DESIGN AND EVALUATION OF A NON-OPIOID TRIPARTITE RELEASE TABLET FOR CHRONIC INFLAMMATORY PAIN.

KUNDAI ROSELYN MAZARURA

A dissertation submitted to the Faculty of Health Sciences, University of the Witwatersrand, in fulfilment of the requirements for the degree of Master of Pharmacy

Supervisor

Prof. Yahya E. Choonara

Department of Pharmacy and Pharmacology, University of the Witwatersrand, South Africa

Co-Supervisors

Prof. Pradeep Kumar

Department of Pharmacy and Pharmacology, University of the Witwatersrand, South Africa

Dr. Armorel van Eyk

Department of Pharmacy and Pharmacology, University of the Witwatersrand, South Africa

2024

DECLARATION

I, Mazarura R. Kundai, declare that this dissertation is my own work. It has been submitted for the degree of Master of Pharmacy in the Faculty of Health Sciences at the University of the Witwatersrand, Johannesburg, South Africa. It has not been submitted before for any degree or examination at this or any other University.

This 16th day of April 2024.

X

Kundai Mazarura
Ms

PUBLICATION

Kundai R. Mazarura, Pradeep Kumar & Yahya E. Choonara (2022): Customized 3D printed multi-drug systems: an effective and efficient approach to polypharmacy, Expert Opinion on Drug Delivery, DOI: 10.1080/17425247.2022.2121816

To link to this article: https://doi.org/10.1080/17425247.2022.2121816

ABSTRACT

Formulation-based approaches towards curbing the prescription opioid crisis include the discovery and development of non-opioid analgesics such as the novel benzyloxy-cyclopentyladenosine (BnOCPA). A more expedited approach involves the development of combinatorial systems of already existing non-addicting analgesics to tap into unexplored synergistic potentials. Despite the recent advances in drug delivery systems, tablets still hold the position of being the most widely used oral dosage form, particularly in the management of chronic ailments; it is cost-effective, non-invasive, and does not require administration expertise.

Challenges in the production of complex geometry combinatorial, multi-drug tablets remain to some extent enigmatic to pharmaceutical researchers, hence the steady paradigm shift from traditional compression to 3-dimensional printing. Although it is superior in multiple aspects, the technique is still in its nascent stages with limited information on regulatory guidelines. Therefore, the aim of this work was to design and develop a non-opioid tripartite controlled-release tablet for efficient chronic inflammatory pain management. Because adherence to adjunct gastroprotective agents (GPAs) in non-steroidal anti-inflammatory drugs (NSAIDs) users has been established to be suboptimal, esomeprazole magnesium trihydrate (ESM) was added to the drug delivery system (DDS). The rationale behind the design was based on inherent drug properties, target release sites, desired therapeutic effects, and allowance for drug release manipulation, therefore a tablet was assembled, constituting an immediate-release top layer formulation of 250 mg paracetamol (PAR) for an early onset of analgesia; a cup layer for the delayed and retarded release of 100 mg of diclofenac sodium (DS) and 250 mg of PAR in tandem, and lastly a core containing a press-coated 20 mg ESM pill.

A reproducible and efficient Reverse-Phase High-Performance Liquid Chromatographic (RP-HPLC) method was developed and validated for the simultaneous detection of the APIs over the concentration ranges studied. Deleterious drug-excipient incompatibilities were ruled out through pre-formulation investigations by FTIR, DSC, and TGA analyses. Combining both wet and dry granulation methodologies; the chosen formulation and polymers (7.5% hydroxypropyl methylcellulose (HPMC) K15M, 25.3% eudagrit L (EL) 100-55, and 10.5% croscarmellose sodium (CCS)), while considering the quality target product profiles (QTPPs), critical process parameters (CPP), and critical material attributes (CMAs), resulted in the development of a pragmatic tablet delivering fifty percent of the PAR dosage in the initial 30 minutes, with a cumulative release of 95.0% ± 0.08% and 94.9% ±3.87% for DS and ESM, respectively.

Through in-process quality control tests, the validity of the manufacturing process was confirmed, with all results falling within pharmacopeial specifications. The release mechanism of PAR and DS from the cup after the 2-hour mark distinctly followed the Hixson-Crowell model where the geometrical characteristic of the cup was maintained with surface erosion. Visuals from scanning electron microscopy (SEM) analysis obtained prior to and during dissolution, confirmed hydration gravimetric analysis results as well as bulk and surface erosion mechanisms. The obtained *ex vivo* analysis results showed retarded permeation rates of the tabletted APIs compared to the APIs in their pure state. Therefore, it is imperative to consider improving the existing models employed for *ex-vivo* permeability studies of tableted formulations, with a particular focus on exploring the impact of excipients/polymers on drug permeation.

ACKNOWLEDGEMENTS

My sincere appreciation goes to my esteemed supervisors for not only their invaluable support and supervision but also for entrusting me with this project and allowing me to live out my passion for medicine manufacturing. Through their redirections and solutions, drawn from their immense knowledge pools and experience I managed to see the project to the end.

I also want to thank the WADDP researchers for creating an environment that is conducive to research, inspiring, and positively influential in every way, with specific acknowledgment of Ahmed Abdelgader for generously sharing his expertise on the operation of the tablet press machine and much more.

Despite having a limited understanding of what this stage of my academic path entailed, my parents were highly supportive in every way possible, for which I am exceedingly grateful. I'd want to thank my friends and brother Tapiwa Mazarura, (fellow academics) who brought joy to what could have been a lonely 2-3 years of my life.

The 2023 academic year would not have been possible without the scholarship I received from MINDS; my thanks go to them as well.

Above all, I thank God the Father, Son, and Holy Spirit, *“in whom I live and move and have my being*." I thank Him for keeping me safe in the late-night hours on the days the research demanded it.

DEDICATION

This work is dedicated to my late grandfathers, my paternal grandfather, who treasured knowledge acquisition even in his old age, and my maternal grandfather, who died in pain in 2021 with the conviction that I could make him a magical pill with no side effects to alleviate his pain.

TABLE OF CONTENTS

LIST OF FIGURES

LIST OF TABLES

LIST OF ABBREVIATIONS

3DP	3 Dimensional Printed
4IR	4th Industrial Revolution
ABS	Acrylonitrile Butadiene Styrene
ACN	Acetonitrile
APIs	Active Pharmaceutical Ingredients
ATR-FTIR	Attenuated Total Reflectance-Fourier Transform Infrared
BCS	Biopharmaceutics Classification System
BHN	Brinell Hardness Number
BIJ	Binder Ink Jetting
BnOCPA	Benzyloxy-cyclopentyladenosine
CAGR	Compound Annual Growth Rate
CCS	Croscarmellose Sodium
CMAs	Critical Material Attributes
COX	Cyclooxygenase
CPOP	Controlled Porosity Osmotic Pump
CPPs	Critical Process Parameters
CQAs	Critical Quality Attributes
DDSs	Drug-Delivery Systems
DIW	Direct Ink Writing
DLP	Digital Light Processing
DMD	Digital Micro-Mirror Device
DPPO	Diphenyl (2,4,6-Trimethylbenzoyl)-Phosphine Oxide
DR	Delayed Release
DS	Diclofenac Sodium
DSC	Differential Scanning Calorimetry
EC	Ethyl Cellulose
EL	Eudragit L
EFV	Efavirenz
ESM	Esomeprazole Magnesium Tri-Hydrate
EVA	Ethylene Vinyl Acetate
EXT	Extrusion (at room Temperature)

FDA	Food and Drug Administration
FDC	Franz Diffusion Cell
FDM	Fused Deposition Modelling
FTC	Emtricitabine
FTIR	Fourier Transform Infrared Spectroscopy
GIT	Gastrointestinal Tract
GPAs	Gastroprotective Agents
HME	Hot Melt-Extrusion
HPC	Hydroxypropyl Cellulose
HPMC	Hydroxypropyl Methylcellulose
ICH	International Conference Harmonization
IMP	Impregnation
INH	Isoniazid
IPQC	In-Process Quality Control
IR	Immediate release
LD	Levodopa
LOD	Limit of Detection
LOQ	Limit of Quantification
MCC	Microcrystalline
NaCMC	Sodium carboxymethylcellulose
NSAIDs	Non-Steroidal Anti-Inflammatory Drugs
ODT	Orally Disintegrating Tablet
PAM	Pressure Assisted Microsyringe
PAR	Paracetamol
PAT	Process Analytical Technology
PBPK	Physiologic-Based Pharmacokinetic
PBS	Phosphate Buffered Saline
PCL	Poly Ɛ-Caprolactone
PDDS	Pulsatile Drug Delivery Systems
PDLA	Poly D-Lactic Acid
PDLLA	Poly-D,L-Lactic Acid
PEC	Polyelectrolyte Complexes
PEEK	Polyether Ether Ketone
PEKK	Polyether Ketone

PEO	Polyethylene Oxide
PGE2	Prostaglandin (E2)
PLA	Polylactic Acid
PLLA	Poly-L-Lactic Acid
PoC	Point-Of-Care
PPIs	Proton Pump Inhibitor
PVA	Polyvinyl Alcohol
PVP	Polyvinylpyrrolidone
QbD	Quality by Design
QbT	Quality by Testing
QTPP	Quality Target Product Profile
RP-HPLC	Reverse Phase-High Performance Liquid Chromatography
RSD	Relative Standard Deviation
SEM	Scanning Electron Microscopy
SFF	Solid Freeform Technology
SGF	Simulated Gastric Fluid
SLA	Stereolithography
SLM	Selective Laser Melting
SLS	Selective Laser Sintering
SLS	Sodium Lauryl Sulphate
SMEDDS	Self-Micro Emulsifying Drug Delivery Systems
SNEDDS	Self-Nanoemulsifying Drug Delivery Systems
SR	Sustained Release
SSG	Sodium Starch Glycolate
SSIF	Simulated Small Intestinal Fluid
TDF	Tenofovir Disoproxil Fumarate
TGA	Thermogravimetric Analysis
TLC	Thin Layer Chromatography
UPLC-MS	Ultra-Performance Liquid Chromatography-Mass Spectrometry
UV	Ultra-Violet Visible
WHO	World Health Organisation

CHAPTER 1

INTRODUCTION AND MOTIVATION FOR THE STUDY

1.1 Background

An ongoing conundrum for healthcare professionals has been how to effectively manage chronic pain without posing risks of tolerance, dependence, and addiction, with nearly 1 in every 5 South Africans suffering from chronic pain, limbic joint pain, and back pain making up 43.6%, and 30.5% of the pain, respectively (Kamerman *et al.,* 2020). The range of available pharmacological treatment options for long-term management is predominantly restricted to non-steroidal anti-inflammatory drugs (NSAIDs) and/or opioid analgesics. Frequently, patients choose opioids as their preferred choice due to their well-established effectiveness in pain relief and occasional mood-altering benefits (Engel-Rebitzer *et al.,* 2021; Dowel *et al.,* 2022; Seidel *et al.,* 2022; Castle *et al.,* 2023). Of late, rising rates of opioid overdose deaths have raised questions about prescribing opioids for chronic pain management. Worldwide, about 0.5 million deaths are attributable to drug use of which more than 70% of these deaths are related to opioids, with more than 30% of those deaths being a result of overdose. Because of the risk of serious harm, without sufficient evidence for benefits, current guidelines discourage opioid prescribing for chronic pain (Dowel *et al.,* 2022). "*Opioid misuse and abuse remain a serious public health crisis facing the country. Preventing new addiction through fostering the development of novel non-opioid analgesics is an important priority for the FDA*," Patrizia Cavazzoni, M.D., director of the FDA's Centre for Drug Evaluation and Research (FDA, 2022).

The pathophysiology of persistent inflammatory pain commonly found in joint diseases includes signalling initiated by peripheral terminals of sensory neurons (Chen, Yang and Grosser, 2013; Seidel *et al.,* 2022). The presence of algogens such as prostaglandins, particularly E2 (PGE2), in the synovium and synovial fluid capable of exciting or sensitizing peripheral nociceptors, describes the generation of pain in inflammatory joint diseases. PGE2 is a product of the hydrolysis of arachidonic acid, a reaction catalysed by cyclooxygenase enzyme 2 (COX-2) (Di Carlo, Smerilli and Salaffi, 2021), Figure 1.1. The pathophysiology explains the rationale behind the use of COX inhibitors in associated conditions. On the other hand, inhibition in the synthesis of prostaglandins in patients on chronic Non-Steroidal Anti-Inflammatory Drugs (NSAIDs) induces clinically significant ulceration, bleeding, and/or obstruction. The pathogenesis of NSAID-induced ulceration and bleeding involves three key pathways: inhibition of cyclooxygenase (COX)-1 activity, inhibition of COX-2 activity, and direct cytotoxic effects on the epithelium (Wallace, 2008). Selective COX-2 inhibitors were at some

point hailed for their non-ulcer-inducing mechanism due to their COX-1 sparing pathway until the role of the COX-2 pathway was identified in the pathogenesis of NSAID-induced damage, including evidence of increased risks of myocardial infarction to the point of withdrawal from general use. Therefore, regardless of the NSAID of choice, concomitant proton pump inhibitor (PPIs) co-therapy is crucial. There exists comprehensive evidence on the effectiveness of PPIs over standard doses of H_2 receptor antagonists and that they are as effective as, but better tolerated than misoprostol in ulcer prophylaxis (Rancis *et al.,* 2002; Dieppe, Shah Ebrahim and Jüni, 2004; Wallace, 2008; Lazzaroni and Porro, 2009).

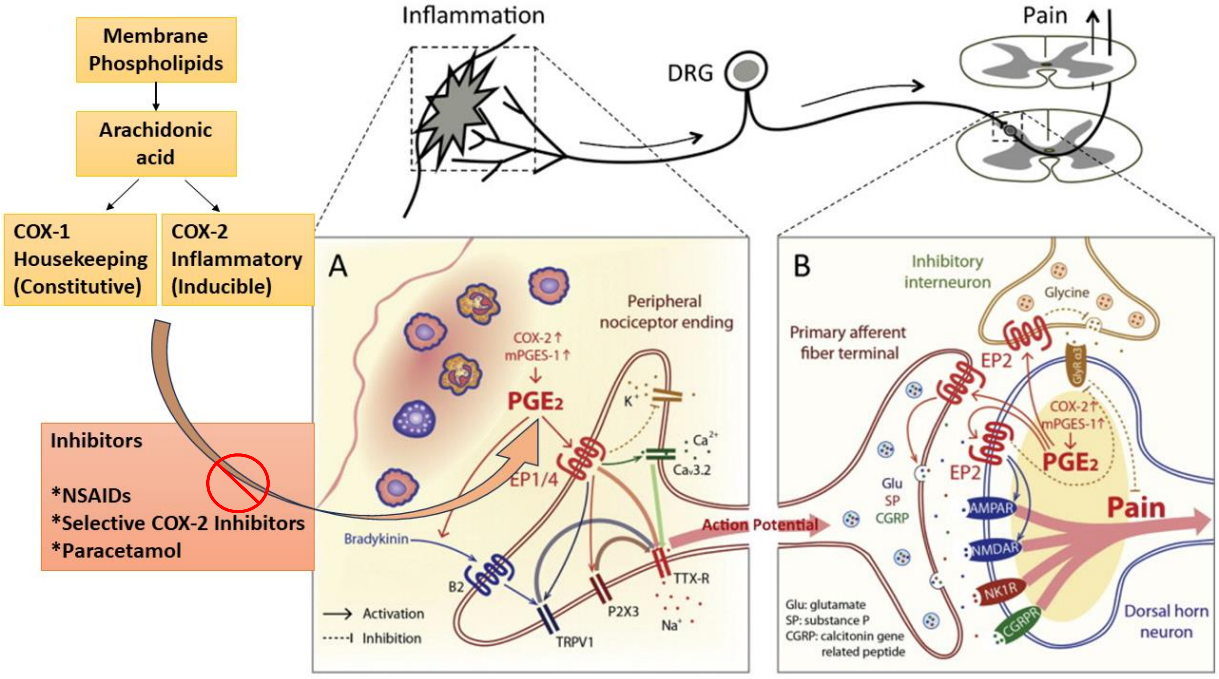

Figure 1.1: Molecular mechanisms that mediate PGE2-induced pain hypersensitivity inflammation. (A) COX-2 and mPGES-1 are upregulated in both injured cells and infiltrating immune cells in inflamed tissues, which increases PGE2 concentrations at peripheral nociceptor terminals. (B) Inflammation upregulates COX-2 and mPGES-1 expression in the spinal cord and increases PGE2 production. PGE2, mainly acting on EP2 receptors, contributes to central sensitization through both presynaptic and post-synaptic mechanisms. Modified and reprinted with permission from (Chen, Yang and Grosser, 2013).

The tablet remains the go-to dosage form in most pharmaceutical developments due to its plethora of advantages, particularly in chronic disease management (Hummler *et al.,* 2023). Controlled pulsatile-release multi-drug solid oral dosage forms have been instrumental in treating various chronic ailments improving adherence and compliance patterns in most patients (Huynh and Lee, 2015). Pulsatile drug delivery systems (PDDS), i.e., systems in which the drug is released suddenly after a well-defined lag time according to the circadian rhythm of the disease, are classified as either, time-controlled pulsatile release (single or multiple unit system), internal stimuli-induced or external stimuli-induced release systems

(Sokar *et al.,* 2013). The dosage forms of these can either follow capsule, pellet, or tablet configurations amongst which is the 'core-in-cup' tablet system. A typical core-in-cup tablet system consists of three different parts: a core tablet, containing the active ingredient, an impermeable outer shell, and a top cover plug layer of a soluble polymer, (Danckwerts and Watt, 1998; Nagaraju *et al.,* 2009; Sokar *et al.,* 2013; Srinija and Lakshmi, 2016; ElMeshad *et al.,* 2020) (Figure 1.2).

Nonetheless, the present study proposes to employ the same concept in developing a drug delivery system comprising an enterically press-coated esomeprazole magnesium trihydrate (ESM) core pill, an insoluble pH-dependant plug barrier, a delayed release (DR) cup formulation layer of diclofenac sodium (DS) and paracetamol (PAR), and an Immediate release (IR) top layer of PAR. In addition to the discovery and development of non-opioid analgesics such as the novel VX-548 (moving into Phase III clinical trials) and benzyloxy-cyclopentyladenosine (BnOCPA); an expedited approach towards formulation-based interventions involves research on combinations of currently available active pharmaceutical ingredients (APIs) to tap into unexplored synergistic potentials of non-addicting analgesics (Kingwell, 2022; Wall *et al.,* 2022).

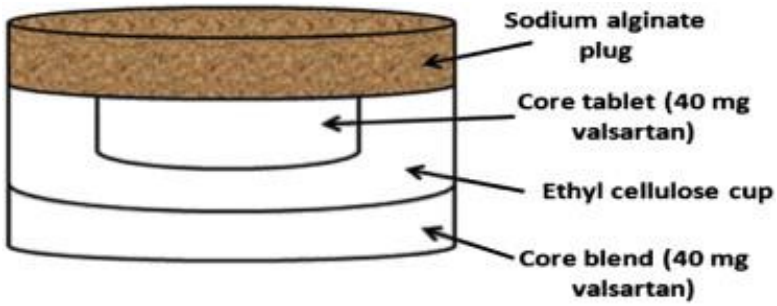

Figure 1.2: Core-in-Cup PDDS. Reprinted with permission from (Sokar *et al.,* 2013).

1.2 Rationale Behind the Design and Combination

High-income countries have suffered strains in their health and financial systems as a result of the global crisis, unfortunately, the health systems of developing countries are even less prepared should the opioid epidemic occur (Harker *et al.,* 2020). In order to lessen the forecasted burdens, there is a need to ensure a reduction in the number of new cases of addiction, whether from intentional or unintentional abuse. A pharmaceutical approach in ensuring this involves encouraging the discovery, development, and re-development of low-abuse potential, non-addicting analgesic formulations for prescription to opioid-naïve chronic patients.

Adherence to adjunct gastroprotective agents (GPAs) in NSAID users has been established to be suboptimal; in fact, it was discovered in one study that more than one-third of NSAID users did not use the prescribed GPAs daily, which resulted in a 16% increase in GIT complications for every 10% decrease in adherence (Van Soest *et al.,* 2007). Therefore, this study proposes a familiar analgesic combination of PAR and DS, comprising prophylactic ESM for potential and convenient use in the long-term symptomatic relief of inflammatory pain in chronically ill patients.

The rationale behind the design was based on inherent drug properties, target release sites, desired therapeutic effects, and allowance for drug release manipulation. Whilst diclofenac potassium is formulated for release in the stomach, often as IR tablets, DS due to its resistance to dissolution in low pH gastric milieu, is designed for duodenal release (Williams and Buvanendran, 2011). Following oral administration, DS uniquely accumulates in synovial fluid which may explain why its duration of therapeutic effect is considerably longer than the plasma half-life of 1 to 2 hr, the dose range for adults with joint inflammatory pain is 150 – 200 mg/24hrs in adults (Williams and Buvanendran, 2011). Various pieces of research have comprehensively proved the synergism between PAR and DS, including new data on the analgesic mechanisms of PAR, confirming its efficacy in multimodal, non-opioid, or opioid-sparing, therapies for the treatment of both acute and chronic pain (Przybyła, Szychowski and Gmiński, 2021; Freo, 2022).

The top layer constitutes an immediate-release formulation of PAR, 250 mg for an early onset of analgesia. The cup layer was formulated for the delayed and retarded release of 100 mg of DS and 250 mg of PAR in tandem. Lastly, the core is a press-coated 20 mg ESM pill. Because ESM rapidly degrades at low pH, i.e., gastric milieu, a low solubility barrier plug was placed between the IR layer and DR layer. A schematic depicting the desired release profile is represented in Figure 1.3.

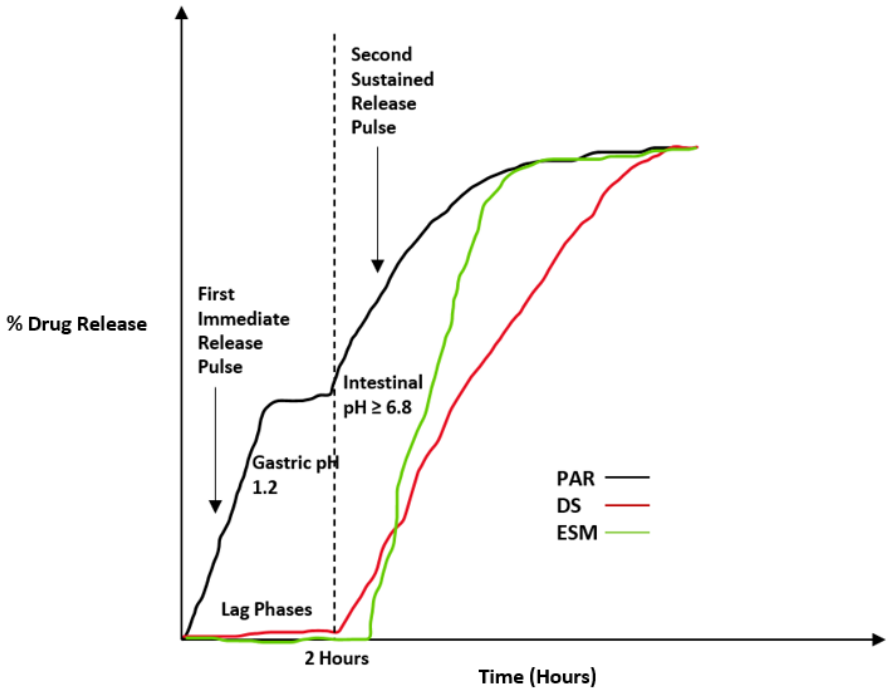

Figure 1.3: Schematic of the ideal desired release profiles**.**

1.3 Aims and Objectives of the Study.

The aim of this study was to design and develop a non-opioid tripartite controlled-release tablet for chronic inflammatory pain. The above aim was attained via the following objectives:

1. Performing pre-formulation studies to characterise and screen various polymer combinations for potential use in the formulation, including developing and validating an HPLC method for the simultaneous detection of the APIs.
2. Designing and formulating a tripartite controlled-release tablet and performing process validation tests by analysing the matrices' hardness, uniformity of mass, friability, and thickness.
3. Characterisation of the tablet by performing physicochemical studies to determine stability and molecular interactions within the matrix and between the layers.
4. Elucidation of the physico-mechanical properties of the DDS through matrix hydration, erosion, and textural analyses.
5. Performing *in vitro* drug release studies to determine the drug release profile of the DDS and predict the potential release mechanism of the system.
6. Performing *ex vivo* permeability studies on porcine duodenal tissue to determine the effect of tableting on the permeability profiles of the active ingredients.

1.4 Overview of This Dissertation

Chapter One: This chapter provides an introduction and background of this current study. Details on the motivation for undertaking this study, the rationale, aims and objectives for the study were presented.

Chapter Two: This chapter presents a comprehensive literature review on controlled-release multi-drug oral systems, with concise insight into the currently employed and novel formulation techniques. Included therein is a summary of different 3D printing technologies applied in the fabrication of customised solid oral drug delivery systems, such as extrusion-based printing further subdivided into fused deposition modelling (FDM) and extrusion at room temperature (EXT), amongst others. The chapter ends with an expert opinion on how identified hindrances in the full implementation of these novel techniques may be tackled.

Chapter Three: This chapter outlines all the pre-formulation investigations undertaken on potential formulation components. Details on the effects of potential polymers/excipients on APIs' characteristics as determined via DSC, TGA and FTIR analyses are presented. Outlined as a part of the chapter are steps taken towards the development and validation of an HPLC method for the simultaneous quantitation of the APIs during dissolution and permeability analysis.

Chapter Four: This chapter entails the preliminary design and developmental stage, in which working formulations were determined through *in vitro* dissolution studies carried out on various drug-loaded structural components of the tablet matrix. In order to distinctly establish working concentrations of the functional polymers for each formulation layer, partial blanks were formulated and compressed for investigation. Analyses performed highlight the influence of key polymers such as super-disintegrant croscarmellose sodium (CCS), hydroxypropyl methylcellulose (HPMC K15M), eudragit L 100-55 (EL 100-55) as well as the efficiency of the plug as an added protection from gastric degradation of the core formulation.

Chapter Five: This chapter focuses on the assemblage of the complete and optimal drug delivery system, based on the findings from the previous chapter, including *in vitro* release studies and all in-process validation tests. Included therein is the characterisation of the final formulation, i.e., establishment of the DDS's physico-mechanical properties through matrix hydration, erosion, and textural analyses.

Chapter Six: This chapter expounds on the methodology applied in evaluating the *ex vivo* permeability characteristics of the drug compounds in combination through porcine duodenal tissue. Highlighted in the chapter is the effect of tableting excipients/polymers on available methods of permeability analysis.

Chapter Seven: Concludes on the present research, presenting recommendations for future work.

CHAPTER 2

LITERATURE REVIEW ON NOVEL FORMULATION TECHNIQUES FOR CONTROLLED RELEASE MULTI-DRUG SYSTEMS

Expert Opinion on Drug Delivery

ISSN: (Print) (Online) Journal homepage: https://www.tandfonline.com/loi/iedd20

Customized 3D printed multi-drug systems: an effective and efficient approach to polypharmacy

Kundai R. Mazarura, Pradeep Kumar & Yahya E. Choonara

To cite this article: Kundai R. Mazarura, Pradeep Kumar & Yahya E. Choonara (2022): Customized 3D printed multi-drug systems: an effective and efficient approach to polypharmacy, Expert Opinion on Drug Delivery, DOI: 10.1080/17425247.2022.2121816

To link to this article: https://doi.org/10.1080/17425247.2022.2121816

2.1 Introduction

Because of the prevalence and chronicity of both communicable and non-communicable diseases such as hypertension, tuberculosis, and diabetes, patients are often prescribed long-term regimens comprising multiple medications (Gradman *et al.,* 2013; Weverling *et al.,* 1998; Cruz *et al.,* 2018). While there is no set definition of polypharmacy, it is commonly described as the concurrent prescribing of at least four or five medicines, for instance, a typical regimen for a hypertensive patient with hypercholesterolemia contains Enalapril 10 mg, Carvedilol 10 mg, Spironolactone 10 mg, Hydrochlorothiazide 25 mg at least once daily, and Simvastatin 20mg (STG, 2015). Following administration requirements to the letter is a sine qua non for effective polypharmacy. Unfortunately, both intentional and non-intentional non-adherence are frequent consequences of polypharmacy (Payne and Avery, 2011).

Poor medication adherence has been linked to a deterioration in the prognosis of patients with non-communicable diseases, coupled with other negative effects such as increased mortality and costs (Diseases *et al.,* 2021). Recent findings from a study examining the factors associated with non-adherence among older patients with multimorbidity and polypharmacy showed a 79.6% prevalence of non-adherence in 74 non-institutionalized patients aged ≥65

years with ≥2 chronic conditions (González-Bueno *et al.,* 2021). The former statistics cohere with Butler and co-workers' previous findings, in which non-adherence was associated with 4 to 11% of all hospitalizations and 7.6% of emergency visits, with a staggering overall incidence of 40 to 86% (Butler *et al.,* 2011). A formulation-based solution to the pressing issues of polypharmacy was the introduction of fixed dose combinations (FDCs) commonly referred to as "polypills" targeted at reducing the risk of mortality and cardiovascular events (Abushouk *et al.,* 2022). In 2016, polypills were formally recommended and included in the European Guidelines on cardiovascular disease prevention and the World Health Organization proposed polypills as a significant strategy for improving cardiovascular disease management (Piepoli *et al.,* 2016; WHO, 2016).

As the name suggests these formulations contain multiple active ingredients, each with a different pharmacological effect. A commercially available example is Polycap™ constituting enteric-coated aspirin, ramipril, simvastatin, atenolol, and hydrochlorothiazide, other examples include Ramitorva™ (aspirin, ramipril, and atorvastatin), and Starpill™ (aspirin, losartan, atenolol, and atorvastatin) (Yusuf *et al.,* 2009; Webster, Castellano and Onuma, 2017). The development of the majority of polypills was motivated by the serious burden and incidence of cardiovascular disorders, however, the concerns around polypharmacy are not limited to cardiovascular diseases. Furthermore, the rationale behind multi-drug systems hinges on the effectiveness of combined therapy, simplified treatment regimens, reduced production and storage costs, and efficient supply chain and logistics, in addition to the highlighted grounds of enhanced adherence and compliance (Webster, Castellano and Onuma, 2017). However, polypills like any other intervention have their drawbacks, notably the production process, which has proven to be quite complex. Different procedures are utilized in the classic compression process, such as granulation of all active components, individual granulation of actives, and drug separation by layering in circumstances where there are incompatibles and interactions between the actives (Webster, Castellano and Onuma, 2017).

More importantly, the mass production of the polypill has been criticised for its one-size-fits-all approach, which disregards individual patient needs that is, some patients may require higher or lower dosages of particular active moieties within the formulation, while others may not require all of the drugs contained within the formulation (Abushouk *et al.,* 2022). Moreover, bioavailability profiles and dosing requirements of paediatric, adult, and geriatric populations vary. Although traditional techniques may be used to customise a pill for a patient, the methods are neither cost-effective nor practicable for continuous fast on-demand production (Webster, Castellano and Onuma, 2017). This calls for more innovative and flexible production techniques that will allow the smooth fabrication of bespoke drug combinations. One such

technology is 3-dimensional (3D) Printing, an innovation posing significant promise for patient patient-centred therapy (Jamróz *et al.,* 2018). The combination of these two ideas (3D printing and multi-drug Systems) represents another step forward in the revolutionisation of healthcare. This review will investigate the promising paradigm shift from one medication for all to personalised patient-centred medicines, providing an overview of the current state of 3D printing techniques for multi-active dosage forms, polymers, and excipients used and their effects, the market view, limitations, and potential barriers to full implementation.

2.2 Summary on 3D Printing Technologies

3D printing has been described by terms such as layered manufacturing, additive manufacturing, computer automated manufacturing, fast prototyping, solid freeform technology (SFF), and even artistic science from its inception in the early 1970s (Abdulhameed *et al.,* 2019; El-bassyouni, 2020). It has a plethora of applications in engineering, dentistry, building, aeronautics, bone regeneration, as well as pharmacy (Choonara *et al.,* 2016). To produce a solid entity, the printing process involves layer-by-layer deposition of 'ink' material based on a pre-designed 3D digital model. Although it has been around for some time, its use in the pharmaceutical sector is still in its nascent stages, and its full potential has yet to be realized (Jamróz *et al.,* 2018; Zhu *et al.,* 2020). A lot of research has been done on 3D printing in the medical sector, with a vast amount of literature for reference on topics such as the selection of appropriate excipients, printable actives, strategies to achieve different drug-release profiles, and the advantages of various methodologies (Goyanes *et al.,* 2015; Awad *et al.,* 2018; Horst, 2018).

Operations of the different types of 3D printing technologies have been extensively explained in several publications with provisions for the different ways of classifying them (Goyanes *et al.,* 2015; Horst, 2018; Abdulhameed *et al.,* 2019; Zhu *et al.,* 2020). A simple classification system by Jamroz et al. included powder solidification, liquid solidification, and extrusion. Extrusion-based printing is frequently utilized in the production of solid oral dosage forms. The approach is further subdivided into fused deposition modelling (FDM) and extrusion at room temperature (EXT), the latter of which is confined to thermolabile drugs (Jamróz *et al.,* 2018). In liquid solidification, the object is built by either droplet solidification (Drop on Drop deposition or Ink Jetting) or solidification of photosensitive liquid (Stereolithography/SLA), whereas in powder solidification, the object is built by either solidification of powdered material by high energy beam (Selective laser sintering/ SLS) or liquid binding of powdered material (Drop on solid deposition or Binder Ink Jetting (BIJ) (Jamróz *et al.,* 2018). Modifications were made to SLA to allow for faster, better resolution, and more efficient processing via the incorporation of a digital micro-mirror device (DMD) in the optical path of the laser. Whilst SLA printers,

require vast amounts of resin for printing, digital light processing (DLP) printers allow for customized resin reservoirs and lesser amounts of resin. Promising applications of DLP 3DP include printing medical devices, microneedle-mediated drug delivery systems (Lim, Ng and Kang, 2017; Bloomquist *et al.,* 2018), and more recently solid oral dosage forms, illustrated in Figure 2.1 below (Kadry *et al.,* 2019).

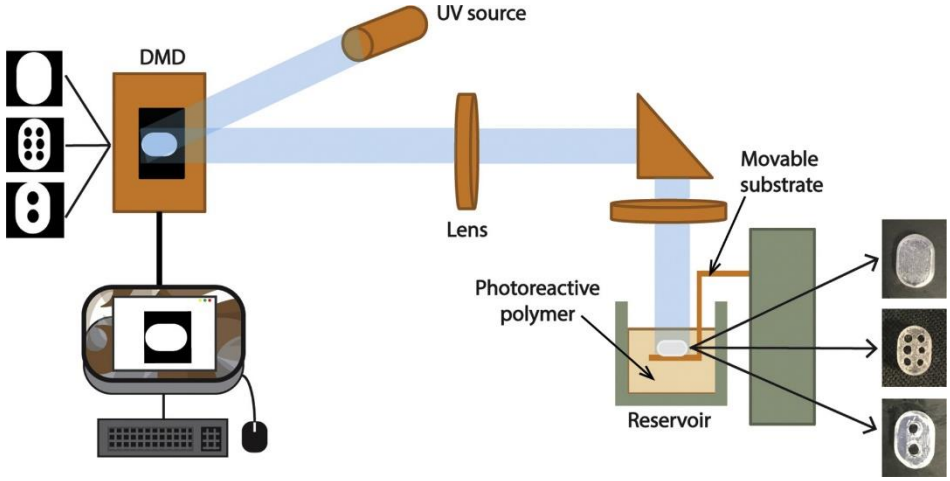

Figure 2.1: Schematic diagram of the Digital Micromirror Device (DMD) stereolithography (DLP 3DP) setup including designs and images of 3D printed theophylline tablets. Reproduced with permission from (Kadry *et al.,* 2019) © 2019 Elsevier B.V. Ltd.

The advantages of 3D printing in medication formulation far outweigh the negatives. It enables the compartmentalization of drug components, which is especially essential in multi-drug systems where interactions and incompatibilities between medicines and excipients are possible. Furthermore, unlike traditional techniques, 3D printing is more versatile, allowing for adjustments in shape and size to meet the specific demands of a patient (Alhnan *et al.,* 2016). From bi-layered tablets to 6-layer tablets, researchers have proved the versatility of 3D printing (Gioumouxouzis *et al.,* 2018; Robles-martinez *et al.,* 2019). Although 3D printing has many advantages, some of the few minor drawbacks include the final product's look with perceptible exterior flaws, and post-processing of the product, particularly in powder-based and extrusion-based 3D printing (Alhnan *et al.,* 2016).

2.3 Customisation in Different Population Groups

2.3.1 Visually Impaired Patients

For visually impaired patients, receiving medications may present challenges like trouble reading labels and differentiating drugs, especially if the once annotated packaging has been damaged or lost (Andreadis *et al.,* 2022). 3D printing opens up the possibility of printing Braille characters directly onto the pills. Successful attempts were made in printing orally disintegrating tablets and Intraoral films with embedded Braille and Moon characters. Visually

impaired volunteers who took part in the haptic *in vivo* evaluation studies confirmed the readability of the embedded text and the potential for personalized treatment with 3D printing (Eleftheriadis and Fatouros, 2021).

2.3.2 Paediatric Patients

The pharmacotherapy of children requires very specific guidelines in regard to dosing and special attention to safety and efficacy. A child's sensitivity to bitter ingredients makes easy administration and taste key factors to consider in dosage form design for this group (Andreadis *et al.,* 2022). Personalized paediatric formulations can be prepared using 3D printing, however, ingredients used in 3D printed dosage forms intended for administration to children need to be extensively studied for their possible toxicity. Researchers have attempted nonetheless to develop delivery systems that appeal to the population, such as chewable gelatine-based gummies in the form of Lego™ bricks, including capsules and orodispersible miniprintlets, and cartoon-based ibuprofen and paracetamol-loaded chocolate chewable tablets (Rycerz *et al.,* 2019; Karavasili *et al.,* 2020; Eduardo, Ana and José, 2021).

2.3.3 Geriatric Patients

Multimorbidity is a more common occurrence in older patients making them the most susceptible to the deleterious effects of polypharmacy. It is this population group that will benefit the most from 3D printed multidrug systems, customised to each one's therapeutics needs (Andreadis *et al.,* 2022). Figure 2.2 illustrates the concept of customised therapy achieved by 3D printing versus mass-produced conventional systems.

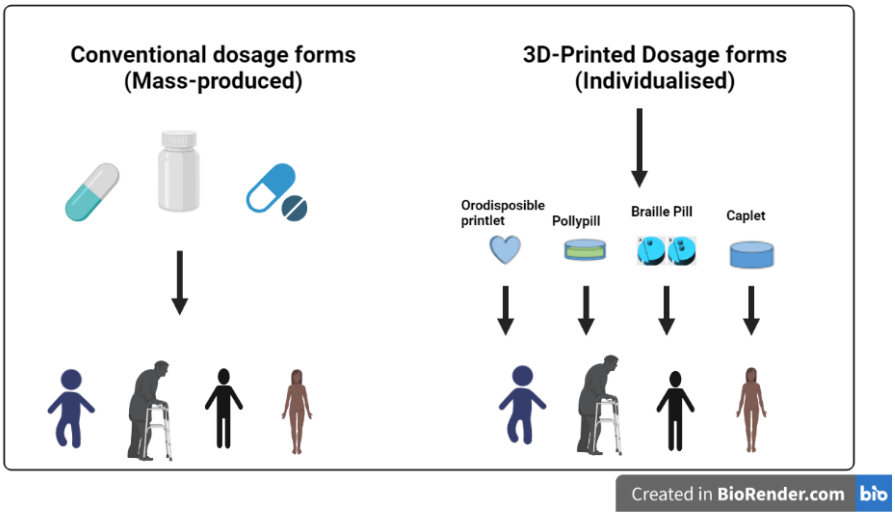

Figure 2.2: Comparison between mass-produced conventional dosage forms-based therapy and 3D printing-based personalized therapy. Adapted with permission from (El-Bassyouni, 2020) © 2020 Elsevier.

2.4 3D Printed Multi-Drug Dosage Forms

Spitram® (levetiracetam), a single-active formulation for the treatment of seizures, is the only 3D printed formulation with Food and Drug Administration (FDA) clearance to date (Kassem, Sarkar and Nguyen, 2022). The development of 3D printed multi-system models is presently based on proof-of-concept approaches. Oral dosage forms such as captopril, nifedipine, and glipizide, fixed-dose combinations efavirenz (EFV), tenofovir disoproxil fumarate (TDF), and emtricitabine), and a 6-layered pill containing paracetamol, caffeine, naproxen, chloramphenicol, prednisolone, and aspirin make up the majority of these formulations. These formulations were printed using a variety of 3D printing methods (Khaled *et al.,* 2015b; Robles-martinez *et al.,* 2019; Siyawamwaya *et al.,* 2019a). Multidrug systems are not only limited to oral dosage forms, but the technology has also found application in drug-eluting implants (Domsta and Seidlitz, 2021). Among the numerous approaches available, nozzle-based printing, particularly fused deposition modelling, has been the most popular among researchers (Kassem, Sarkar and Nguyen, 2022).

2.4.1 3D Printed Oral Multi-Drug Formulations

2.4.1.1 Formulations Printed by Fused Deposition Modelling

One noteworthy advantage of FDM in multi-drug formulation development is that it allows for multi-material printing, which allows for the extrusion of more than one drug-loaded filament in a single printing process (Long *et al.,* 2017). Hot melt-extrusion (HME) is a stand-alone process used to manufacture API and polymer filaments (feedstock) prior to FDM printing. The method uses heat and pressure to melt and extrude the mixture via an orifice (Repka *et al.,* 2018; Lubrizol, 2019). The extruded mixture is aligned with a 3D printer in HME-based printing to create the item based on the pre-designed digital model (Zhang *et al.,* 2017). HME has proved useful in the creation of solid dispersions, alleviating problems associated with poorly soluble APIs and therefore improving dissolution rates and bioavailability (Repka *et al.,* 2018). The drug loading method in filament production determines the amount of drug that can be loaded which in turn influences the rate of drug release from the eventual 3D printed solid dosage form. Drug loading by impregnation is limited to a low of about 2% w/w and yields rapid drug release, of which both scenarios may not be ideal for multi-drug systems requiring sustained release mechanisms. By employing HME in drug-filament production, both higher drug loading and prolonged release profiles can be achieved (Karavasili *et al.,* 2020). This was demonstrated by Thanawuth *et al.,* (2021), in a study where drug release studies were carried out on three, 3D printed tablet formulations, two low-dose formulations, one made from impregnation (IMP)-produced drug-loaded filaments and the other from HME-produced drug-loaded filaments, the third was also HME-produced but with a higher loading (30 % w/w), PLL

(PVA) was the choice of polymer in all formulations. The results confirmed that drug loading determined by the technique directly influences drug release, both the IMP and HME-produced filaments with low drug loading yielded faster release profiles compared to the high drug loaded-HME-produced-tablets, in which release was extended to 24 hours with a swelling-erosion mechanism (Thanawuth *et al.,* 2021).

With growing interest in additive manufacturing of personalised medication with complex geometries, integrating and synchronizing FMD and HME using process analytical technology (PAT) tools could potentially lead to continuous, larger-scale production of efficient and cost-effective multi-drug delivery (Long *et al.,* 2017; Wesholowski *et al.,* 2019). Raman Spectrometer, Laser-Based Diameter Measuring Module, Acoustic Emission Sensor, High-speed camera, and Rheometer are some possible PAT instruments that may be included into the HME-FDM process and are favourable to multi-drug systems. APIs can be quantified, deterioration identified in-line, dosing accuracy increased, viscosity measurement avoiding nozzle clogging, no pauses in the printing process, and texture analysis guaranteeing smooth feeding of filaments into 3D printers (Hagrasy *et al.,* 2013; Korte and Quodbach, 2018; Yang *et al.,* 2018; Andrews *et al.,* 2019; Ponsar, Wiedey and Quodbach, 2020). Figure 2.3 and 2.3 b illustrate printing processes with and without the inclusion of PAT.

Because various medicines have varying release kinetics and absorption locations, it is critical to consider aspects that will affect transit durations through particular areas of the gastrointestinal tract when developing controlled-release multiple-drug delivery systems (Aulton and Taylor, 2013). For example, metformin and glimepiride, two medicines used to treat Type 2 diabetes, (administered as a fixed dose combination or as separate medications) have different absorption sites, metformin is mostly absorbed in the small intestine, whereas Glimepiride is absorbed in the stomach (Hwang *et al.,* 2013; STG, 2015). Based on these criteria, to ensure optimum pharmacotherapy, researchers employed HME/FDM 3D printing to fabricate a bi-layered, controlled-release solid dosage form of metformin and glimepiride (Gioumouxouzis *et al.,* 2018). Similarly, Windolf and co-workers recently fabricated mini floating polypills for Parkinson's Disease combining Levodopa, benserazide, and pramipexole in various dosing for personalized therapy (Windolf *et al.,* 2022).

A new Melt Extrusion Deposition (MED™) 3D printing technology has been created to improve the use of FDM by addressing drawbacks such as the requirement for pre-fabrication of printable drug-loaded filament and printing precision. The MED™ method combines powdered active components and excipient ingredients as starting materials, eliminating the need for

prior filament production. Reproducible, accurate, and larger-scale production can be performed using high-throughput printer nozzle arrays, handling numerous materials, and precise deposition control. This new technology, combined with compartmental model designs, allows for the fabrication of bespoke multi-drug systems with modulated release kinetics from each compartment (Zheng *et al.,* 2021).

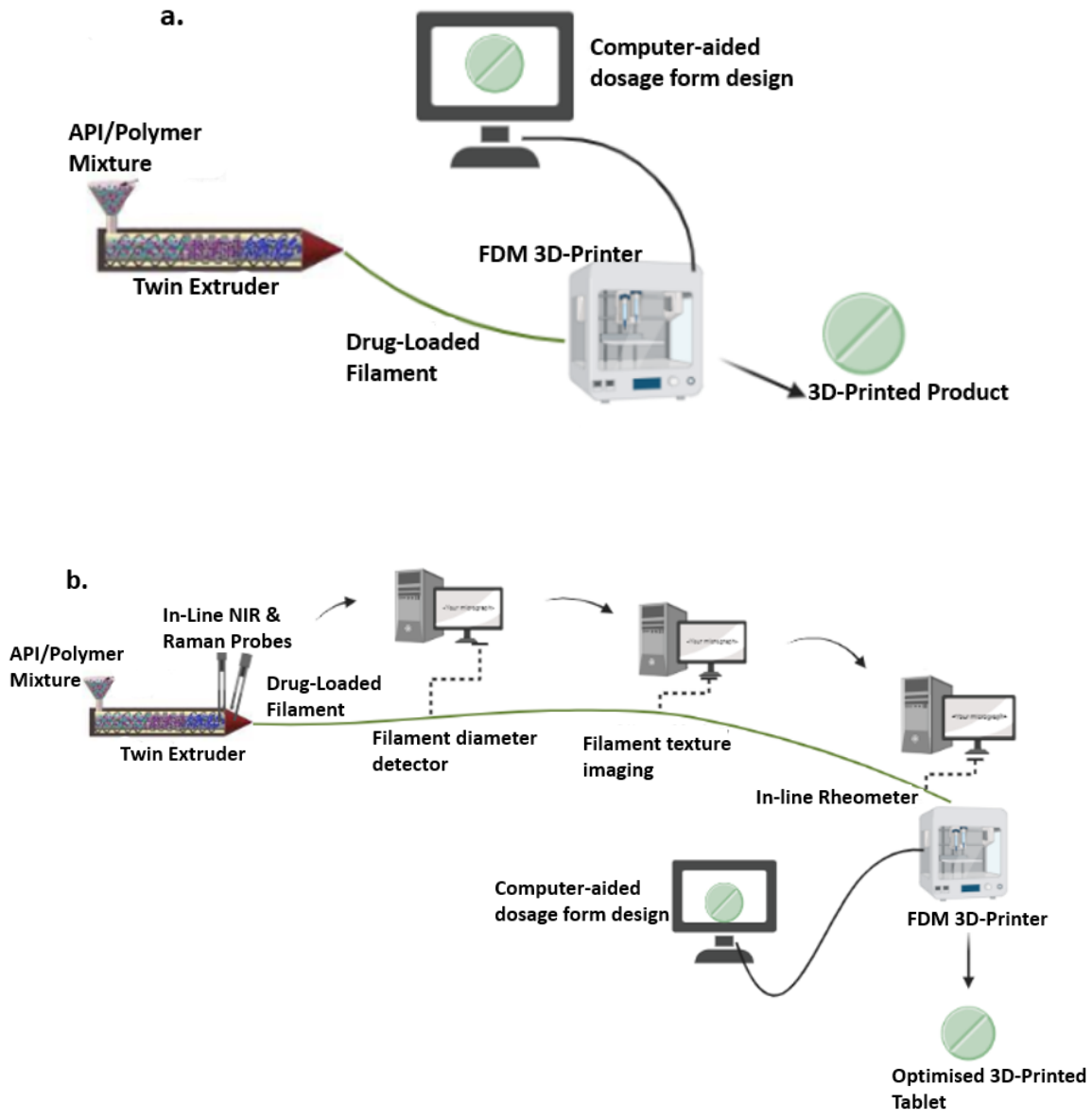

Figure 2.3: a. HME coupled FDM 3D printing procedure without in-line PAT tools b. HME coupled FDM 3D printing with PAT tools.

2.4.1.2 Formulations Printed by Pressure Assisted Microsyringe Extrusion

Thermal deterioration is an unavoidable drawback of HME-FMD printing, limiting the number of medicines and materials that may be produced using the technology, also known as Pressure Assisted Microsyringe (PAM), extrusion at room temperature does not require high temperatures. Rather the process involves the preparation of a semisolid gel or paste consisting of drug/s and additives. The mass is then continuously extruded layer by layer through a syringe-based tool-head. Thus, by employing multi-syringe systems, this technique can yield multi-active solid dosage forms with varying kinetics, Figure 2.4 a (Jamróz *et al.,* 2018; Azad *et al.,* 2020). Khaled and colleagues (2015) used room-temperature extrusion to create a multi-compartment, multi-drug system consisting of nifedipine, captopril, and glipizide. The formulation was designed to solve issues found in the treatment of hypertension and type 2 diabetes, such as dosage dumping, burst phenomena, short elimination half-life, and short duration of action (Khaled *et al.,* 2015b). Captopril was released through controlled osmosis by incorporating an osmogen sodium chloride into the core of the captopril compartment, whereas the other two actives were released via diffusion processes, as shown in Figure 2.4b.

Controlled porosity osmotic pump tablets use osmotic pressure principles for controlled release, overcoming the impact of the gastrointestinal tract's physiological condition (Shahi *et al.,* 2012; Sahoo *et al.,* 2015). This approach is not only simple to use, but it is also appealing to patients since it decreases dose frequency while providing the benefit of a longer duration of action. Zero-order release, independent of physiological parameters such as pH can be achieved. The manufacture of a controlled porosity osmotic pump (CPOP) involves the encapsulation of an osmogen core with a semipermeable membrane, which rapidly dissolves when in contact with an aqueous medium creating a micro-porous membrane (Sahoo *et al.,* 2015). Another recent study used extrusion-based printing at room temperature to obtain a higher bioavailability of efavirenz (EFV), tenofovir disoproxil fumarate (TDF), and emtricitabine (FTC) compared to a non-3D printed commercial version of the same medicines, Atripla® for improved HIV therapy (Siyawamwaya *et al.,* 2019b). Nonetheless, extrusion-based printed DDS have unappealing characteristics such as low resolution (depending on nozzle size) and poor mechanical qualities, necessitating the use of more precise methods such as SLA (Domsta and Seidlitz, 2021).

2.4.1.3 Formulations Printed by Stereolithography

Stereolithography (SLA) is the original 3D printing method, having been used in pharmaceutical technology for the first time in 1984 (Jamróz *et al.,* 2018). It is a laser-based technology that uses photo-polymerisation to create a solid three-dimensional object from a photocurable viscous liquid enclosed in a vat. A layer is generated by a laser beam following a g-coded pattern, then the platform is lowered into the vat for the second layer, and so on until the item is finished (Melchels, Feijen and Grijpma, 2010; Abaci *et al.,* 2021). Its advantages over nozzle-based methods include greater dimensional precision, a finer finish, and a lack of dependency on heat for manufacturing. More significantly, unlike SLA, FDM is restricted to a small number of spatially separated medicines in a formulation (Pereira *et al.,* 2019; Robles-martinez *et al.,* 2019). As a result, Martinez and colleagues used SLA 3D printing for the first time to create a multi-layered tablet containing six drugs: paracetamol, caffeine, naproxen, chloramphenicol, prednisolone, and aspirin (Robles-martinez *et al.,* 2019). However, considerations such as the possibility of API deterioration owing to laser projection onto the drug-loaded solution and the requirement for extra API in the manufacture of the photocurable resin, restrain its complete usage in production (Abaci *et al.,* 2021). Recently, SLA was employed in the development of multifunctional nanocomposite pills, in which both nanoparticles and conventional solid dosage form designs make up a drug delivery system. The procedure entails the creation of vat photo-polymerised monoliths that serve as reservoirs for drug-loaded nano-carriers. Similarly, researchers may be able to develop more novel nanocomposites for multi-modal and multi-compartment drug delivery systems suitable for multiple drug systems using SLA-assisted 3D printing (Sharma *et al.,* 2022).

2.4.1.4 Formulations Printed by Selective Laser Sintering

Selective laser sintering (SLS) is yet another type of laser-based printing that has had limited application in 3D printed oral multi-drug systems. This is most likely due to the laser beam's high-energy input, which raises concerns about the likelihood of API and pharmaceutical excipient deterioration (Alhnan *et al.,* 2016). Unlike similar powder bed-based techniques, the process is faster, and does not require a binder solution; instead, the powdered printing material is exposed to radiation, which will either partially or fully melt it for layered fabrication. In SLS-printed oral dosage forms, two drug loading approaches can be used: prior to sintering and after sintering. The former entails preparing an API and excipient/s powder mixture, which is then added to the powder bed for laser-based fabrication of the drug-loaded tablets (Abaci *et al.,* 2021). Drug loading after printing is considered a safer approach because the API is not exposed to laser radiation. In this approach, a non-drug loaded excipient-based delivery system is printed and the API is loaded using coating procedures or infilling techniques. SLS

was used for the dual printing of miniprintlets with two rate-controlling systems incorporating two model drugs, paracetamol and ibuprofen, whereby one drug was released immediately from a kollicoat instant release matrix, whilst the release of the second drug was sustained over an extended period using ethyl cellulose (Awad *et al.,* 2019). Great potential exists in the use of SLS in oral dosage forms, particularly multi-drug permutations with distinct and uniform dosing, permitting discrete separation of the APIs and resolving problems of incompatibility and physical interaction, which are major drawbacks in most multi-drug formulations. Table 2.1 provides examples for each of the afore-explained techniques.

Table 2.1: Summary of 3D Printed multi-drug oral dosage forms.

Drug Combination	**3DP Technique applied**	**Shape and design.**	**Reference**
Nifedipine, Captopril and Glipizide.	Extrusion at room temperature.	Cylinder. Compartmentalised: Top compartment, Nifedipine and Glipizide, release by diffusion. The bottom compartment, Captopril, release by osmosis.	(Khaled *et al.,* 2015b)
Efavirenz, Tenofovir Disoproxil fumarate and Emtricitabine.	Extrusion at room temperature.	Prism Separate layers of Efavirenz, Tenofovir and Emtricitabine.	(Siyawamwaya *et al.,* 2019b)
Paracetamol, Caffeine, Naproxen, Chloramphenicol, Prednisolone and Aspirin.	SLA	Cylinder and ring shape 6 distinct layers of each drug, with different release profiles.	(Robles-martinez *et al.,* 2019)
Lisinopril dihydrate, Indapamide, Rosuvastatin calcium and Amlodipine besylate.	Fused deposition modelling (FDM)	Cylindrical. Layered design, each layer constituting a different drug.	(Pereira *et al.,* 2019)
Aspirin, Hydrochlorothiazide Pravastatin, Atenolol, and Ramipril.	Extrusion-based printing.	Cylindrical. Aspirin and Hydrochlorothiazide immediate release compartment and Atenolol, Pravastatin, and Ramipril sustained release compartments.	(Khaled *et al.,* 2015a)
Metformin and Glimepiride	HME-based Fused Deposition Modelling.	Bilayer oral solid dosage form combining metformin for prolonged and glimepiride for immediate drug delivery.	(Gioumouxouzis *et al.,* 2018)

Levodopa (LD) Benserazide (BZ) and Pramipexole (PDM).	HME-based Fused Deposition Modelling.	Cylindrical. PDM and polyvinyl alcohol for rapid drug release and a fixed combination of LD/BZ (4:1) in an ethylene-vinyl acetate copolymer matrix for prolonged drug release.	(Windolf *et al.,* 2022)
Isoniazid and Rifampicin	HME-based Fused Deposition Modelling	Compartmentalised shells. Each compartment physically sealed for effective retardation of in vitro API release	(Genina *et al.,* 2017)
Paracetamol and Ibuprofen.	SLS	Spherical Miniprintlets. Two distinct regions; Immediate release and Sustained release.	(Awad *et al.,* 2019)
Irbesartan, atenolol, hydrochlorothiazide and amlodipine	SLA	Cylindrical, 2 types of layered designs, Type 1 Irbesartan and Atenolol on the outer layers and, hydrochlorothiazide and amlodipine in the inner layers. Type 2 Amplodipine and hydrochlorothiazide on the outer layers and irbesartan and atenolol in the inner layers.	(Xu *et al.,* 2020)

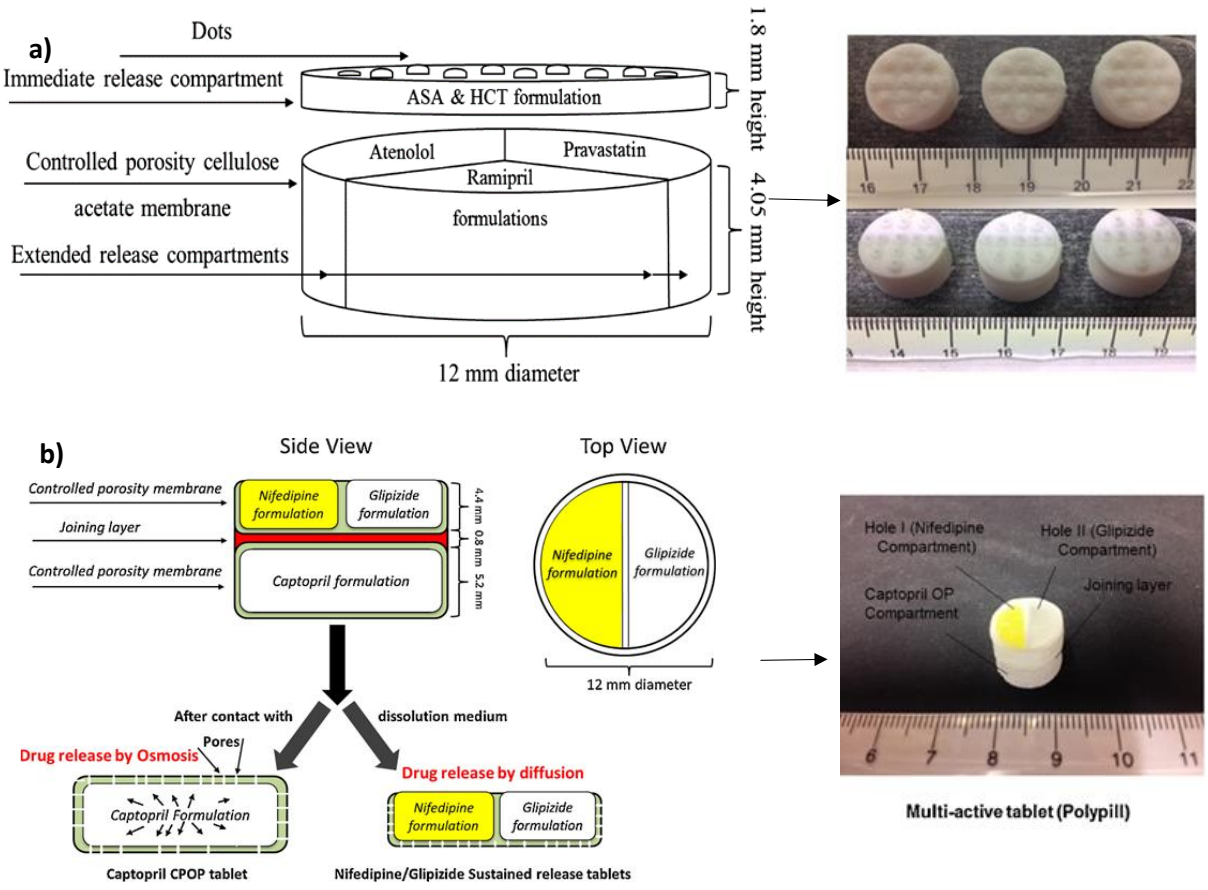

Figure 2.4: Selected images of 3D printed multi-drug system configurations. Reproduced with permission from a) (Khaled *et al.,* 2015c) 2015 Elsevier; b) (Khaled *et al.,* 2015a) © 2015 Elsevier.

2.4.2 3D Printed Multi-Drug Eluting Implants

The term “drug-eluting implants” refers to drug delivery systems and devices that consist of drugs released in surrounding tissue areas after implantation or insertion as a means of achieving targeted therapy (Domsta and Seidlitz, 2021). There are various forms of implants depending on the area of application. Types such as catheters and screws were considered in this study. The most prevalent application of multidrug implants is in bone-related conditions (Gbureck *et al.,* 2007; Wu, Zheng, Guo and Huang, 2009; Wu, Zheng, Guo and Sun, 2009; Vorndran *et al.,* 2010; Inzana *et al.,* 2015; Li *et al.,* 2015; Zhu *et al.,* 2015; Wu *et al.,* 2016; Trombetta *et al.,* 2019; Chou *et al.,* 2021). Unlike in oral systems, the commonly employed printing technique for implants is binder ink jetting, the advantages of which (over the other techniques) include low costs, fast production, multi-material printing, no need for supporting structures, low-temperature processing and high porosity products (Domsta and Seidlitz, 2021).

Drug loading in 3D printed implants is done either pre-, during or post-printing. Incorporation of the drug pre-printing is normally applied in FDM/HME, whereby API and polymer filaments are made in an extruder. Binder inkjet printing enables the incorporation of drugs into the implant during the printing process as they can be added to the binder solution (Wu, Zheng, Guo and Huang, 2009; Inzana *et al.,* 2015; Wu *et al.,* 2016; Trombetta *et al.,* 2019). The drugs that are incorporated into the implant matrix before or during the printing process have to withstand all conditions of the preparations and the actual printing process. Consequently, some sensitive drugs are excluded from those mechanisms due to their degradation properties. Post-printing loading on or into the 3D printed implant can either be done by, coating (Boyer, Ballard, *et al.,* 2018; Boyer, Woerner, *et al.,* 2018; Poudel *et al.,* 2020), immersion into the drug solution under a vacuum to aid absorption, incubation with sublimated iodine (Boyer, Woerner, *et al.,* 2018), use of supercritical carbon dioxide (Ngo *et al.,* 2020) or manual filling of the processed drug into the 3D printed hollow or reservoir device (Arany *et al.,* 2020; Stewart, Domínguez-Robles, McIlorum, Gonzalez, *et al.,* 2020; Stewart, Domínguez-Robles, McIlorum, Mancuso, *et al.,* 2020). These mechanisms can be quite cumbersome and are limited to porous implants. Table 2.2 provides a summary of developed 3D printed multi-drug implants.

Table 2.2: 3D Printed multi-drug implants.

Implant type	Drugs loaded	3DP Technique	Design and Objective	Reference
Stents and Catheters.	Gentamicin Sulphate, Methotrexate	HME/FDM	Disc, bead, catheter. 3D printing of different constructs with antibiotic or chemotherapeutic-eluting filament.	(Weisman *et al.,* 2019)
Bone treatment screws	Vancomycin Hydrochloride, Ofloxacin, Tetracycline Hydrochloride	Binder Ink jetting	Cylinder Drug adsorption and desorption of low-temperature 3D printed ceramic scaffolds.	(Gbureck *et al.,* 2007)
	Levofloxacin, Rifampicin Isoniazid,	Binder Ink jetting	Multi-layered cylinder. For the bi-modal release profile.	(Wu, Zheng, Guo and Huang, 2009)
	Isoniazid Rifampicin	Binder Ink Jetting	Programmed sequentially release of multidrug implant.	(Wu, Zheng, Guo and Sun, 2009)
	Levofloxacin, Tobramycin	Binder Ink Jetting	For bone tuberculosis treatment for treatment of chronic osteomyelitis.	(Wu *et al.,* 2016)
	Vancomycin, Heparin, rhBMP-2	Binder Ink Jetting	Scaffold Bio-ceramic implants with high accuracy of drug deposition to modify the release.	(Vorndran *et al.,* 2010)
	Isoniazid, Rifampicin	Extrusion	Scaffold. 3D printed scaffolds with antitubercular drugs in animal model	(Li *et al.,* 2015; Zhu *et al.,* 2015)
	Rifampicin, Vancomycin	Binder Ink Jetting	Scaffold. Simultaneous local delivery of Rifampicin and Vancomycin from 3D printed ceramic scaffolds for bone infection treatment examined in a mouse model.	(Inzana *et al.,* 2015)
	Rifampicin, Sitafloxacin	Binder Ink Jetting	Scaffold. 3D printing of antibacterial scaffolds for osteomyelitis treatment.	(Trombetta *et al.,* 2019)
	Vancomycin, Ceftazidime	Extrusion	Screw. Influence of Printing parameter on drug-eluting screws 3D printed by a solution-technique	(Chou *et al.,* 2021)

2.5 Additive Materials Used in 3D Printing of Multi-Drug Systems

One of the major constraints preventing mass adoption of 3D printing for biomedical manufacturing is a lack of 3D printing biomaterials that is, polymers, biomaterials, hydrogels, and bioinks that are functional for 3D printing, biocompatible, and perform well from a biomechanical standpoint (Pugliese *et al.,* 2021). Of the aforementioned 3D printing materials,

polymers are the most commonly employed biomaterial in multi-drug systems (Khaled *et al.,* 2015b, 2015a; Awad *et al.,* 2019; Robles-martinez *et al.,* 2019; Siyawamwaya *et al.,* 2019b). The ability to modulate the release of different actives in multi-drug systems forms the basis upon which polymers are selected in the 3D printing thereof. Other equally important characteristics include the materials' printability, ease of processability, cost, biocompatibility, and degradation rates. In fused deposition modelling (FDM) techniques polymers are processed into drug-loaded filaments prior to printing, SLS in the form of powder beads, solutions in SLA, and gels in direct ink writing (DIW). Polymers are incorporated as either binders, disintegrants, compression aids, diluents, or fillers for modulation of drug release. Because of their application versatility, polymers are employed in pharmaceutical 3D printing for a variety of purposes, such as controlling dosage shape, size, and drug release. More importantly, the majority of them are biocompatible, biodegradable, have manipulable mechanical properties, and degradation rates, and can be dissolved in rapidly evaporating organic solvents such as dichloromethane (Pugliese *et al.,* 2021).

The type of polymer or material employed in 3D printing depends on the technique being applied although some polymers may be used in more than one technique. Generally, in FDM/HME printing thermoplastic polymers such as polycarbonate, acrylonitrile butadiene styrene (ABS), polylactic acid (PLA) and nylon are used; SLS uses Poly ε-caprolactone (PCL) and polyamides, in inkjet printing any polymer that can be supplied as powder may be used (Jain *et al.,* 2018) whilst in SLA, liquid photosensitive polymers such as epoxy or an acrylate based resin e.g polyethylene glycol diacrylate and photoinitiators such as diphenyl (2,4,6-trimethylbenzoyl)-phosphine oxide (DPPO) are employed (Healy *et al.,* 2019). Numerous polymers of natural and synthetic origin have found applications in biomedical 3D printing. For instance, natural polymers like gelatine, collagen, alginate, and chitosan are usually utilized, but they frequently necessitate cross-linkers which could be cytotoxic, thus synthetic polymers have recently gained attention for 3D printing to avoid such manner of drawbacks (Gross *et al.,* 2014; Stansbury and Idacavage, 2016; Ligon *et al.,* 2017).

Cellulose-based polymers have long been used in the pharmaceutical industry to produce solid dosage forms, and they have shown great promise in 3D printing techniques. Of the two main cellulose derivatives, cellulose ethers comprise of the commonly employed methylcellulose, ethyl cellulose (EC), hydroxypropyl cellulose (HPC). The derivatives of which are formed by substitutions with methyl and hydroxypropyl groups yielding the likes of hydroxypropyl methylcellulose (HPMC), a widely studied polymer. Drug release from HPMC matrices is retarded using higher molecular weight and viscosity grades. As the degree of

substitutions increases, the solubility profiles shift from dilute alkali to water and finally to an organic-solvent-soluble stage (Raj *et al.,* 2021).

A promising approach in controlled release systems, is the quarternisation of polymers, that is, the addition of an amino group, for example, PQ-10 also known as quaternized hydroxyethylcellulose ethoxylate, a cationic cellulose derivative. The unique ability of these polyelectrolyte complexes (PEC) to self-assemble has sparked interest in 3D printing applications, including multidrug systems (Siyawamwaya *et al.,* 2017). In a recent study by Siyawamwaya and colleagues, a novel PEC of electrostatically bonded PQ-10 and humic acid was synthesised and used as bio-ink in 3D printing an antiretroviral multi-drug system for enhanced bioavailability, as shown in Figure 2.5.

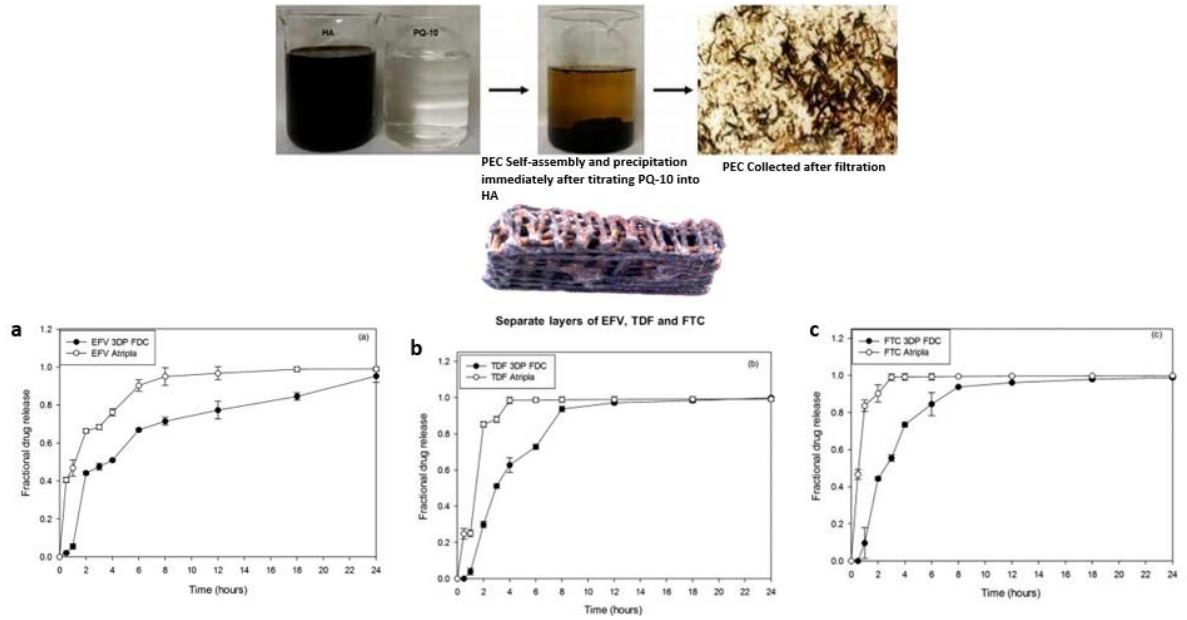

Figure 2.5: Picture of the self-assembly of HA and PQ-10 and the fibrous PECs collected by filtration before drying. SEM image of 3D printed FDC, alongside prolonged drug release profiles of a) Efavirenz (EFV), b) Tenofovir Disoproxil Fumarate (TDF) and c) Emtricitabine (FTC) in comparison to the commercial version, Atripla®. Reproduced with permission from (Siyawamwaya *et al.,* 2019a) 2019 Elsevier.

PCL and PLA are low-cost, biodegradable, non-toxic, hydrophobic polyesters, which can be used alone or in combination. PCL has a melting point of 55–60 °C, *Tg* of −54 °C, is soluble in organic solvents and is commonly used for long-term implant delivery devices due to its very low in vivo degradation and can be used in tablets and nanotubes (Langer, Basu and Domb, 2016). Several forms of PLA exist because of the chirality of the starting monomers, i.e., lactic acid (L) and lactide (D). These L or D configurations own various properties and

have the ability to form stereo-complexes between the L-PLA and D-PLA forms giving rise to; PDLA PLGA poly (lactic-co-glycolic acid), PLLA (poly-l-lactic acid) and PDLLA (poly-d,l-lactic acid) (Ligon *et al.,* 2017; Azad *et al.,* 2020). The latter two possess favourable thermal and mechanical properties, a T*g* range of 55–65 °C and mechanical strength of 1.9 to 4.8 GPa. Therefore, PCL is often blended with the chiral forms of PLA to achieve better erosion properties (Jain *et al.,* 2018).

Eudragit® represents a set of synthetic polymethacrylate, non-biodegradable, non-absorbable, nontoxic and amorphous polymers. According to Evonik, all Eudragit polymers have thermoplastic properties, low glass transition temperatures (between 9 °C and > 150 °C), high thermostability, and high miscibility with APIs and other excipients (Evonik, 2018). Varying the functional group on the polymer dictates the type of drug release it is best suited for. For example, the Eudragit E series, soluble at low pH is used in immediate-release formulations, L and S series show delayed release in drug formulations. Eudragit® RL and Eudgrait® RS are insoluble with pH-independent swelling, Eudragit® RL has high permeability while Eudragit® RS has low permeability. Thus, combining the series together enables pharmaceuticals with customized time-controlled release profiles. As a water-insoluble thermoplastic polymer, EC is often used for its sustained release capabilities in FDM 3D printing (Thakral, Thakral and Majumdar, 2013; Okwuosa *et al.,* 2017).

Other immediate release polymers include HPMC E5 and PVA a biocompatible, hydrophilic thermoplastic polymer, exhibiting a T*g* of 85 °C, a melting point range of 180 to 228 °C. PVA is suitable for immediate-release tablets as it dissolves more readily in hydrochloric acid (Azad *et al.,* 2020). Khaled in the construction of a multidrug compartmentalised system, employed croscarmellose sodium (CCS), sodium starch glycolate (SSG) (disintegrants), polyvinylpyrrolidone (PVP K30) (a binder) and D-mannitol (a filler), in making the joining layer of the two compartments. It was designed to disintegrate quickly within the 1st hour of the dissolution test and allow the tablet to split into two parts with different drug release mechanisms (Khaled *et al.,* 2015b). PVA may also be used in making individualised gastro-resistant tablets, by creating a drug-loaded PVA core with an enteric shell. Another study also suggests that the total drug release can be achieved within 3 minutes by reducing the infill rate of PVP tablets to 50 %, which in turn increases the porosity of tablets (Okwuosa *et al.,* 2017; Kempin *et al.,* 2018). For the manufacturing of implants, biocompatible and biodegradable polymers such as PLA, poly(lactic-co-glycolic acid) (PLGA) or polycaprolactone (PCL) are commonly used, others include cellulose derivatives, PVA, Eudragit, ethylene vinyl acetate (EVA), polyethylene oxide (PEO) and thermoplastic polyurethane (TPU) (Shaqour *et*

al., 2020). Wu et al (Wu *et al.,* 2016), employed one of the chiral forms of PLA, PDLLA (Mw = 100 kDa) in the fabrication of a 3D printed multi-drug implant for chronic osteomyelitis.

2.5.1 Other High Functionality Polymers

The advent of 3D printed biomedicals has stimulated the development of a whole range of high-performance polymers such as polyether ether ketone (PEEK), polyether ketone (PEKK), Polyetherimide (ULTEM) and engineering ceramics like alumina, zirconia and silica. The unique properties of these polymers, that is resistance to extreme heat, incredible hardness, biocompatibility, and rubber-like qualities, set them apart. PEEK is the most popular of the aforementioned materials. Its popularity is attributed to a variety of favourable properties, including heat resistance of up to 260 °C, water resistance, lightweight compared to metals, and, most importantly, biocompatibility. All current PEEK materials for 3D printing are obtainable as filaments and can be 3D printed using FDM machines (Beamler, 2019). Kang *et al.,* successfully employed FDM in the development of PEEK implants for bone mandibular defects, producing a novel mandibular reconstruction model with high stability, proven by deformation results (Kang *et al.,* 2021). However, PEEK, like other high-functionality polymers, has its limitations, including poor integration with surrounding bone tissue post-implantation. Therefore, to improve PEEK bioactivity, numerous strategies for functionalizing the PEEK surface and changing the PEEK structure have been proposed (Gu *et al.,* 2021). Composites such as graphene and nanomaterials, and even 4D materials also fall under the category of high-performance polymers.

2.6 Limitations and Barriers to Implementation

Many specialists around the world share the ambition for 3D printing, with new research papers being published more frequently than not to highlight the technology's potential in formulation development and patient care. Regardless of the hype, countries are certainly encountering difficulties in introducing and implementing this technology within the pharmaceutical sectors. Aprecia Pharmaceuticals' Spritam® (Levetiracetam), the first and only commercialised 3D printed pharmaceutical to this date confirms this. Large biopharmaceutical firms have shown little interest in this field (Wright, 2005).

2.6.1 Regulatory Constraints

Despite the FDA's (United States of America) efforts as forerunners in implementing 3D printing, as evidenced by the Guide provided in 2017 (Reddy *et al.,* 2020), there are still some grey areas in terms of regulatory requirements, making it a big hurdle for manufacturers worldwide (Bhusnure *et al.,* 2016). Biomedical systems, unlike other 3D printed products,

require special attention when it comes to rules and constraints. Compared to the conventional ways of developing oral dosage forms, 3D printing processes are distinct and still novel in many pharmaceutical manufacturing sectors. As a result, quality control testing on items such as tablets needs to be revised. Promisingly, in March 2021, the Medicines and Healthcare Products Regulatory Agency (MHRA) proposed a new regulatory framework towards the development of point-of-care manufacturing and supply, including 3D printing technologies for customised medicine production (Abdul and Trenfield, 2022).

2.6.2 Processing Parameters

2.6.2.1 Material Attributes and Selection

The type of binders used varies depending on the product being created. Biocompatible binders must be considered in order to develop biomedical products, and knowledge about these binders is still restricted. The materials employed must be of good quality and safe for use in the body of the patient; the only materials that are compatible are those that are organically based, which are unfortunately presently scarce (Shahrubudin *et al.,* 2020). 3D printed dosage forms possess low mechanical properties, which may be favourable in the case of oral dosage forms designed for immediate release. Nonetheless, the printed product should have acceptable tensile, compressional strength and flexible rigidity where applicable. The optimum bone tissue scaffold, for example, has macro-pores of 300–900 μm and porosity of 60–95 % in load-bearing bone tissue regeneration. Fortunately, with Selective Laser Melting (SLM) 3D printing technique, porous titanium implants with great osteo-integration in vivo performance with pore size 400–1000 μm can be fabricated (Shahrubudin *et al.,* 2020).

2.6.2.2 Printer Accuracy

Low dimensional accuracy may seem counterintuitive when discussing 3D printing, yet depending on the object being developed, such as implants and body parts, high levels of accuracy may be important. When employing randomly selected equipment and materials, producing 3D printed biomedical items with the exact size and structure is difficult. Low dimensional accuracy products will not fit in the body, lowering clinical success rates. The difficulty is to overcome product shrinkage throughout the curing and cooling process.

2.6.2.3 Return on Investment (ROI)

Additionally, respondents in a survey done in Malaysia highlighted four hurdles to the implementation of 3D printing with regard to management: re-education of workers, high-priced products, a lack of guidelines, and cyber-security issues. Because the technology is still a relatively new notion in many circles, basic operational knowledge may be insufficient.

Employees will need to enhance their education and skill levels for organizations to implement 3D printing, as well as obtain experience in various physicochemical and biological features of active pharmaceutical ingredients (APIs) (Shahrubudin *et al.,* 2020).

One of the most significant costs associated with adopting 3D printing technology in the manufacturing industry is the cost of purchasing a 3D printing machine. A 3D printer is relatively expensive with costs being determined by its capabilities; a lower cost indicates lesser print quality and materials, (Shahrubudin *et al.,* 2020). These costs and other high start-up costs have indeed limited the implementation of 3D printed systems in many companies, especially in cases where the return is not certain. Finally, yet importantly, fear and lack of acceptance are significant hurdles to the future use of 3D printed biomedicines, as with any other cutting-edge technology breakthrough, particularly in the medical profession. Given the constraints and limits connected with the products' creation, this is understandable to some extent (Safi, Thiessen and Schmailzl, 2018).

2.7 Cost Implications and Projected Market Views

Nonadherence to chronic medications was estimated to cost the United States $100 billion to $289 billion per year, similar trends were observed in the European Union, with nonadherence costs of up to €1.25 billion per year. Several assessment studies have been done on the cost-effectiveness of a combination medication for cardiovascular conditions (Gaziano, Opie and Weinstein, 2006; van Gils *et al.,* 2011; López-Jaramillo *et al.,* 2018) and in all studies, incremental cost-effectiveness was demonstrated. For example, in the United Kingdom, it was projected that implementing fixed-dose therapy for primary prophylaxis in elderly patients could result in a net gain of £2,000 per year of life, plus the prevention of a first myocardial infarction or stroke (Hilson and Nhonoli, 1991). And, as fewer people are hospitalised for cardiovascular-related complications, costs are also reduced.

3D printing polypills will almost certainly result in even lower overall costs. The cost implications of 3D printing pharmaceutical products have a significant potential for lower production costs, but this is not true in all production arenas. On a large scale, conventional methods of mass production of non-customized pharmaceuticals are more affordable than 3D printing. In small-scale settings, where products are made on demand for a patient's unique needs, cost savings can be seen (Banks, 2013; Choonara *et al.,* 2016). As a result, using 3D printing to create customized multi-drug systems would be a cost-effective solution for both patients and small-scale pharmaceutical companies (Ventola, 2014).

Reduction in manufacturing costs can be attributed to the elimination of excessive additives, normally employed in traditional methods of manufacturing. A decrease in the number of additives will also result in a decreased final product weight. When compared to traditional methods, the time it takes to create a 3D printed medicinal product is significantly shorter, as additional processing steps such as granulation, milling, and drying may not be necessary (Ventola, 2014). Similarly, traditional methods of implant fabrication have been shown to take longer than 3D printing. More cubic centimetres can be built in an hour with 3D printing, while still producing a high-quality product (Banks, 2013). Thus, with increased productivity, the cost of the final product is also reduced.

Despite the fact that 3D printing accounts for less than 1% of the global manufacturing market, it is poised to become an indispensable tool for production workflows (Cost and Impact, 2021). Stratasys, Materialise NV, and ETEC are currently some of the major players in the 3D printing of healthcare products. North America; Europe and Asia-Pacific account for about 45 %, 40 % percent of market shares. Devices make up the largest chunk of 3D printed products, and implants take the lead in terms of application, followed by external wearables (Gibbs, 2020). The Healthcare products 3D printing market is currently valued at US$261.3 million, with a forecasted market value of US$1,121.6 million for Latin America, the Middle East, and Africa by 2031. During the forecast period 2021-2031, the market in the rest of Latin America, the Middle East, and Africa is expected to grow at a Compound Annual Growth Rate (CAGR) of 15.7 %. The market is expected to grow at a CAGR of 14.9 % of the projected timeframe 2021-2026, and 16.4 % in the second half of the projected period 2026-2031 (Cost and Impact, 2021).

2.8 Conclusion

With the Fourth Industrial Revolution (4IR), the need to simplify processes in different facets of life has never been greater and the medical field is slowly adapting to this technological era. The health and wellbeing of patients is a priority for health professionals thus all efforts put into improving drug delivery are done in the interest of the patients. This review has reiterated the numerous advantages of employing 3D printing for pharmaceutical products namely, customization and personalization, particularly in multi-drug systems, reduction in pill burden, improved adherence patterns, cost-effectiveness, increased productivity, democratization of design and manufacturing, and improved interprofessional collaboration (Ventola, 2014).

The techniques applied to 3D printing of multi-drug systems each carry their own unique set of advantages, FDM/HME techniques are the go-to for both oral dosage forms and implants,

with processing advantages such as multi-material printing, safe operating environments, low cost and wider choice of polymers such as HPMC, PLA, PCL and ABS. Nonetheless, there is a general lack of additive materials functional for 3D printing that is, polymers, biomaterials, hydrogels, and bioinks, that tick all the boxes in terms of biocompatibility, biodegradable profile, toxicity and performance from a biomechanical standpoint.

3D printing has been presented as a faultless intervention, capable of producing a solid object at the push of a button; this is clearly not the case. Limitations and challenges in the areas of processing and management and more importantly regulatory constraints have been identified as significant obstacles to its full adoption. Not neglecting the issue of acceptance, the general populace has always displayed some reluctance in embracing techno-medical advances, as seen with the COVID-19 mRNA vaccines (Id *et al.,* 2021). Thus, educational programs especially for patients in need of customised medication and introducing the subject in pharmacy curricula to equip future healthcare professionals is of paramount importance. As highlighted in the present review, the advancement of this branch of pharmacology will improve the treatment of both rare and common diseases including, cardiovascular conditions, tuberculosis, HIV and bone-related cases (Dvoretskaya, 2020). Furthermore, the use of various 3D printing techniques in the treatment of a variety of other chronic diseases such as Alzheimer's disease, arthritis, asthma, cancer, epilepsy, and stroke has been investigated. Their utility however in chronic disease management is still in its early stages, and more concrete studies and evidence are needed (Varghese *et al.,* 2022).

The UK government recently published the 'UK Genome Strategy 2020' and the 'Life Sciences Vision 2021,' both of which prioritize personalised medicine within healthcare. With start-up companies like FabRX pushing the agenda even further, coming up with the world's first breakthrough pharmaceutical 3D printer for personalised medicines, the M3DIMAKER™, consisting of a sleek hardware system that enables printing using different nozzles, suitable for multi-drug systems (*FabRx*, 2022; Abdul and Trenfield, 2022) . Unfortunately, studies on 3D printing technology have centred on developments in Europe and the USA, with limited developments in developing countries. Therefore, pharmaceutical researchers and pharmacists are encouraged to share knowledge and communicate recent advances in research and practices through social media guided by professionalism and ethics (Algahtani, 2021). Financially, 3D printing multi-drug systems are a cost-effective alternative. Small-scale on-demand production, reduction in excipients, and increased productivity due to a reduction in the time required to create a 3D printed medicinal product. In conclusion, the evolution of drug delivery systems is driven by a need to better the overall patient experience and outcome.

On-demand fabrication of controlled release multi-active systems, of different geometries for once-off administration, is not only a lucrative business idea but also one that will offer convenience, better adherence, and ultimately improved chronic patient outcomes.

2.9 Expert Opinion

A search for the term 3D printing on Pubmed.gov (National Library of Medicine) currently yields over 16 000 results, indicating a major increase from 3700 in 2020 ('National Library of Medicine', 2022). While trying to predict a complete shift may be difficult, the implementation of 3D printed systems is at this point ineluctable. Studies have clearly demonstrated the benefits; what remains is making them a reality. Raising awareness, not only among the public but also among pharmacy professionals, is a good place to start. A survey on 156 hospital pharmacists in Saudi Arabia was recently conducted to assess their knowledge and perceptions of 3D printing in the pharmaceutical sector. The findings revealed that while approximately 53 % of pharmacists were aware of 3D printing technology in general, only 14–16 % of pharmacists were aware of the specific application of 3D printing in drug dispensing. Participants had an optimistic response to the concept of personalized medicine and believed that 3D printing could provide a promising solution for both formulating and dispensing personalized medicine in pharmacies. A promising 67% demonstrated interest and willingness to learn (Algahtani, 2021).

Having printers in large manufacturing plants may not be a good starting point; instead, point-of-care (PoC) 3D printing centres, that is, hospitals, clinics, and pharmacies wherein healthcare professionals customize and develop a 3D printed medical device on demand. Unfortunately, the idea of having multiple local printing sites, comes with its own set of challenges one being the difficulty in monitoring the quality of all printed products as well as other regulatory ambiguities. Nonetheless, reviewers anticipate that the FDA will soon adopt new regulations that directly address PoC 3D printing, owing to its rapid adoption in healthcare organizations (Trenfield *et al.,* 2018). As humankind progresses, software engineers can develop applications that will enable smoother workflow amongst health care professionals and patients. However, upscaling techniques and the incorporation of PAT for in-process non-destructive quality control tests can help facilitate large-scale commercial printing of systems such as polypills (Beitler *et al.,* 2022).

The majority of 3D printed biomedical have been tested in in vitro models and animal models (Siyawamwaya *et al.,* 2019a). A collective presentation of results obtained from studies involving human subjects will instil more confidence in these productions and accelerate the

implementation thereof. Selected researchers such as Goyanes *et al.,* (2015), have demonstrated the effectiveness of 3D printed systems in human subjects and information on clinical trials completed and underway may be obtained from clinicaltrials.gov. With growing interest in innovative drug delivery, it is clear that 3D printing is not the end of it, as evidenced by the emerging realm of the novel 4D printing. The development of drug delivery systems capable of releasing drugs at the optimal time and anatomical location is an integral part of the drug development industry. 3D printing can achieve drug delivery control, precision in drug dosages, and on-demand structure production. 4D printing enables even more precise control over the spatial distribution of various systems that can self-fold or self-unfold to encapsulate and release drugs or in a programmable manner (‘du Toit *et al.,* 2020). These systems fold and unfold in response to a variety of stimuli, which may include changes in osmolarity, temperature, humidity, light, or electric and magnetic stimuli. 4D printing is therefore a time-dependent and printer-independent innovation, with dynamic advantages over 3D printing; nevertheless, the majority of materials used in 4D printing are currently not bio-medically appropriate, thus as in 3D printing more research is needed (Lukin *et al.,* 2019).

Underlying all aspects stipulated in this review is the point that, 3D printing of medicals, and more germane to this study, multi-active systems, is not only beneficial but also essential. Undeniably, large pharmaceutical companies may not be alacritous to manufacturing a customised product for a limited consumer target, hence the more feasible and economical idea of having the printers incorporated in pharmacy and hospital settings.

CHAPTER 3

PRE-FORMULATION INVESTIGATIONS AND LIQUID CHROMATOGRAPHIC METHOD DEVELOPMENT AND VALIDATION FOR THE SIMULTANEOUS QUANTITATION OF THE ACTIVE INGREDIENTS

3.1 Introduction

Following API selection, the choice of suitable additives compatible with the APIs is crucial in building quality into a pharmaceutical drug product. Amongst other functions, these additives must enable drug administration, provide the intended drug release, and increase the formulation's stability and bioavailability. Therefore, physicochemical pre-formulation studies on formulation components can provide justification for the selection and non-selection of certain inactive ingredients (Chadha and Bhandari, 2014; Gorain *et al.,* 2018).

Various analytical techniques may be applied in detecting both physical and chemical drug-drug and or drug-excipient interactions, as well as affirming default characteristics of the APIs for purity and identity confirmation. These techniques include thermal analysis via differential scanning calorimetry (DSC) and thermogravimetric analysis (TGA) testing, spectroscopic techniques, as well as chromatography. Through DSC analysis the glass transition temperatures (*T*g) and melting points may be determined (Chadha and Bhandari, 2014). Polymers exhibit either glassy or rubbery characteristics at body temperature thus determining the rate of bioerosion. However, scholars have concluded that the data produced by thermal approaches is not only difficult to interpret, but that the interactions identified during DSC experiments at high temperatures may not be indicative of those observed under normal storage circumstances (Segall, 2019). TGA provides further details on the thermal behaviour of the analytes i.e., the rate of change in weight as a function of temperature.

Vibrational spectroscopy by means of Fourier Transform Infrared Spectroscopy (FTIR) analysis is sensitive to the chemical structure of the compound, as shown in Figure 3.1, where each bond vibration is measured as an analysing parameter (ChemSpider, 2021). Thus, a change in vibration can aid in determining the solid-state characterisation behaviour of drug-excipient combinations and hence potentially establish intermolecular interactions (Gorain *et al.,* 2018). Therefore, any pharmaceutical interaction type, including dehydration or hydrate formation, desalting, morphological changes, or inter-change between amorphous and crystalline can easily be identified by this technique, through decreases in peak intensity, emergence of additional peaks or disappearance thereof (Liltorp *et al.,* 2011).

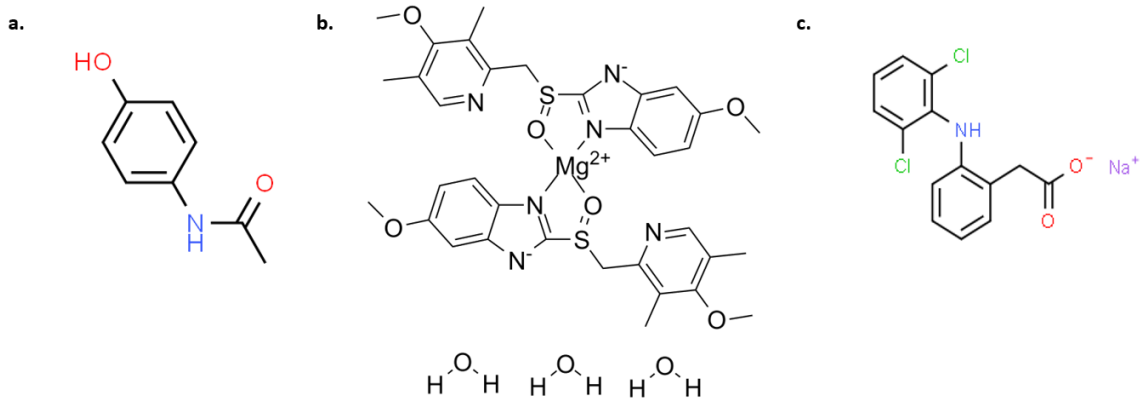

Figure 3.1: Chemical structures of a. PAR, b. ESM c. DS. Adapted from (Chemspider, 2021).

Key to the pre-formulation stage is the development and establishment of a reproducible reliable assay method for the quantitation of the actives in the resultant formulation. The ratio in which actives are combined in fixed-dose combinations can at times present challenges in assay method development, demonstrated and tackled by Youssef and others who developed different and effective methods for the estimation of Paracetamol, Pseudoephedrine and Brompheniramine in the dosage ratio of 250:15:1 (Youssef *et al.,* 2019). Because the compounds are well-researched, several methods for their determination individually and in combination with other drugs have been developed and validated. This includes thin layer chromatography (TLC), high-performance liquid chromatography (HPLC), and Ultra-Violet (UV) spectrophotometry and ultra-performance liquid chromatography (UPLC) (Jain *et al.,* 2011; Sharma *et al.,* 2011; Samlayawala and Koradia, 2014; Farid and Abdelaleem, 2016; Khan *et al.,* 2016; Rahman, 2019; Sharma and Medical, 2018). Nonetheless, after a thorough literature survey and owing to the fact the proposed combination is new, there is presently no method for the separation and quantification of PAR, DS and ESM in a combined dosage form. The aim of this chapter is to present all pre-formulation investigations undertaken on APIs and potential formulation components, including the development and validation of an HPLC method for the simultaneous quantitation of the APIs.

3.2 Materials and methods

3.2.1 Materials

Reference standards of paracetamol (PAR), diclofenac sodium (DS), and esomeprazole magnesium trihydrate (ESM) were sourced from Sigma-Aldrich (St. Louis, Missouri, USA).

ESM bulk was purchased from DLD Scientific, South Africa. Different polymer blends for potential use in the formulation including hydroxypropyl methylcellulose (HPMC) K15M, Croscarmellose Sodium (CCS), Sodium Carboxy Methyl Cellulose (NaCMC), Polyvinylpyrrolidone (PVP), Starch, HPMC E50LV, Eudagrit® L 100-55 (EL 100-55) were all sourced from Sigma-Aldrich (St. Louis, Missouri, USA). Analytical reagents used included pharmaceutical-grade purified water, Acetonitrile (HPLC grade) (Honeywell Burdick and Jackson, Muskegon, MI, USA), Orthophosphoric acid 85%(w/w) (HPLC grade) (Fluka, St. Louis, Missouri, USA).

3.2.2 Fourier Transform Infrared Spectroscopic Analysis

FTIR spectroscopy was done on the Perkin Elmer Spectrum100 Series, (Beaconfield,UK) to determine the molecular structures of the APIs and different polymer-API combinations. Samples were prepared in a ratio of 1:1, taking into account the composition of each potential layer. For better resolution, the number of scans was set at 20, and the wavenumber was maintained at 4000 to 650 cm^{-1}.

3.2.3 Differential Scanning Calorimetry Analysis

The Mettler-Toledo TC15, TA Controller System (Switzerland) with a DSC instrument (Mettler DSC 20, Mettler-Toledo AG, Switzerland) was used to obtain base thermograms for each API and subsequent API-Polymer combinations. An indium calibration was performed for the analyses and samples of 10 mg were transferred to aluminium pans, sealed, and punctured to remove excess pressure. The heating rate was set at 10 °C per minute and the temperature range was 30 – 300 °C. Samples of API and polymer combinations as per the layers of the DDS were made in the ratio 1:1 and milled using a mortar and pestle (Hobbs *et al.,* 2009).

3.2.4 Thermogravimetry Analysis

Thermogravimetry analysis (TGA) on the same samples was done on the PerkinElmer, TGA 4000 (Llantrisant, Wales, UK). The samples were heated from 30 to 900 °C with a 10 °C/min heating rate under the continuous flow of nitrogen. Thermograms generated were presented as percentage weight against temperature graphs.

3.2.5 HPLC Method Development and Validation

Principal to the development of an HPLC method for the estimation of an assay and quantitative determination of drug products, is the selection of the mode of chromatography. The selection of the modality relies on the nature of the sample that necessitates segregation. Generally, the employment of reverse-phase chromatography (wherein the mobile phase is polar, and the stationary phase is nonpolar) is the favoured approach for a majority of the substances. Substances possessing higher polarity will experience earlier elution, while those with lower polarity will elute at a later stage. However, in the case of isomer (enantiomers)

separation, normal-phase chromatography, characterized by a nonpolar mobile phase and a polar stationary phase, is utilized (Lakka and Kuppan, 2019). The superiority of the reverse-phase mode of chromatography stems from its extraordinary spectrum of applications encompassing various molecular sizes, polarities, and ionicities, exemplary resolution as well as its adaptability and the existence of relatively uncomplicated albeit semi-empirical techniques for method establishment (Poole, 2023).

3.2.5.1 Wavelength Selection

An overlain spectrum (Figure 3.2) was obtained from UV-VIS spectrophotometric analysis of the three drugs to estimate the wavelength at which all three drugs absorbed maximally. Based on the obtained spectrum the wavelength of choice would have been in the 230 nm to 235 nm range. Consequently, analysis at this wavelength range yielded exaggerated chromatograms of PAR, whilst peaks of the other two drugs were significantly diminished, this was largely influenced by the drugs' ratio i.e., 25:10:1 (PAR: DS: ESM) backed–up by the Beer-Lambert's Law. Therefore, this approach to wavelength selection (Samlayawala and Koradia, 2014) was disregarded, and a wavelength (300 nm) that would favour the absorbance of ESM whilst thwarting that of PAR was selected.

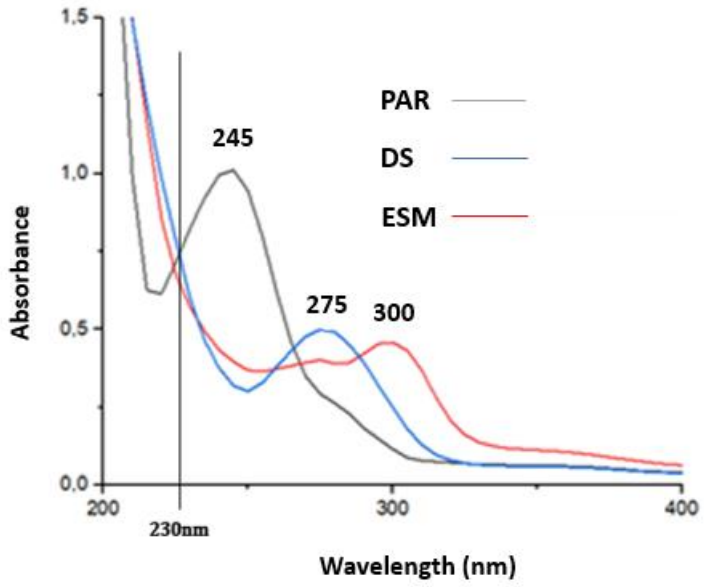

Figure 3.2: Overlain spectra of the three actives obtained by UV-Vis Spectrophotometric analysis.

3.2.5.2 Method Development and Optimization

Before validating the method, experimental analyses were conducted on the drugs in combination to achieve optimum separation. Trials were based on API monographs and validated methods for binary combinations, as referenced in the introduction. The retention times of each drug were noted as a function of altering mobile phase composition, ratios, pH, flow rate, and wavelength.

3.2.5.3 Method Validation

The method was validated using International Conference Harmonization (ICH) guidelines, with emphasis on linearity range, detection limit, quantitation limit, accuracy, precision (repeatability and intermediate precision), specificity, and robustness. Furthermore, stability studies were conducted on the standards (Guedes and Guedes, 2006).

3.2.5.3.1 Preparation of Standards

Stock solutions of concentrations 1500 µg/ml, 500 µg/ml, and 500 µg/ml for PAR, DS and ESM, respectively were prepared from pure samples of the APIs. Accurately weighed samples of each drug were dissolved in 50ml of the mobile phase which was selected as 50 mM phosphate buffer (Na_2HPO_4): ACN (70:30, v/v), at pH 7.0 adjusted using Orthophosphoric Acid 85 %. The solutions were thoroughly vortexed for 10 minutes to ensure complete dissolution. Given the final implementation of the technique, namely the analysis of drug release through dissolution, the target concentration for each drug was calculated and set as the maximum theoretical concentration to be measured following a complete dissolution run in 900 ml of dissolution media, expressed as µg of the total drug dose in a tablet per ml. Also taking into account that half the total dose of PAR would be released in the initial dissolution vessel prior to being transferred to the subsequent 900 ml vessel. Therefore, to determine the linearity ranges for each drug, the following working standards were prepared by serial dilution with the mobile phase; PAR (20, 50, 100, 150, 200, 500 µg/ml), DS (10, 20, 50, 100, 200, 250, 500 µg/ml), ESM (2, 5, 7.5, 10, 20, 50, 100 µg/ml), inclusive of and above the 25 – 200 % (of the target) concentration range (Guedes and Guedes, 2006). The stock solutions were filtered using 0.45 µm nylon syringe filters prior to preparing the diluted samples.

3.2.5.3.2 Linearity, LOD, and LOQ Determination

Linearity refers to the capacity of an analytical technique to yield a reaction that is commensurate with the concentration or quantity of the substance being analysed in the specimen. In the event that the methodology is linear, the outcome of the tests is directly proportional or can be ascertained with a well-established mathematical conversion in relation to the analyte concentration within a specified range (Yadav and Bharkatiya, 2017). Analysis was done in triplicate on the working standards prepared above. The limit of detection (LOD)

and limit of quantification (LOQ) were calculated using Equations 3.1 and 3.2 after determining standard deviation (SD) and standard error (SE) values from each set of regression statistics (Bliesner, 2006).

$$LOD = 3.3\sigma/S \qquad \textbf{Equation 3.1}$$

$$LOQ = 10\sigma/S \qquad \textbf{Equation 3.2}$$

Where;

σ is the SD of the data response, and

S is the slope of the calibration curve.

3.2.5.3.3 Method Precision Analysis

The expression denotes the proximity of concordance (extent of dispersion) amidst a succession of computations procured from manifold samplings of identical standards under the stipulated conditions. Precision is a gauge of the replicability of the comprehensive analytical method. It encompasses two elements: repeatability and intermediate precision and intermediate precision (Yadav and Bharkatiya, 2017). Thus, Inter-day precision i.e., between-day precision, and Intra-day precision (within-day) were determined by evaluating three replicates at three different concentrations for each API (Table 3.4) across three days of analysis (ICHQ2R1, 2014). The % RSD of the assay or recovery values should not be greater than 2.0 % (Bliesner, 2006).

3.2.5.3.4 Specificity Analysis

Specificity refers to the capability to unequivocally evaluate the analyte even when there are various components that are likely to be present. These components may encompass impurities, degradants, matrices, and so forth. In cases where an individual analytical procedure lacks specificity, this shortcoming can potentially be offset by other complementary analytical procedures (Yadav and Bharkatiya, 2017). The specificity of the developed method was assessed by injecting solutions i-iii (3 times) in order to demonstrate the absence of interference with the elution of the drugs, through chromatogram comparisons.

i. Blank (mobile phase)

ii. Placebo (excipients only)

iii. Sample (Tablet i.e., excipients and APIs)

3.2.5.3.5 Accuracy Analysis

Accuracy is described as the proximity of a measured value to the true or accepted value. It is ascertained by implementing the method to samples that have known quantities of the analyte added. These samples must be evaluated against standard and blank solutions to ensure the absence of any interference. The accuracy is then calculated from the test results as a percentage of the analyte that is retrieved by the assay (Yadav and Bharkatiya, 2017). Each individual sample recovery should lie within the range of 98 % to 102 %, The mean recovery acceptance criteria should be 100 ± 2 % for an assay of an active ingredient in a drug product, over a spiking range of 80 to 120% of the target concentration (Bliesner, 2006; Samlayawala and Koradia, 2014).

i) On standards

A select standard per drug was spiked at 3 different concentration levels i.e., 85 %, 90 % and 100 %, using calculated aliquots from respective stock solutions. Analysis of each set of the three spiked samples was done in triplicate (ICHQ2R1, 2014).

ii) Tablet

The method was tested on preliminary tablet formulations containing 1000 mg PAR, 100 mg, DS and, 20 mg ESM. One tablet was crushed and transferred into a 250 ml volumetric flask, solubilised using acetonitrile and further diluted to the mark using the phosphate buffer. The resultant solution was diluted to yield a theoretical concentration ratio within the LOD range per drug.

3.2.5.3.6 Robustness Analysis

In order to assess the capacity of the analytical method to remain unaffected by small variations in method parameters, deliberate changes in the flow rate (± 0.2 ml/min), temperature (± 5 ˚C) and mobile phase ratio (± 5 %) were made to the method. The parameter of merit considered was the % recovery, which principally should meet the 98 % to 102% acceptance criteria (Bliesner, 2006).

3.2.5.3.7 Stability Analysis

The stability of standards was established under normal benchtop conditions, over a period of 24 hours. ESM standards were left in the autosampler as protection from photolysis (Bliesner, 2006; Al-Salloum and Al-sabti, 2019). The stability of frozen (4 ˚C) and thawed standards was also assessed beyond 2 weeks. The acceptance criteria that the variation in results between the initial, fresh standards and the analytes should not differ by >2 % was set (Hobbs, 2009).

3.3 Results

3.3.1 FTIR Analysis

Secondary interactions including hydrogen bonding and hydrophobic interactions were probed via FTIR analysis of individual APIs, key polymers, and potential combinations, as shown in Figure 3.3. The observed infra-radiation spectrum obtained for ESM showed all the characteristic peaks of the drug corresponding with literature findings (Panti, 2021). These peaks include the C=O group at 1612 and 1570 cm^{-1}, the broad peak of the C=N group, the peak at 3417 cm^{-1} of the N–H group and the C=C group at 2949 cm^{-1}. As seen in Figure 3.3, these characteristic peaks were maintained in the ESM+MCC spectrum, and that of the core (inclusive of EL 100-55) appeared to be an overlap of the ESM+MCC spectra, confirming compatibility in usage (Kwon *et al.,* 2022).

Band characteristics of DS were observed in the DS spectrum at; 3388 cm^{-1} the N–H stretch vibration, the phenyl groups (C=C) at 1577 cm^{-1} and the substituted phenyl group stretch at 748 cm^{-1} (Shen *et al.,* 2011). Suspicions of hydrogen bonding between the listed characteristic peaks of DS and those of EL 100-55 i.e., the broadband O–H stretch in the range of 3400–2200 cm^{-1}, methyl and methylene bands at 2981 cm^{-1} and 2929 cm^{-1}, carbonyl groups at 1735 cm^{-1} and the two ester-linkage bands (C–O) at 1270 cm^{-1} and 1175 cm^{-1}. This interaction reflects good compatibility between the two, which may subsequently lead to full control in the release of DS from the cup formulation layer as a function of EL 100 -55. Prior investigations have ruled out interactions between PAR and the listed excipients, and the obtained spectra of the Immediate Release (IR) layer, DR cup and polymer combinations confirm these findings (Gorain *et al.,* 2018).

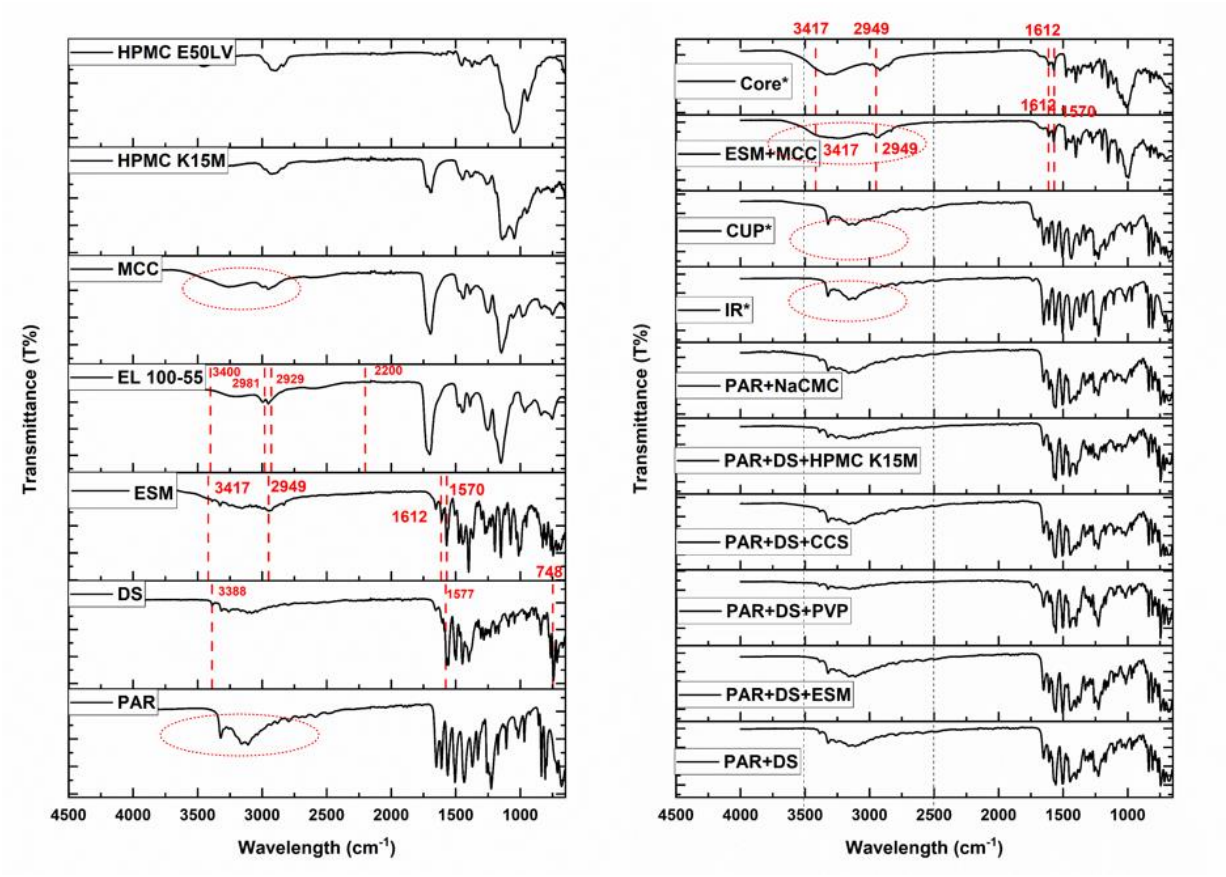

*Immediate Release (IR) (PAR, CCS, PVP), DR cup (PAR, DS, EL 100-55, HPMC K15M), Core (ESM, MCC, EL 100-55)

Figure 3.3: FTIR spectra of individual APIs (PAR, DS, ESM), key polymers (HPMC E50LV, HPMC K15M, MCC, EL 100-55), and potential API and polymer combinations as per formulation layers (left to right).

3.3.2 DSC and TGA Analysis

Onset, Peak, and Endset temperatures and Integral values for each obtained thermogram (Figure 3.4 a and b) were tabulated for concise comparison, (Table 3.1). Typical of a pure DS sample a single endothermic response corresponding to a melting point of 289.67 ˚C was observed (Shen *et al.,* 2011). A broad glass-transitional endotherm suggestive of an amorphous material was observed for EL 100-55 from 199.12 to 236.60 ˚C. The combination of the DR cup constituents resulted in a melting point lower than that of DS, EL 100-55 and PAR.

Thermal analysis of PAR showed an endothermal peak due to the fusion of the substance at 173.06 ˚C consistent with the literature data on the melting point of PAR (168–172 ˚C). No remarkable deviations or additional peaks were observed in the subsequent thermograms of samples containing PAR. Through TGA analysis (Figure 3.5) PAR was proven to be thermally stable, with complete thermal composition until about 173 ˚C, followed by another decomposition event occurring at about 360 ˚C with a 67% loss in weight (Jendrzejewska *et*

al., 2020). Both endothermic and exothermic peaks were observed in the thermogram of ESM, at 196 ˚C and 240 ˚C, respectively, higher than observations made by (Panti, 2021) and (Liu *et al.,* 2018) both of whom had different findings, indicating the variability in the thermal behaviour of ESM as a compound.

Table 3.1: Integral, Onset and Endset temperature values for the individual API, excipient, and combined samples.

	Integral	**Onset Temperature**	**Peak Temperature**	**Endset Temperature**
	(mJ±SD)	**(°C±SD)**		
PAR	-2037.79	169.31	173.06	178.44
DS	-4481.51	279.47	289.67	293.98
ESM	-2552.69	25.47	196.70	299.86
EL 100-55	-881.95	199.12	223.09	236.60
HPMC K15M	-2301.63	24.98	73.53	299.66
MCC	-892.42	10.96	84.12	127.99
PAR+DS	-981.60	155.40	159.04	164.78
PAR+DS+ESM	-2278.46	149.10	153.84	159.29
PAR+DS+CCS	-5850.48	153.02	159.17	167.94
PAR+DS+PVP	-2557.44	25.00	157.76	242.05
PAR+DS+HPMC	-3247.64	153.90	158.60	165.26
DR Formulation*	677.22	164.32	171.66	177.22
IR Formulation*	-1434.98	164.41	171.55	177.25
Core Formulation*	-597.13	153.58	153.72	157.35

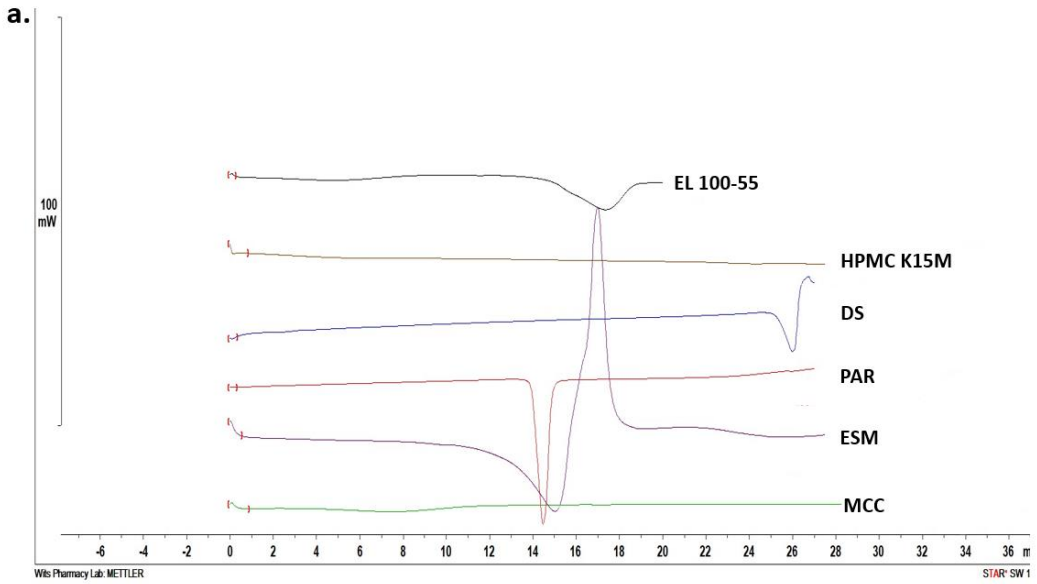

b.

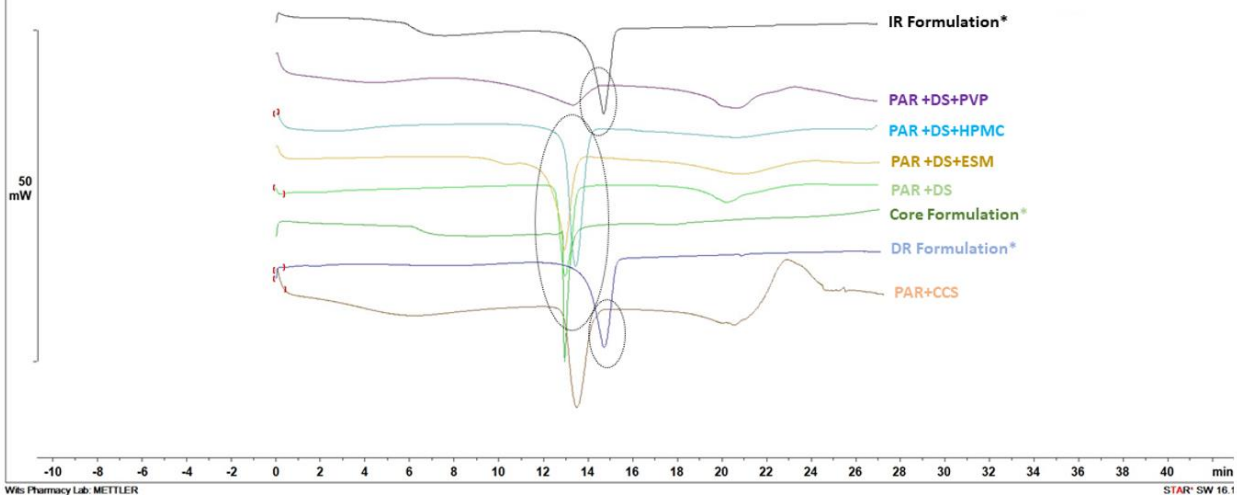

*Immediate Release (IR) (PAR, CCS, PVP), DR cup (PAR, DS, EL 100-55, HPMC K15M), Core (ESM, MCC, EL 100-55)

Figure 3.4: DSC thermograms of a. Individual APIs, key polymers, and b. potential combinations.

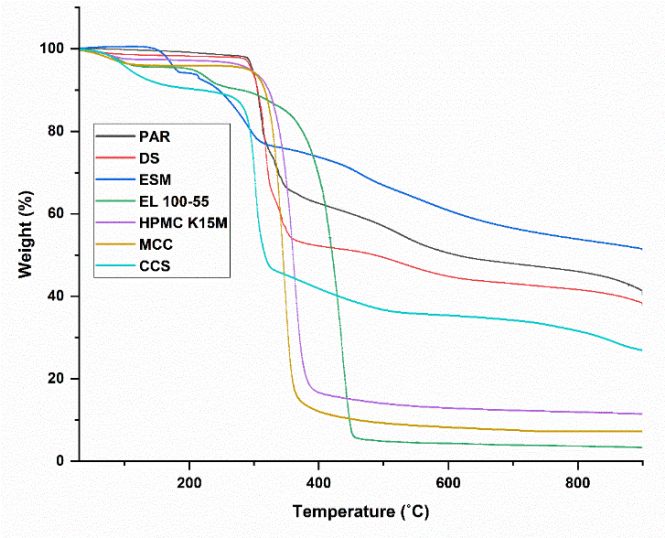

Figure 3.5: TGA curves of individual APIs and key polymers.

3.3.3 Method Development and Validation

3.3.3.1 Method Development

Mobile phase combinations of Water (65 %): Acetonitrile (30 %): Glacial Acetic Acid (5 %), and Methanol (70 %): Phosphate Buffer (Na_2HPO_4) pH 7.3 (30 %) yielded problems of either co-elution, poorly resolved peaks, or prolonged retention times. Benchtop acid degradation of ESM occurred rapidly in buffer systems with low pH. As a result, a neutral (pH 7) mobile phase of 70% 50 mM phosphate buffer (Na_2HPO_4) and 30 % acetonitrile was employed. The mobile phase was thoroughly filtered using 0.45 µm filter paper before each analysis. Table 3.2 outlines the final and optimised method employed.

Table 3.2: Summary of Reverse Phase RP-HPLC conditions applied.

Parameter	Criteria
Column	Phenomenex® - Luna® C18,150 mm x 4.6 mm and particle size 5 µm.
Mobile Phase	A: Acetonitrile (30%) B: Phosphate Buffer (Na_2HPO_4) (70%) (50 mM, pH 7)
Flow rate	1 ml/min
Detection wavelength	300 nm
Injection Volume	20 µl
Run time	10 minutes
Column Temperature	25 °C
Elution technique	Isocratic

3.3.3.2 Method Validation

3.3.3.2.1 Linearity, LOD, and LOQ

Table 3.3 displays the results obtained showing correlation coefficients greater than 0.999 for all APIs (Guedes and Guedes, 2006). The *y*-intercept should not significantly depart from zero i.e., the peak area response of the *y*-intercept should be less than 5 % of the response of the nominal 100 % concentration value (Bliesner, 2006). All three APIs showed *y*-intercepts significantly close to the origin, i.e., < 5 % of the target concentration's response for each drug in the final formulation in dissolution media. Figure 3.6 (a–c) shows the respective standard curves and chromatograms obtained for each drug. The LOQ and LOD fell within the range of acceptable criteria of ≤15 % and ≤20 % of the nominal concentration, respectively (Sithole *et al.,* 2021).

Table 3.3: Summary of regression statistics, LOD and LOQ values for the APIs.

Parameter	PAR	DS	ESM
Linearity range (µg/ml)	20 - 500	50 - 500	2 - 100
Correlation Coefficient	0.9998	0.9998	0.9994
% Response of Y-intercept	2.35	3.89	4.37
Slope	2491.66	17663.50	53931.00
SE of Intercept	4097.48	34516.10	26454.01
SD of Intercept	10036.74	77180.34	69990.74
LOD (µg/ml)	13.29	14.42	4.28
LOQ (µg/ml)	40.28	43.70	12.98

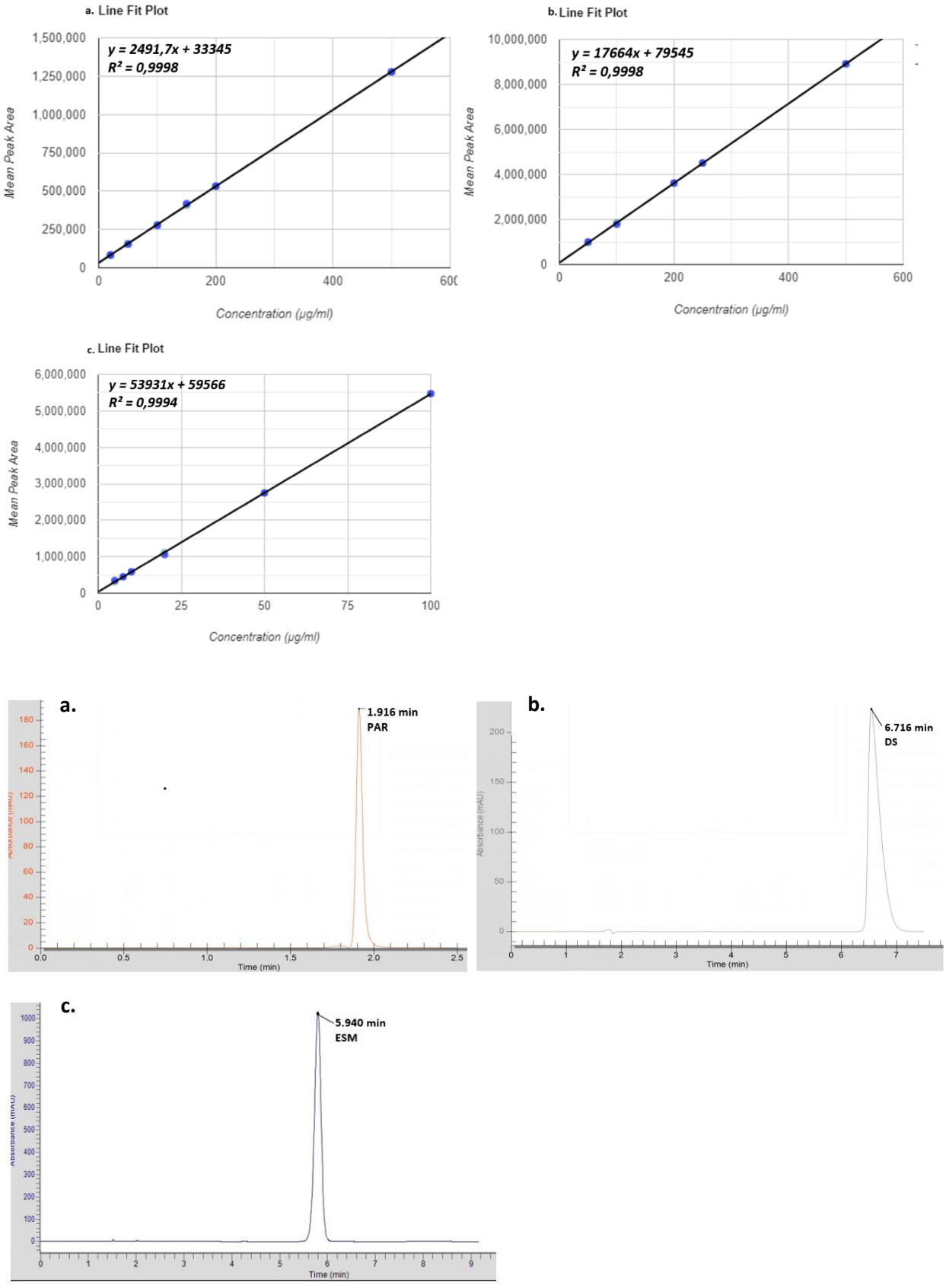

Figure 3.6: Regression lines and respective representative chromatograms showing the retention of a. PAR at 1.916 min, b. DS at 6.716 min, and c. ESM at 5.940 min.

3.3.3.2.2 Method Precision and Accuracy

The acceptance criteria for each spiked sample's recovery should lie within the range of 98 % to 102 % (Bliesner, 2006). Both analyses of the standards and the tablet proved the accuracy of the method in simultaneously quantifying the 3 APIS (Table 3.5, 3.6, and Figure 3.7). For precision the % RSD of the assay should not be greater than 2.0 %, no deviations above 2 % were observed in the 3 concentrations see Table 3.4 below (Bliesner, 2006).

Table 3.4: Summary of precision results (n=3).

		Intra-Day		**Inter-Day**	
API	**Concentration (µg/ml)**	**Mean Peak Area ± SD**	**% RSD**	**Mean Peak Area ± SD**	**% RSD**
PAR	20	84069.13 ± 622.82	0.74	85073.76 ± 882.66	1.04
	150	419777.57 ± 565.26	0.14	422739.71 ± 965.03	0.23
	500	1272293.19 ± 1642.71	0.13	1281166.82 ± 2879.06	0.22
DS	50	1008508.69 ± 2196.10	0.22	1004206.11 ± 2419.94	0.24
	200	3616091.24 ± 452.07	0.01	3618129.47 ± 1993.91	0.06
	500	8900603.53 ± 35464.95	0.39	8873691.55 ± 47814.06	0.54
ESM	2	236899.86 ± 821.85	0.34	239088.26 ± 505.11	0.21
	10	487202.85 ± 1268.75	0.26	620947.79 ± 979.35	0.16
	100	4339415.037 ± 23732.46	0.55	5516351.029 ± 2187.03	0.04

Table 3.5: Summary of accuracy results on standards (n=3).

API	**Initial Standard Concentration**	**Spike Level %**	**Mean % Recovery ± SD**	**% RSD**
PAR	20	80	100.12 ± 0.59	0.59
		95	100.23 ± 2.97	2.96
		100	99.46 ± 1.99	2.00
DS	100	80	100.68 ± 0.09	0.09
		95	98.85 ± 0.93	0.95
		100	99.85 ± 0.14	0.14
ESM	20	80	99.03 ± 1.35	1.36
		95	98.02 ± 0.49	0.50
		100	98.73 ± 0.71	0.72

Table 3.6: Summary of accuracy results on tablet formulation dilution (n=3).

API	Dilution 500:25:5 (µg/ml)	
	Mean % Recovery ± SD	**% RSD**
PAR	97.55 ± 0.37	0.38
DS	98.60 ± 1.40	1.42
ESM	97.64 ± 0.21	0.22

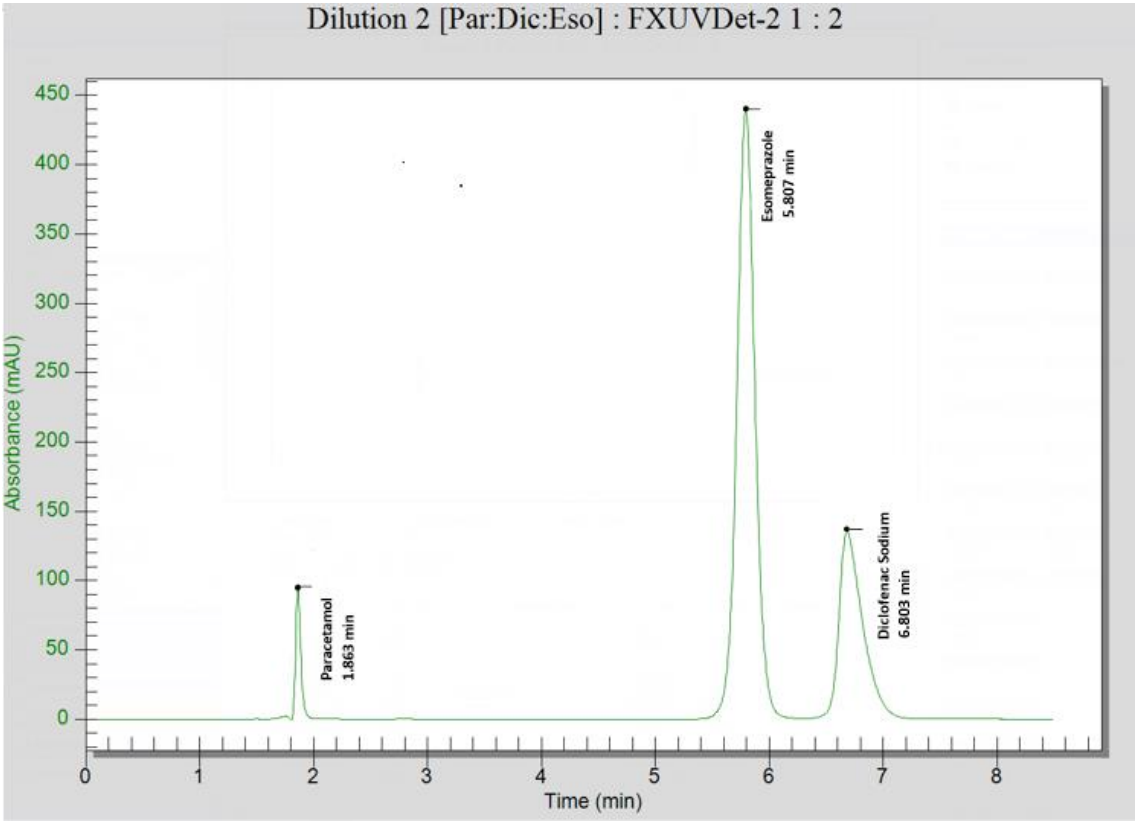

Figure 3.7: Chromatogram showing the retention of PAR at 1.863 min, ESM at 5.807 min, and DS at 6.803 min in a combined sample containing 1 mg/ml of each drug (1:1:1).

3.3.3.2.3 Robustness Analysis

The conclusion drawn from this analysis was that the method only yields the best results at the established conditions as variations e.g., changing the flow rate by +0.2, resulted in significant deviations. Temperature and mobile phase changes demonstrated some level of robustness for PAR and DS, whilst ESM showed greater sensitivity to alterations in these parameters (Table 3.7). Therefore, the method may still be applied in identifying, and quantifying the 3 APIs in combinations should minimal changes (less than the analysed e.g., ±2˚C ± 0.5 ml/min) be encountered during other analyses.

Table 3.7: Summary of robustness assessment (n=3).

	HPLC Parameter		API % Recovery					
	Set Conditions	**Alteration**	**PAR 150 (µg/ml)**	**% RSD**	**DS 200 (µg/ml)**	**% RSD**	**ESM 100 (µg/ml)**	**% RSD**
Flow Rate	1 ml/min	1.2	93.10 ± 0.12	0.13	85.01 ± 2.11	2.48	80.03 ± 2.04	2.55
		0.8	104.13 ± 1.28	1.23	101.50 ±1.35	1.33	95.28 ± 1.71	1.79
Temperature	25 ˚C	30˚C	100.75 ± 2.90	2.88	100.00 ± 1.03	1.03	91.24 ± 0.07	0.08
		20˚C	90.15 ±1.73	1.92	106.10 ± 3.04	2.87	87.72 ± 2.16	2.46
Mobile Phase	70:30	65:35	102.83 ± 1.25	1.22	107.00 ± 0.93	0.87	98.65 ± 0.98	0.99

3.3.3.2.4 Stability Analysis

The acceptance criteria that the difference should be <2% was met for the benchtop 24-hour samples of PAR and DS, whilst degradation was evident in ESM. Potential contributions to the instability of ESM may be attributed to UV-photolysis and hydrolysis all characteristic of ESM (Nalwade *et al.,* 2012). From the frozen samples, DS showed the greatest stability, (Table 3.8).

Table 3.8: Stability assessment on standards (n=3 injections).

	PAR (500 µg/ml) Standard Mean Peak Area = 1290983.727		**DS (200 µg/ml) Standard Mean Peak Area = 3615607.791**		**ESM (100 µg/ml) Standard Mean Peak Area = 5473971.776**	
	Mean Sample Peak Area	**% Difference**	**Mean Sample Peak Area**	**% Difference**	**Mean Sample Peak Area**	**% Difference**
Benchtop (24 hours)	1310667.29	+1.52	3564841.03	-1.40	5254179.351	- 4.02
Freeze-thaw cycles (2 Weeks +)	1149157.16	-10.99	3625894.29	0.28	4825165.28	-11.85

3.3.3.2.5 Specificity/Selectivity Analysis

Based on the results presented in Figure 3.8. no interference occurred in the elution and retention times between the 3 APIs and excipients demonstrating the overall specificity of the method proposed. However, a slight shift in the retention times of ESM and consequently DS was observed in the presence of excipients, by +0.401 minutes and +0.602 minutes, respectively.

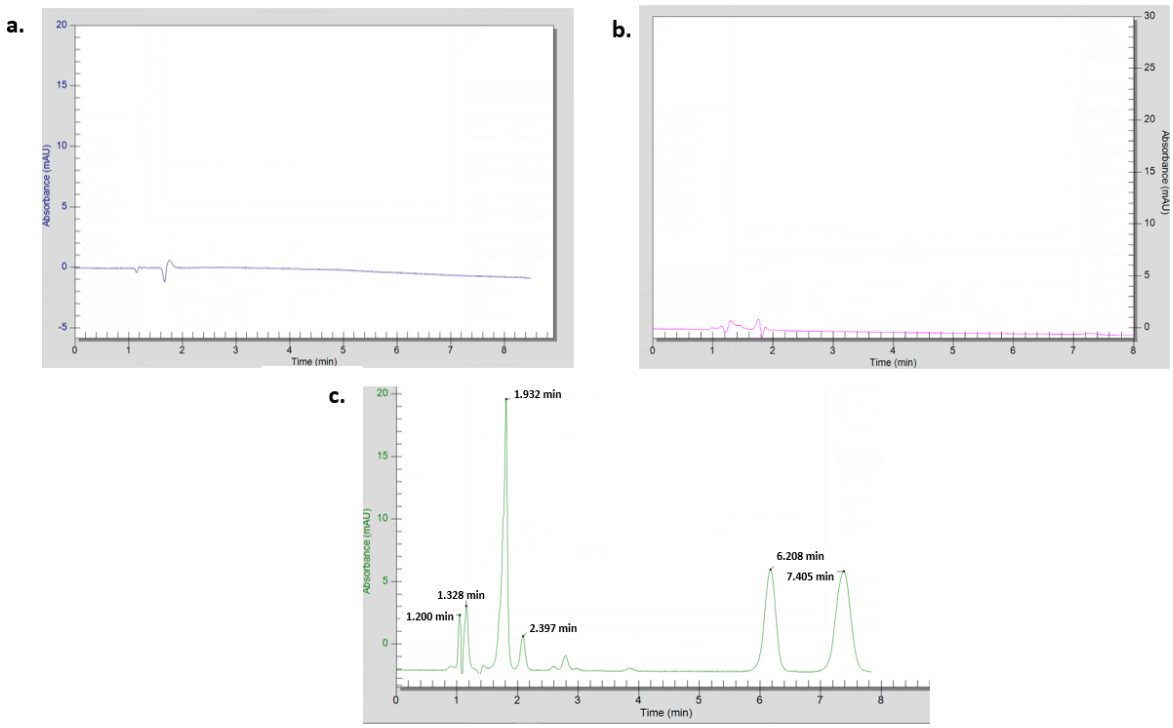

Figure 3.8: Specificity chromatograms of a. the Mobile Phase b. Excipients and c. APIs + Excipients in the ratio 25:5:1 (125:25:5 µg/ml)

3.4 Conclusion

A reproducible, fast, precise, and accurate method was successfully developed and validated for the quantification of the respective APIs in tandem. Further confirmation of the reliability of the method was illustrated in both *in vitro* and *ex vivo* analysis of the tablet formulations, as shown in Chapters 5 and 6 respectively. The purity of the reference standards of the APIs was confirmed through the different characterisation techniques.

Compatibility analysis through rapid DSC screening of the API/excipient/polymer combinations no detrimental interactions were observed. Only slight changes in peak heights, shape, and width due to probable changes in the mixture geometry were observed and drops in API melting point principle to the effect impurities (in this case excipients and polymers) on the melting point of substances (Lisa, 2021). Further investigations were done for FTIR analysis,

from which favourable hydrogen bonding between characteristic groups of EL 100-55 was predicted.

The lack of stability of ESM, as confirmed through HPLC method validation as well as variations established in thermal analysis, served as a precaution in the proceeding development of the DDS, also illustrating the potential need for a stabiliser such as sodium Lauryl sulphate (SLS).

CHAPTER 4

FORMULATION DEVELOPMENT AND COMPARATIVE *IN VITRO* DRUG RELEASE ANALYSIS

4.1 Introduction

The implementation of Quality by Design (QbD) principles in the formulation and development of tablets has become increasingly popular, encompassing the preliminary and systematic risk assessment of critical material attributes (CMAs) and critical process parameters (CPPs) with respect to in-process and finished product critical quality attributes (CQAs) (ICH, 2009; Simão, Chaudhary and Ribeiro, 2023). By definition, the QbD process is a systematic step-by-step process that starts with predefined goals in the form of a quality target product profile (QTPP) stemming from reliable scientific knowledge of the drug product formulation, manufacturing process, and process controls (Mohurle *et al.,* 2019; Simão *et al.,* 2023).

Employment of this approach is advantageous in that unlike Quality by testing (QbT), there is likely to be a reduction in the number of experiments required to produce a cost-effective high-quality product (Chappidi *et al.,* 2019). The complexities in the compression of non-conventional geometries of tablets have been well established, motivating researchers to implement systematic QbD concepts. Whilst literature contains little to no guidelines on the QbD approach in developing complex multi-drug tablet systems (more than 2 structural components), Simão and researchers (Simão *et al.,* 2023) managed to come up with a practical framework appropriate and suitable for application in the development of bilayer tablets through a systematic step-by-step QbD strategy. In a similar manner, where applicable, the development of the present system adopted the QbD approach, as shown in Figure 4.1.

Successful controlled release multidrug systems are an interplay between matrix geometries and functional excipients, and the core-in-cup tablet design amongst others is one that allows dual or even tripartite controlled drug release. The ability to manipulate release patterns in these systems is a function of a wide range of multi-functional polymers that permit release in response to a variety of factors such as time, temperature, pH, and enzymes (van der Merwe *et al.,* 2020; Geraili, Xing and Mequanint, 2021a). Indeed, the presence of dissolved drug particles at the absorption site is a prerequisite for drug absorption. Dissolution testing, therefore, represents a critical step in early drug development, allowing the nascent visualization of preconceived and desired release patterns. *In vitro* drug release testing by dissolution is also useful in identifying the most optimal formulations in the development stage and as a support for quality control specifications (Dressman and Krämer, 2005).

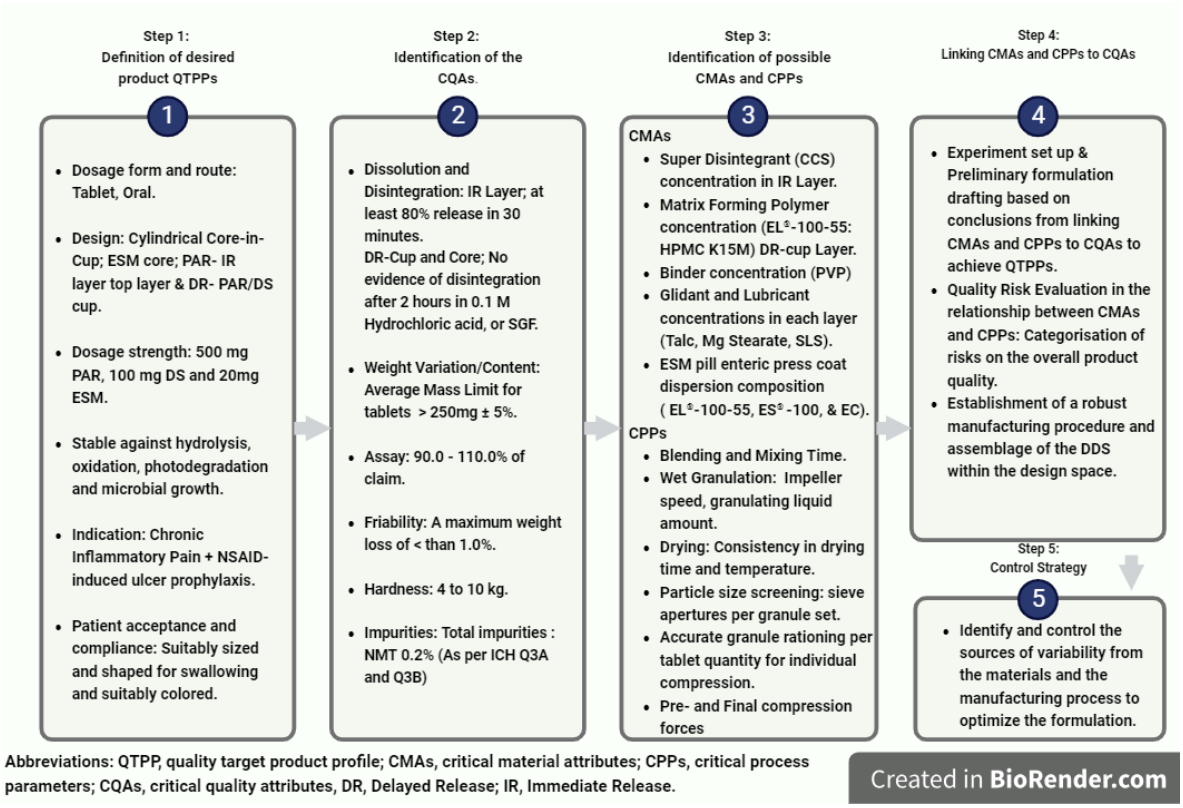

Figure 4.1: Summarisation of the QbD principles applied in the development of the present drug delivery system.

In order to precisely describe release mechanisms, dissolution data must be assessed based on different mathematical functions. Once a suitable function is selected, using derived model parameters such as *k* and r^2 values, the profiles may be classified as either zero order, first order, Higuchi, Hixson–Crowell, Korsmeyer–Peppas, etc (Marcos, 2015).

Although dissolution testing does not conclusively prove that the dosage form will release the drug *in vivo* in an observed manner, it does come one step closer to establishing whether the drug can become available for absorption in terms of being in solution at the sites of absorption. This chapter addresses the selection of polymers that led to the development and design of the DDS including investigative dissolution drug release tests on each formulation. Quality control attributes as evaluated in-process, as well as characterisation of the final optimised formulation, are elaborated on in the next chapter.

4.2 Materials and Methods

4.2.1 Materials

In addition to the materials used in Chapter 3, Sodium Hydroxide pellets, Sodium Lauryl Sulphate (SLS), Eudragit S -100 and Polycaprolactone (PCL), Hydrochloric Acid (HCL), Sodium Chloride (NaCl), Potassium dihydrogen phosphate (KH_2PO_4), Sodium hydrogen phosphate (Na_2HPO_4) were sourced from Sigma-Aldrich (St. Louis, Missouri, USA).

4.2.2 Formulation Development

In order to distinctly observe polymer functions and release characteristics of each structural component of the DDS, partial blanks were formulated and compressed as per the representative schematics in Figure 4.2 a-c. For instance, investigation of the IR Layer involved the compression of the entire DDS comprising a drug-loaded IR Layer and drug-less core and cup polymer matrix formulations. Tables 4.1 – 4.5 below list the formulation constituents of each component of the DDS.

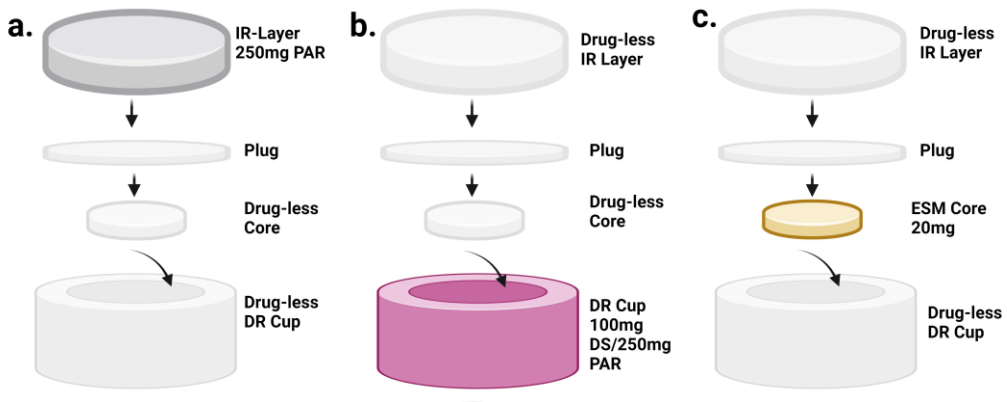

Figure 4.2: Schematic representatives of preliminary drug delivery systems for segregated investigation of each layer.

i. Immediate Release and Delayed Release Layers

Crosslinked carboxymethyl cellulose sodium was the super-disintegrant of choice in the IR layer at 3.1 and 10.6 % (w/w), making up half of the total PAR dose. PVP-K30 was used as the binder at 11.6 and 5.3 % (w/w). At higher than 10 % (w/w) PVP-K30 functions as a disintegrant thus in order to regulate the burst release phenomena HPMC E50 LV at 4 and 5% (w/w) was added to the formulation. The DR cup layer was designed for the retarded enteric release of PAR and DS. DS is a weak acid with compromised solubility at low pH, thus absorption from the gastric region is limited by solubility, justifying the enteric target. In order to successfully retard the release rate and hinder release in the gastric region, combinations

of HPMC K15M: EL 100-55 at 1:3 were employed, (Rajabi-siahboomi, 2008; Jindal and Dua, 2016; Srinija and Lakshmi, 2016; Challener, 2018; Chakraborty, 2022; Evonik, 2022; Kwon *et al.,* 2022). The lubricant and glidant of choice were Magnesium Stearate and Talc, respectively. Wet granulation techniques, employing water as the granulating fluid (*qs*) were applied for both the IR and DR layers, to distinguish the latter layer 15 mg of carmine was added to the granules.

ii. The Core and Plug

As well as being sensitive to moisture, light, and high temperatures, ESM is notorious for its rapid degradation in acidic environments (Van Nguyen, Baek and Lee, 2017). Therefore, the core of the cup was designed to shield it from gastric fluid for at least two hours, i.e., gastric emptying time. MCC was used as the binder, which also possesses glidant, filler, and anti-adherent properties. Once in the intestinal region, the release of ESM must be rapid, hence the inclusion of CCS (22.6 and 8.6 % w/w) (Chakraborty, 2022). The application of SLS in pharmaceutical formulations is multi-faceted, including its use as an emulsifier, release modifier, penetration enhancer, solubilizer, and tablet lubricant (5% SLS has similar lubrication efficiency as 1% Mg^{2+} Stearate with better dissolution due to the improved wetting). Moreover, because the pH range of SLS is from 7 to 9.5, its incorporation into preparations could slightly raise the pH during drug dissolution (Dun *et al.,* 2018; Alshora *et al.,* 2022). SLS was therefore considered for inclusion in the formulation at about 5 % (w/w). Dry granulation and direct compression steps were applied in this instance. As an added precaution against premature exposure, which may result from the immediate disintegration of the top layer, the ESM pills were enterically press-coated in addition to a barrier between the IR and DR cup layers. The solvent-free and heat-free coating method was preferred to maximize the drug's overall stability (Sateesh, 2017).

Table 4.1: Immediate Release Layer formulation composition.

	PAR	**CCS**	**PVP-K30**	**HPMC E50 LV**	***Mg-Stearate**	***Talc**	**Total Weight**
				(mg/tablet)			
IR_1	250.00	10.00	37.60	16.00	5.00	3.00	321.60
(%)	77.74	3.11	11.69	4.98	1.55	0.93	100.00
IR_2	250.00	34.00	17.00	12.60	5.00	3.00	321.60
%	77.74	10.57	5.29	3.92	1.55	0.93	100.00
IR_3	250.00	34.00	17.00	12.60	5.00	6.00	324.60
%	77.02	10.47	5.24	3.88	1.54	1.85	100.00

***Incorporated into granules just before compression.

Table 4.2: Delayed Release cup formulation layer composition.

	PAR	DS	EL 100-55	HPMC K15M	HPMC E50 LV	*Mg-Stearate	*Talc	Total Weight
	(mg/tablet)							
DR_1	250.00	100.00	120.00	41.36	-	5.40	5.00	521.76
(%)	47.90	19.2	23.0	7.9		1.00	1.00	100.00
DR_2	250.00	100.00	140.00	41.36	-	5.40	5.00	541.76
(%)	46.15	18.45	25.84	7.63		1.00	1.00	100.00
DR_3	250.00	100.00	140.00	52.44	-	5.40	5.00	552.84
(%)	45.22	18.08	25.32	9.49		1.00	1.00	100.00
DR_4	250.00	100.00	140.00	41.36	11.08	5.40	5.00	552.84
(%)	45.22	18.08	25.32	7.48	11.08	1.00	1.00	100.00

*Incorporated into granules just before compression

Table 4.3: Core formulation composition.

	ESM	MCC	CCS	Mg-Stearate	SLS	Total Weight
	(mg/tablet)					
C_1	22.30	20.96	12.75	0.45	-	56.46
(%)	39.50	37.12	22.58	0.80	-	100.00
C_2	22.30	41.92	6.38	-	3.50	74.10
(%)	30.10	56.58	8.60		4.72	100.00

Table 4.4: Plug formulation.

	EL 100-55	EC	SSG
	(mg/tablet)		
P1	60.00	66.00	24.00
(%)	40.00	44.00	16.00
P2	30.00	33.00	12.00
(%)	40.00	44.00	16.00

Table 4.5: Core Press Coat composition.

Polymer	***mg/core pill.***
EL 100-55	70
ES-100	70
EC	15
Talc	5
Total	**160**

4.2.3 Pre-Compression Evaluation

The flow properties of each set of granules for each drug-loaded component of the DDS were assessed using Angle of Repose, Cars Index, and Hausner's Ratio determinations. Weighed-out quantities of the granule sets were lightly packed into a hollow glass measuring cylinder. The volumes were noted as the untapped volume, the cylinders were subjected to a fixed number of taps, and this volume was noted as the tapped volume, the two volumes were used to determine the bulk and the tapped densities of each set of granules. The granules were allowed to freely heap from a funnel and respective radii and height measurements were noted. The Angle of Repose, Cars Index, and Hausner's Ratio were thus calculated using equations 4.1 – 4.3 (Nandi *et al.,* 2020). Table 4.6 presents the acceptable ranges of each flow property, as depicted below.

Angle of repose: $\theta = tan^{-1}\frac{h}{r}$

Where **θ** is the Angle of repose,
h is the Height of the pile, and
r is the Radius of the base of the pile **Equation 4.1**

Cars Index: $I = (\mathrm{Dt} - (\frac{Db}{Dt})) * 100$

Where **Dt** is Tapped density, and
Db is Bulk density **Equation 4.2**

Hausner's ratio: $HR = \frac{Dt}{Db}$

Where **Dt** is Tapped density, and
Db is Bulk density. **Equation 4.3**

Table 4.6: Scale of flowability determined by different methods (Sahoo *et al.,* 2015).

Flow property	Angle of Repose	Car's index	Hausner's ratio
Excellent	25-30	< 10	1.00-1.11
Good	31-35	11-15	1.12-1.18
Fair	36-40	16-20	1.19-1.25
Passable	41-45	21-25	1.26-1.34
Poor	46-55	26-31	1.35-1.45
Very poor	56-65	32-37	1.46-1.59
Very very poor	>66	>38	>1.6

4.2.4 Assemblage of the Full DDS

Compression was done on the Manesty Type F3 eccentric (single punch) manual tableting press (Manesty Machines, United Kingdom), Figure 4.2 schematically outlines the order in which the DDS was assembled and compressed. Separately, using a flat faced 7 mm punch and die set, ESM core pills were compressed. Press coating of the core pills was done by means of a slightly larger punch and die set, 9 mm diameter. 50 % of the granules were placed in the die cavity, followed by the central placement of the pill, and then the remaining 50 % was poured on top and fully compressed (Maity and Sa, 2016). Thereafter, accurately weighed quantities of the cup formulation per tablet were loaded into the die cavity, and the cup shape was achieved using a disc-shaped 'device' the size of the coated core pills made from molten Polycaprolactone (PCL). The upper punch was manually lowered for slight pre-compression and raised to remove the 'device', exposing the cup. The coated core pills were manually placed into the cup, followed by a spread of the plug granules, this again was slightly compressed to level out the granules, and finally, the IR formulation was poured on top, and fully compressed. The die capacity was kept constant throughout the compression cycles by lower punch adjustments, and the main compression force as a function of upper punch adjustments was kept at a constant of 23 kN to ensure uniformity in thickness and related mechanical properties.

4.2.5 *In Vitro* Drug Release Studies

In vitro, drug release studies were carried out using a USP dissolution apparatus II (Erweka, Heusenstamm, Germany) equipped with paddles. Dissolution was performed in 900 mL simulated gastric fluid (SGF) pH 1.2 for the first 2 hours and simulated small intestinal fluid (SSIF) pH 6.8 for the remainder of the study, as shown in Table 4.7 (Khan, 2011). The speed and temperature were set at 50 rpm and 37 ± 0.5 °C. 5 mL samples were withdrawn at every specified time interval followed by replacement with an equal quantity of fresh media kept at

37 ± 0.5 °C to maintain sink conditions. Withdrawn samples were filtered using 0.45 µm nylon syringe filters, and past the 2-hour mark, the filtrate was transferred to vials containing 400µL of 0.25 M sodium hydroxide to avoid acid degradation of ESM (Kwon *et al.,* 2022). Each sample's quantitative analysis was done per the conditions stipulated in Chapter 3, Table 3.1. Replacement with fresh media at each time interval may result in a significant deviation from the true drug quantity released at subsequent intervals; therefore, mathematical corrections must be applied to ensure accuracy in % cumulative drug release. Equation 4.4 below was used to determine the corrected amounts of drug released per time interval (Salt, 2021). Kinetic modelling of the dissolution data was done on DDSolver, (a menu-driven add-in program for Microsoft Excel), from which goodness of fit data for each drug and data sets were obtained (Najmi and Sultan, 2022).

$$C_{n,corr} = C_n + \frac{V_s}{V_m}\int_{i=1}^{n-1} * C_i \qquad \textbf{Equation 4.4}$$

Where:

$\mathbf{C_{n,corr}}$ is the corrected concentration at sample interval n,

$\mathbf{C_n}$ is the measured or uncorrected concentration at sample interval µg/ml,

$\mathbf{V_m}$ is the original media volume in the dissolution vessel 900 ml,

$\mathbf{V_s}$ is the volume of sample removed at each time interval 5 ml, and

$\mathbf{C_i}$ is the uncorrected concentration at each previous sample interval µg/ml.

Table 4.7: Constituents of dissolution media.

Component	**SGF (pH 1.2) /1000 ml**	**SSIF (pH 6.8) * /1000 ml**
KH_2PO_4	-	0.144 g
Na_2HPO_4	-	0.795 g
NaCl	2.00 g	9.000 g
HCL (32%)	7.00 ml	-

***** pH was further adjusted using 85% (w/w) phosphoric acid.

4.3 Results

4.3.1 Pre-Compression Powder Flow Analysis

The moisture content of powders is a key property in powder flow characterisation. Thus, the presence of hygroscopic excipients such as PVP, CCS, and MCC in the different sets of granules was influential in the flowability of the granules. In general, flowability decreases with

increasing moisture content due to an increase in cohesion from stronger interparticle liquid bridges (Crouter and Briens, 2014). On the other hand, as displayed in Table 4.8, by means of decreasing interparticle friction and cohesion**,** upping the concentration of Talc as a glidant played a role in improving the flow properties to acceptable ranges for compression. However, high concentrations (> 5%) of Talc have been shown to be detrimental to drug release outcomes, therefore further attempts to improve flow properties by means of increasing the amount of glidant were considered unfeasible (Ammar *et al.,* 2016; Apeji and Olowosulu, 2020; pharmaeducation.net, 2023)**.**

Table 4.8: Flow properties per formulation granules.

	Car's index (%)	**Hausner ratio**	**Angle of Repose (°)**
IR_1	33.59	1.62	46.30
IR_2	22.22	1.29	30.40
IR_3	14.15	1.11	31.56
DR_1	17.15	1.28	39.75
DR_2	14.10	1.21	37.12
DR_3	13.63	1.17	35.71
DR_4	13.33	1.15	34.59
C_1	20.31	1.26	38.60
C_2	22.50	1.31	41.14

4.3.2 Dissolution results and influence of polymers

4.3.2.1 IR Layer: Influence of CCS and PVP-K30 Concentrations

Figure 4.3 shows the release profiles for the attempted IR Layer formulations in pH 1.2 for 1 hour, Table 4.9 summarises the best-fit values for the different release models. In order to achieve an 80 % release within 30 minutes in the IR layer, the CCS concentration had to be increased to 10,6 % (w/w), higher than the normally applied concentration range i.e., 2 – 5% (w/w) for wet granulation (Hiremath, Nuguru and Agrahari, 2018). The hydrophilic nature and swelling characteristics of CCS were highlighted in the presence of less binder i.e., 6% (w/w). Because the use of CCS at such high concentrations is more prevalent in orodispersible formulations where rapid swelling and release occur within seconds in the oral cavity; the inclusion of low-viscosity HPMC E50 LV provided a much more controlled burst phenomenon in IR3 (Parfati & Rani, 2018; Tanuwijaya, 2013). The slight difference in the rate of release seen in IR2 and IR3 may be attributed to the increase in the concertation of Talc, whose mechanism involves a reduction in interparticle friction and cohesion resulting in faster

disintegration, consistent with literature findings on the effects of talc on drug release (Ammar *et al.,* 2016; Wang *et al.,* 2018; Apeji and Olowosulu, 2020). The model of release transitioned from zero order to first order from IR1 to IR3, descriptive of the dissolution of water-soluble drugs in porous matrices, which confirms the rapid swelling and burst observed in the layers (Yadav *et al.,* 2013).

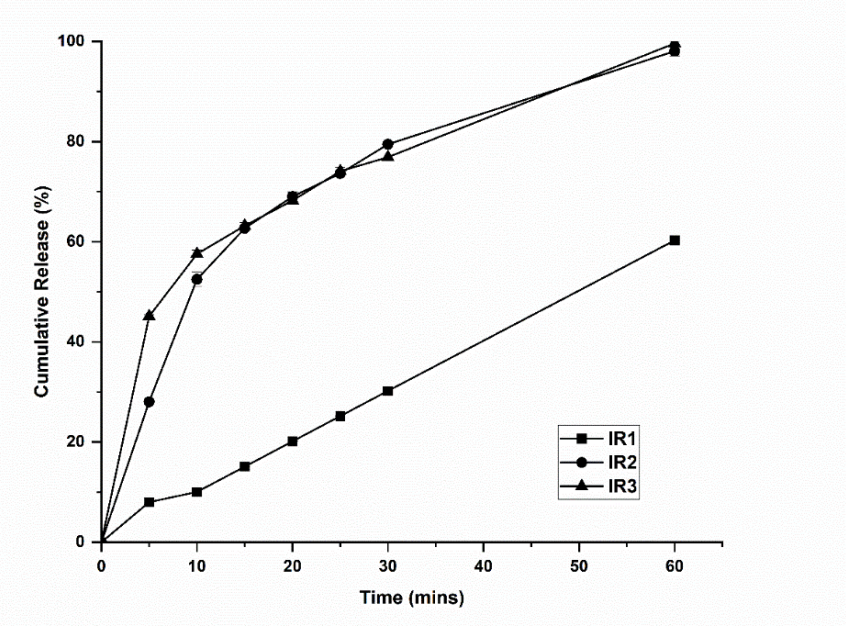

Figure 4.3: IR-Layer drug release profiles in SGF pH 1.2 (n=3; %RSD < 2.00 in all cases).

Table 4.9: Best of fit values: IR Layer (n=3).

		Zero-order	**1st Order**	**Higuchi**	**Korsmeyer-Peppas**
IR_1	r^2	**0.9990**	0.9890	0.9746	0.9987
	k	1.008	0.013	5.797	1.100 *n* = 0.977
IR_2	r^2	0.8733	**0.9943**	0.9827	0.9896
	k	2.232	0.061	14.212	19.893 *n* = 0.400
IR_3	r^2	0.8619	**0.9930**	0.9785	0.9880
	k	2.241	0.063	14.175	20.383 *n* = 0.392

4.3.2.2 DR Cup

Figure 4.4 below shows the release profiles for the attempted DR Layer formulations in pH 1.2 for 2 hours and from 2 to 10 hours in pH 6.8, Tables 4.9.1 and b summarise the best-fit values for the different release models. Generally, the cups demonstrated significant resistance to

disintegration in gastric media, with slight hydration-mediated spillage. One of the cup's critical attributes was the inhibition of drug release in the gastric environment, thus the concentration of EL 100-55 was the first adjustment from DR_1. An increase in the amount of EL 100-55 from 120 mg to 140 mg yielded much more resistance. Because PAR is more soluble than DS, the spillage was confirmed by the quantifiable (by HPLC) presence of PAR in the withdrawn samples, whilst it appeared from the lag phase as though no DS was released in the 2 hours.

The effect of the HPMC K15M concentration was more evident at pH 6.8, as expected, higher concentrations yielded more delayed release. These observations may be attributed to the interaction between the anionic methyl acrylic polymer and cationic products from the ionization of the rest of the components in the matrices. Similar observations have been made in studies where HPMC K15M: EL 100-55 combinations at 10, 20, and 30 % (w/w) were employed to produce sustained release formulations (Takka *et al.,* 2003; Fayed *et al.,* 2013). Notably, the inclusion of low viscosity grade HPMC E50-LV in combination with HPMC K15M was seen to not retard the release as much as HPMC alone at equal concentration.

The dominant model of release in the cup for both PAR and DS was Korsmeyer-Peppas with the diffusion coefficient "n" lying within the range ($1 > n > 0.5$) indicating a non-Fickian nearly zero-order case II transport mechanism via erosion of polymeric chains, instead of pores as seen in Fickian models (Lobo and Costa, 2001; Shah and Khan, 2012). In this case, axial swelling is prevented for a significant period, producing tension of compression on the nucleus as well as keeping it in its dry and vitreous state until the polymeric interface gel advances towards the nucleus. DR4 showed a Super Case II transport mechanism, which simply alludes to a higher speed of solvent diffusion occurring on the surface of the cup, likely due to the reduction in HPMC K15M concentration (Shah and Khan, 2012).

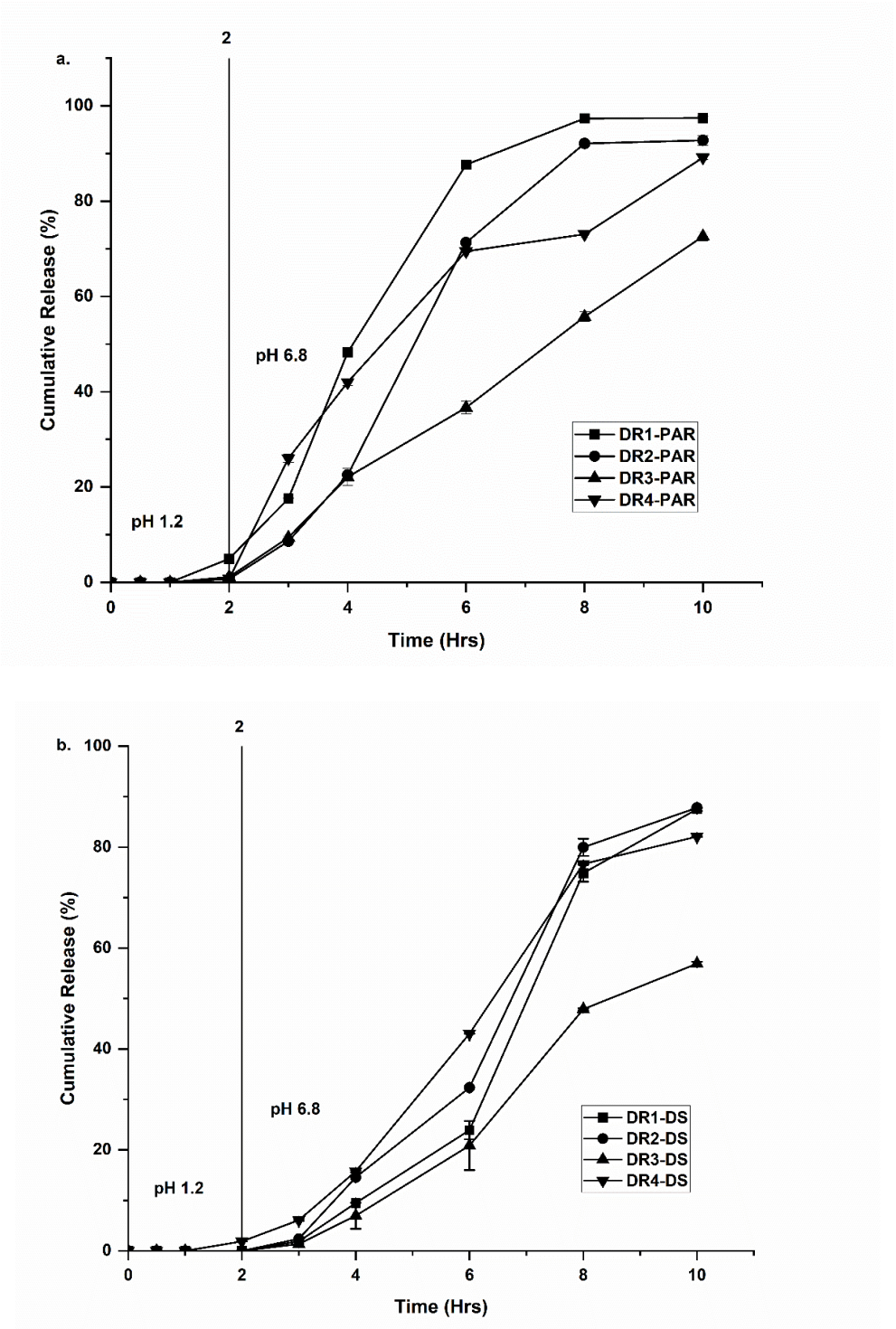

Figure 4.4: a. PAR b. DS DR cup layer drug release profiles in SGF pH 1.2 (0 – 2 hours), SSIF pH 6.8 (2 – 10 hours) (n=3; %RSD < 5.00 in all cases).

Table 4.9.1: a. Best of fit values with Tlag: DR Layer (PAR).

		Zero-order	1st Order	Higuchi	Korsmeyer-Peppas
DR_1	r^2	0.9561	0.9485	0.9855	**0.9926**
	k	12.418	0.248	40.866	54.683 *n* = 0.330
DR_2	r^2	0.9641	0.9281	**0.9892**	0.9855
	k	11.877	0.192	40.670	32.824 *n* = 0.576
DR_3	r^2	0.9900	0.9657	0.9875	**0.9992**
	k	8.086	0.111	24.875	9.991 *n* = 0.949
DR_4	r^2	0.9699	0.9723	0.9957	**0.9967**
	k	10.369	0.190	32.379	39.680 *n* = 0.400

Table 4.9.1: b. Best of fit values with Tlag: DR Layer (DS).

		Zero-order	1st Order	Higuchi	Korsmeyer-Peppas
DR_1	r^2	0.9397	0.8834	0.9928	**0.9957**
	k	9.926	0.126	44.427	13.007 *n* = 1.002
DR_2	r^2	0.9590	0.9076	0.9779	**0.9876**
	k	10.326	0.138	34.553	13.391 *n* = 0.991
DR_3	r^2	0.9405	0.9088	**0.9948**	0.9874
	k	6.524	0.078	26.104	9.911 *n* = 0.947
DR_4	r^2	0.9616	0.9147	0.9883	**0.9944**
	k	8.982	0.114	39.151	6.360 *n* = 1.276

4.3.2.3 Core and Plug Efficiency

The efficiency of the plug in shielding the contents of the core from degradation for at least 2 hours at pH 1.2 was analysed on the uncoated ESM pills, C1. Figure 4.5.a shows the release profiles obtained from the analysis. Following the immediate dissolution of the drug-free IR Layer, detachment of P1 from the cup was observed, exposing uncoated ESM to rapid acid degradation. P2 which is half the formulation of P1, stuck onto the cup much longer than P1 although exposure still occurred within the 2 hours. The variation in results (n=3) (SD > 5.00)

was an indication of the unpredictability and non-definitive behaviour of the plugs, providing no confidence in their efficiency when employed alone without coating. This may be attributed to interparticle bonding between the particles of the cup and the plug, which was evidently stronger in P2 than P1, whilst the intraparticle boding in P1 was independently more robust causing a more pronounced detachment.

Interestingly, the behaviour of the plugs was different in the presence of the coated pills, the expansion from swelling and cellulose-mediated gel-layer formation on the coat's surface cracked open P2, whilst P1 remained significantly intact. As a result of the cracking, fragments of the plug were suspected to have created perforations on the gel surface resulting in minute diffusion of hydrated ESM into acidic media, as shown in Figure 4.6**.** The inclusion of SLS in C2 was seen to improve the overall release of ESM, through stabilisation in dissolution media and improved wetting, (Figure 4.5.b).

The deduced model of release in the coated formulations was Kosmeyer Peppas, with an *n* value corresponding to an anomalous transport diffusion mechanism, which demonstrates drug transport from the gel coat through a combined effect of diffusion and erosion mechanisms (Lobo and Costa, 2001; Shah and Khan, 2012). The anomalous effect is a result of the simultaneous rearrangement of the tablet's polymeric chains and diffusion of dissolution media (Marcos, 2015).

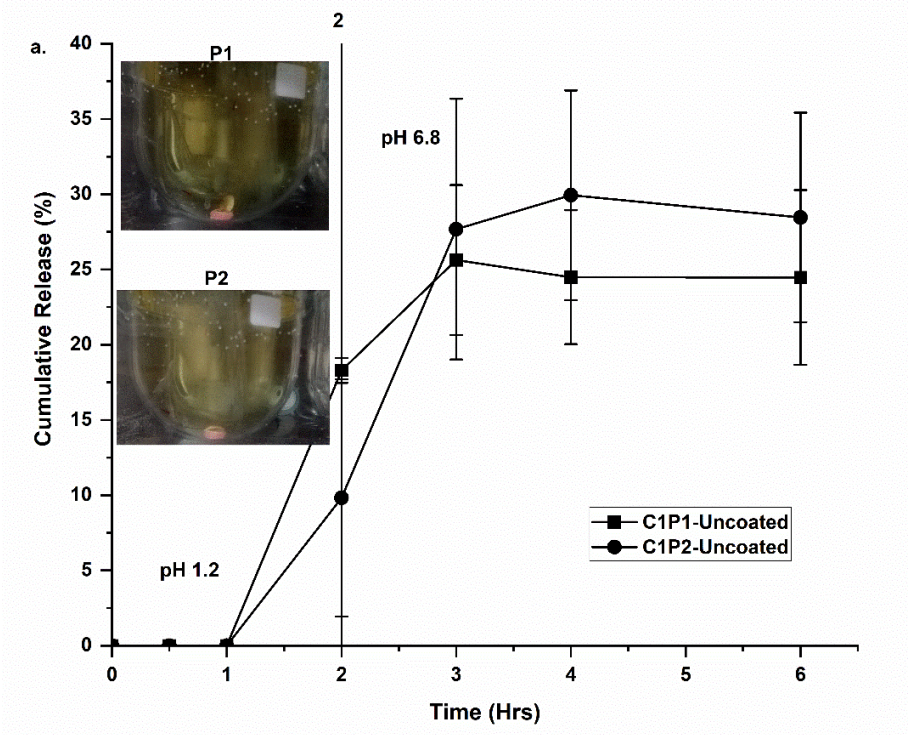

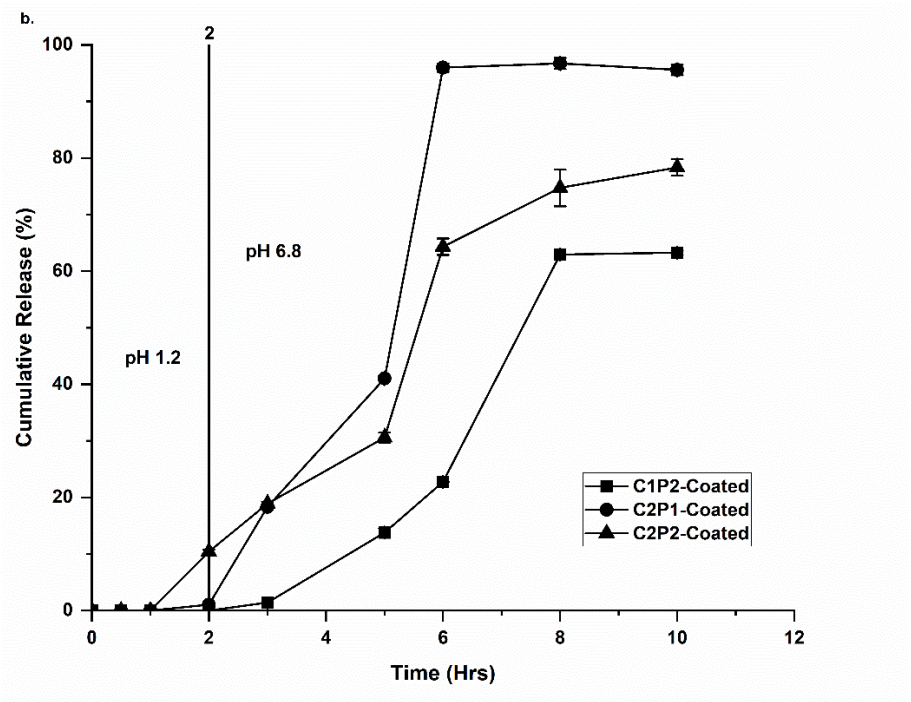

Figure 4.5: a. Uncoated, showing early gastric release of ESM b. coated drug release profiles in SGF pH 1.2 (0 – 2 hours), SSIF pH 6.8 (2 hours onwards) (n=3; 5.00 < %RSD < 10.00 for a., %RSD < 5.00 for b.).

Table 4.9.2: Best of fit values with Tlag: ESM.

		Zero-order	**1st Order**	**Higuchi**	**Korsmeyer-Peppas**
C1P2	r^2	0.9377	0.9039	0.9604	**0.9808**
	k	7.585	0.5490	29.578	27.094 *n* = 0.558
C2P1	r^2	0.9358	0.9020	0.9798	**0.9802**
	k	7.555	0.093	29.602	26.689 *n* = 0.568
C2P2	r^2	0.8757	0.9057	0.9800	**0.9608**
	k	7.053	0.061	29.627	26.707 *n* = 0.567

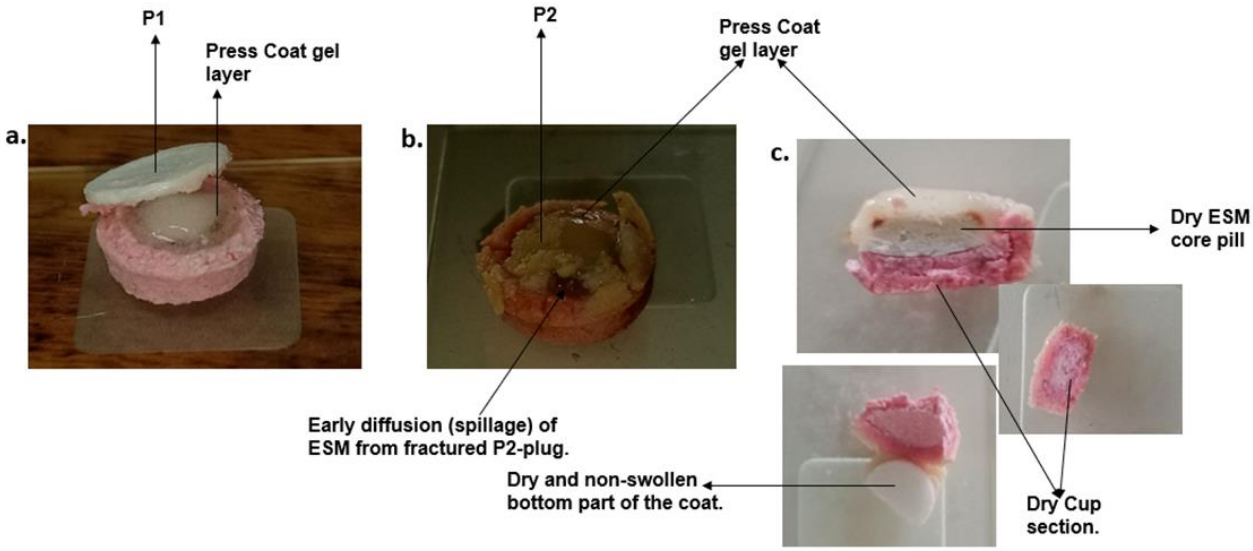

Figure 4.6: Digital visuals of formulation components during dissolution analysis, at pH 1.2 for after the first 2 hours.

4.4 Conclusion

Through careful polymer and design selection in conjunction with critical process parameters and critical material attributes, a formulation capable of meeting most of the target QTTPs and CQAs was achieved at this preliminary level. Through pre-compression analysis the effect of glidant concentration in the presence of hygroscopic polymers, i.e., PVP and CCS was evident. While oro-dispersible tablets capitalize on high concentrations of super disintegrants e.g., CCS > 10% w/w, the use of higher than the recommended 5 % may actually result in the formation of a viscous gel layer that will act as a barrier for disintegration (Hiremath, Nuguru and Agrahari, 2018). Thus, the optimal function of CCS as a super-disintegrant is dependent on binder concentration, higher binder concentration diminishes super-disintegrant function, i.e., an increase in CCS concentration does not equate to faster disintegration when binder concentration is kept constant.

The results obtained from the IR formulation attempts in this section concur with the aforementioned. The selected concentrations of EL 100-55 and HPMC K15M were able to produce a defined lag phase in SGF and sufficient retardation of release in SSIF. The efficiency of the plug as a barrier for the core was limited, with inevitable detachment and or rapture occurring within the 2 hours, thus the resolution to press-coat the ESM pills. Based on this chapter's findings, a complete and optimised DDS was created and evaluated from the different formulation combinations in the following Chapter.

CHAPTER 5

IN-PROCESS EVALUATION POST-COMPRESSION ANALYSIS AND CHARACTERISATION OF THE FINAL FORMULATION

5.1 Introduction

The carefully curated in-process quality tests, including content uniformity, weight variation, hardness, friability, dissolution, disintegration, etc. stem from an interlink between the target finished product's critical quality attributes (CQAs) and critical process parameters (CPPs) (ICH, 2009). Table 5.1 demonstrates the qualitative risk assessment conducted prior to the manufacturing process, as per step 4 outlined in Chapter 4, Figure 4.1. The green cells represent low risk, yellow cells signify medium risk, and red cells indicate high risk.

Table 5.1: Risk estimation matrix presenting initial risk assessment levels of the drug delivery system formulation and manufacturing parameters.

	Process Parameters	Visual Physical Attributes	Assay	Uniformity of Content/ Weight Variation	Hardness/ Friability/ Layers Integrity	Disintegration Time/ Dissolution	Water Content
IR and DR-cup Layers	Blending						
	Wet Granulation						
	Sifting/Size screening						
	Drying						
	Milling						
	Lubrication						-
Core and Press coat blends.	Blending						-
	Co-Sifting/ Size screening						-
	Lubrication						-
Compression	Precompression force of the cup Layer						-
	Precompression force of the Plug Layer						-
	Final Compression force of IR Layer.						-

A comparison of the raw material characteristics as established in Chapter 3, with those of the final product is necessary for ruling out any deleterious drug-processing and or drug-polymer interactions. This entails the determination of the finished product's polymeric structural variations through FTIR and thermal analysis by DSC and TGA analysis. Elucidation of the physico-mechanical properties of the DDS through matrix hydration, erosion, and textural analyses is also essential in characterising the finished product. The synergistic combination of mechanical interlocking, elastoplastic deformation, and fragmentation during the densification of granules through compression conveys the final shape and mechanical strength of the tablet formed (Cabiscol *et al.,* 2018). Whilst hardness test results are essential to confirm the resistance from external mechanical stress, textural profiling allows for the prediction of the tablets' ability to withstand internal stress, i.e., in the GIT to prevent erratic tablet erosion (Siyawamwaya *et al.,* 2019). Matrix hydration and erosion analysis in the dissolution milieu are also key in providing a more detailed description of the mechanism of release.

The mechanisms of release from different controlled-release tablets vary depending on the function and properties of the polymers employed as carriers. These mechanisms include chemically mediated (erosion and degradation), ion-exchange, diffusion, solvent-activated (swelling and osmotic), stimuli- responsive, and dissolution (Rathbone, 2012; Geraili, Xing and Mequanint, 2021) as shown in Figure 5.1. Drugs dispersed in matrices undergo erosion-controlled release mechanisms when the loaded matrix starts to erode before diffusion occurs, the vice versa describes diffusion-controlled release systems. Erosion mechanisms can either be surface or bulk, bulk-erosion degradation occurs simultaneously inside and outside of the matrix upon contact with media. In surface erosion, the initial geometry of the matrix is preserved as a result of degradation of the polymer particles from the surface, and more protection of a hydrophobic core which may comprise highly labile drugs. Both forms of erosion may be observed in one system (Peppas and Narasimhan, 2014; Maclean *et al.,* 2023).

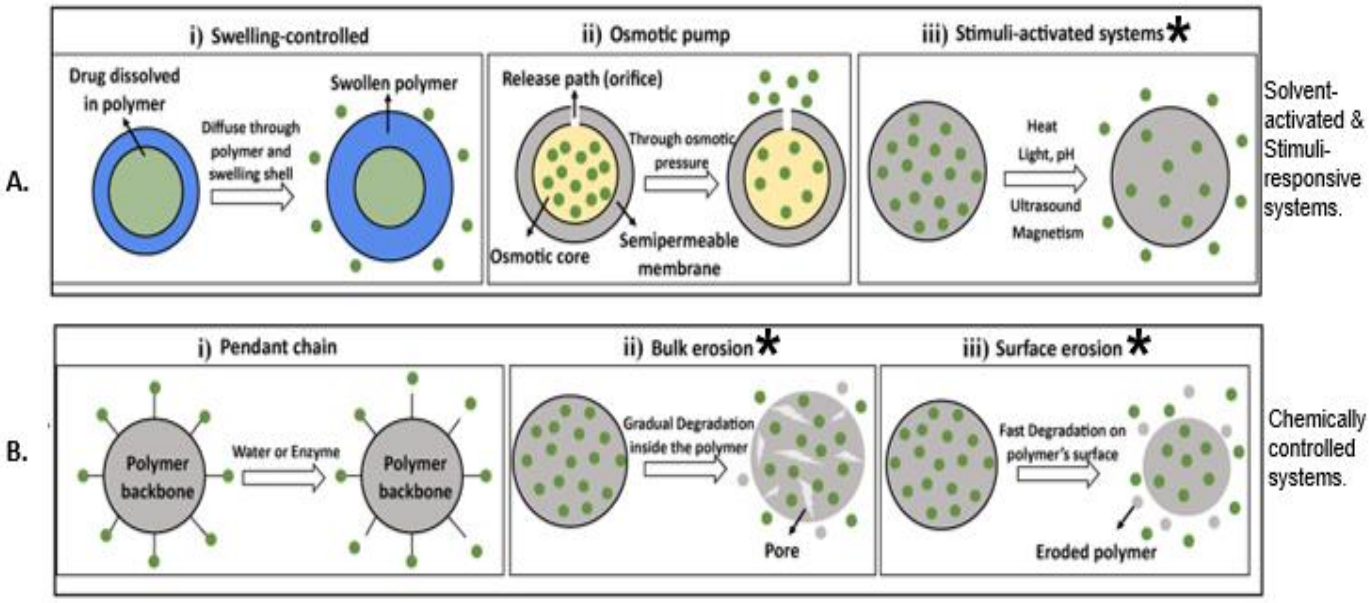

Figure 5.1: Polymeric controlled-release mechanisms. Schematic Illustration Of (A) Solvent-Activated and Stimuli-Responsive Systems. (i) The swelling-controlled system shows drug diffusion through the expandable hydrogel. (ii) The designed orifice in an osmotic-controlled system lets drug molecules release out with an adjustable release rate. (iii) External physical stimuli activate the responsive polymeric carriers to release their cargo in a controllable manner. (B) Chemically mediated Controlled Release Systems (i) Detachment of drug molecules from pendant side-chain polymeric systems (ii) Bulk erosion (iii) Surface versus mechanisms through erodible systems. Adapted from (Geraili, Xing and Mequanint, 2021).

A more qualitative assessment of the shape, morphology, porosity, size distribution, crystal form, and of the compressed tablet can be achieved by Scanning electron microscopy (SEM). This information can be correlated to assess dissolution behaviour, bioavailability, and crystalline structure. The focus of this chapter is on the assemblage of the complete and optimal DDS, based on the findings in the previous chapter, including *in vitro* release studies and all in-process validation tests. Included herein is the characterisation of the final formulation.

5.2 Materials and Methods

5.2.1 Materials

The materials used in this Chapter are the same as those used in Chapter Five. Only pharmaceutical-grade excipients routinely employed in the pharmaceutical industry were employed in this study.

5.2.2 Preparation of the Drug Delivery System

Different formulations were derived from the investigations in the previous chapter, see Table 5.2 below. Preparation of the DDSs was done as per the method and schematic stipulated in section 4.2.4 and Figure 5.2 respectively.

Table 5.2**:** Resultant formulations.

	F1	**F2**	**F3**
IR Layer	IR_3	IR_3	IR_3
Plug	P1	P2	P2
Core	C2	C2	C2
DR cup Layer	DR3	DR3	DR4
Total Theoretical Weight (mg)	**1261.54**	**1186.54**	**1186.54**

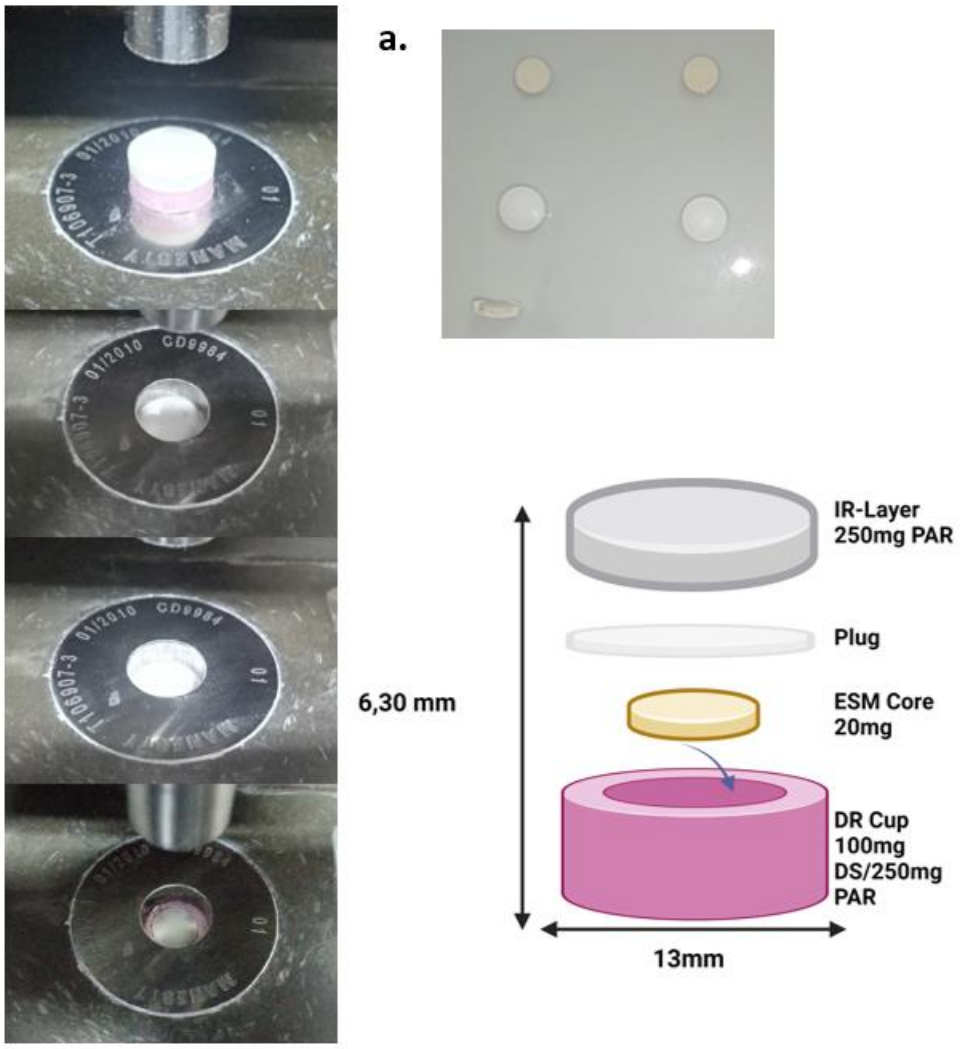

Figure 5.2: Presentation of a. Uncoated and Press-Coated ESM Core Pills; and overall manufacturing procedure.

5.2.3 In-Process Quality Control Evaluation

A range of in-process quality control (IPQC) tests were performed on a sample size of 10 units to ascertain the validity of the manufacturing process. The maximal diametral crushing force was determined through hardness testing on a Hardness Tester (Pharma Test, Hainburg, Germany), using Equation 5.1, the tensile strength of the tablets was subsequently calculated (Juban *et al.,* no date; Vodáčková *et al.,* 2018). Friability was determined on a Friabilator (Erweka D-63150, Heusenstamm, Germany) at 25 rpm for 4 minutes. A digital calliper of 25 x 0.01 mm capacity (Taizhou hangyu tools gauge and blades Co., Ltd., Wenqiao, Zhejiang, China) was used to determine the thickness of the matrices. Content uniformity is a fundamental quality attribute for tablets with set limits for deviations, nonetheless, if the drug component forms the greater part of the tablet, weight variation evaluations can be used to assess drug dose variations. Any variation in weight is indicative of API variation, the opposite is thus true for low drug-loaded formulations (Aulton and Taylor, 2013). Weight variation analyses were done by determining the weight of each tablet using an analytical digital balance (Mettler, Model AE 240, Griefensee, Switzerland).

$$TS = \frac{2F}{\pi Dh} \qquad \textbf{Equation 5.1}$$

Where:

$\boldsymbol{TS}$ is the tensile strength (MPa),

$\boldsymbol{F}$ is the crushing force (N),

D is the diameter of the tablet (mm), and

$\boldsymbol{h}$ is the height of the tablet (mm).

5.2.4 Indentation Hardness Test

Analysis was done on the TA.XTplus Texture Analyser (Stable Micro Systems, England) fitted with a 5 mm Spherical Probe and a 5 kg load cell. The indentation hardness was represented by a conversion to the Brinell Hardness Number (BHN) (Equation 5.2). The textural settings used to calculate the BHN values are depicted in Table 5.3.

Brinell Hardness Number (BHN): $BHN = \frac{2F}{\pi D(\sqrt{D^2 - d^2})}$ **Equation 5.2**

Where :

F is the force generated from indentation (N),

D, the diameter of the spherical probe indenter (5 mm), and

d the indentation depth (3 mm).

Figure 5.3 depicts a typical force (N) versus distance (mm) graph generated from an indentation test per tablet for the calculation of BHN values.

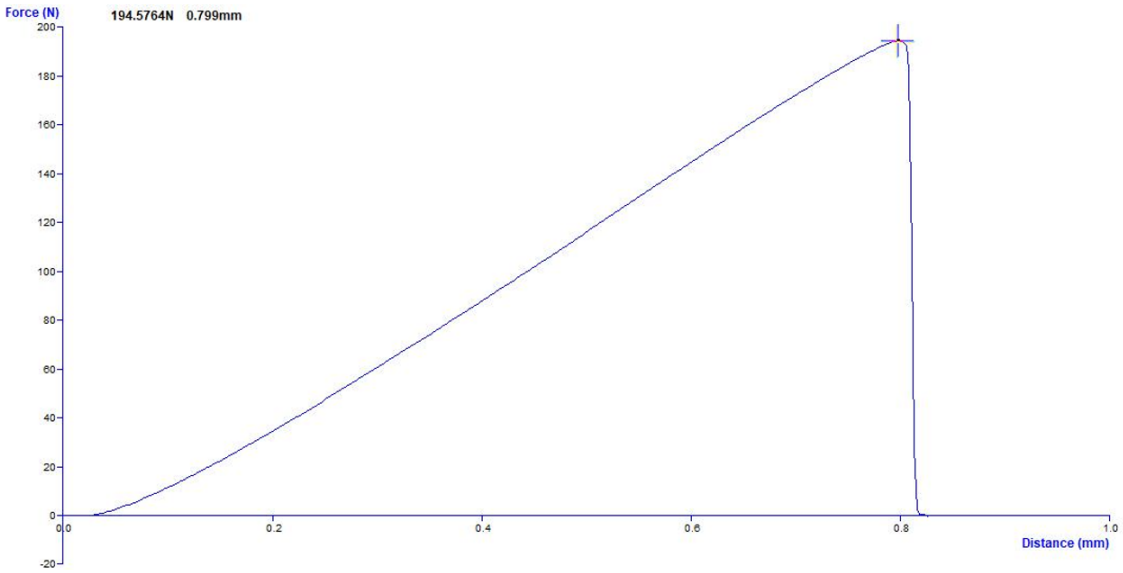

Figure 5.3: Typical Force(N) versus Distance (mm) profile .

Table 5.3: Texture Analyser settings applied.

Test Parameters	Settings
Pre-Test speed	1.00
Test Speed	0.50
Post-test speed	1.00
Compressive distance (mm)	1.00
Trigger Force (N)	5.00

5.2.5 Gravimetric Analysis Through Water Uptake and Erosion Studies

The two hydration characteristics were assessed under the same *in vitro* dissolution conditions stated in Chapter 4, Section 4.2.5, with the exclusion of the IR layer, due to its immediate disintegration. The remainder of the DDS was removed at regular intervals, blotted carefully with tissue paper, and weighed. Equation 5.3 was used to calculate the % water uptake at each removal until a decline in the uptake was observed. Similarly for erosion analysis, the wet tablet samples were withdrawn and oven-dried to a steady weight and using Equation 5.4 the % eroded was calculated.

$$\textbf{Water Uptake} = \frac{W_t - W_i}{W_i} * 100 \qquad \textbf{Equation 5.3}$$

Where:

W_t is the weight at time t, and

W_i is the initial weight of the tablet minus the IR Layer

$$\text{Erosion} = \frac{W_i - W_t}{W_i} * 100 \qquad \text{Equation 5.4}$$

Where:

W_i is the initial weight of the tablet, and

W_t weight of the tablet after drying at interval t.

5.2.6 Determination of polymeric structural variations using Fourier Transmission Infrared spectroscopy

A pulverised tablet sample (F3) was placed on the diamond crystal of an Attenuated Total Reflectance-Fourier Transform Infrared (ATR-FTIR) spectrophotometer equipped with a single reflection diamond MIRTGS detector (PerkinElmer® Spectrum 100 Series FT-IR Spectrometer PerkinElmerLtd., Beaconsfield, UK). Analysis was conducted over a wavenumber range of 6000–450 cm^{-1} at 20 scans.

5.2.7 Determination of the thermal behaviour

Using the same pulverised tablet samples, Thermogravimetry analysis (TGA) was done on the PerkinElmer, TGA 4000 (Llantrisant, Wales, UK). The samples were heated from 30 to 900°C with a 10°C/min heating rate under the continuous flow of nitrogen. Thermograms generated were presented as percentage weight against temperature. DSC analysis was performed on the Mettler-Toledo TC15, TA Controller System (Switzerland) (Mettler DSC 20, Mettler-Toledo AG, Switzerland) equipped with the STARe SW software. An indium calibration was performed for the analyses. Samples of 3 mg to 10 mg were transferred to punctured aluminium pans and sealed immediately. The heating rate was 10 °C per minute and the temperature range captured was 30-300 °C.

5.2.8 Determination of surface morphology using Scanning Electron Microscopy

SEM analysis was done on the SIGMA VP, Zeiss Electron Microscopy, Carl Zeiss Microscopy Ltd; Cambridge, UK. The surface morphology of the tablets was analysed pre- and during dissolution. Sections from the different layers of the dry tablet were carefully cut out, mounted onto stubs with double-sided adhesive carbon tape, and sputter-coated (x2) with both gold and palladium to reduce surface charging and improve conductivity. Samples withdrawn from dissolution were dried completely in an oven at 50°C and likewise coated for analysis. All samples were observed under different magnifications at an accelerated voltage of 5.00 kV.

5.2.9 *In Vitro* Drug Release Analysis

Dissolution studies were carried out as per the method described in Chapter 4, Section 4.2.5, for 24 hours.

5.3 Results

5.3.1 In-Process Quality Control Evaluation

Figure 5.4 shows the general appearances of the tablets and Table 5.4 displays a summary of the results obtained on each physical aspect. The theoretical weights of the tablets as displayed in Table 5.2 above, (including 324.6 mg (IR), 74.10 mg (ESM), 234.10 mg (coated ESM)), translated to upper (5%) and lower (5%) limits of 1324.611-1198.458 mg (F1); 1243.762-1125.308 mg (F2, F3); 77.799-70.390 mg (ESM); 245.799-222.390 mg (coated ESM) respectively, none of the tablets fell outside of these limits. Uniformity in the weight was also confirmed with a % RSD of < 3 % in all cases. The tablets demonstrated dimensional uniformity indicating consistency in tablet press settings with each compression. No separations in the layers were observed after friability assessment, with a % weight loss of less than 1% in all cases. The robustness of the tablets was further confirmed by hardness assessment which was found to be 15.567±0.287 kg for F1, slightly higher than in F2 and F3, attributable to the higher composition of the plug in F1. The same reason may also explain the difference observed in dimensional and weight measurements observed. According to scientific literature (Mužíková *et al.,* 2015), the optimal value of tensile strength of a tablet should lie within the range of 0.56 and 1.12 MPa, this was the case for formulations 1 to 3.

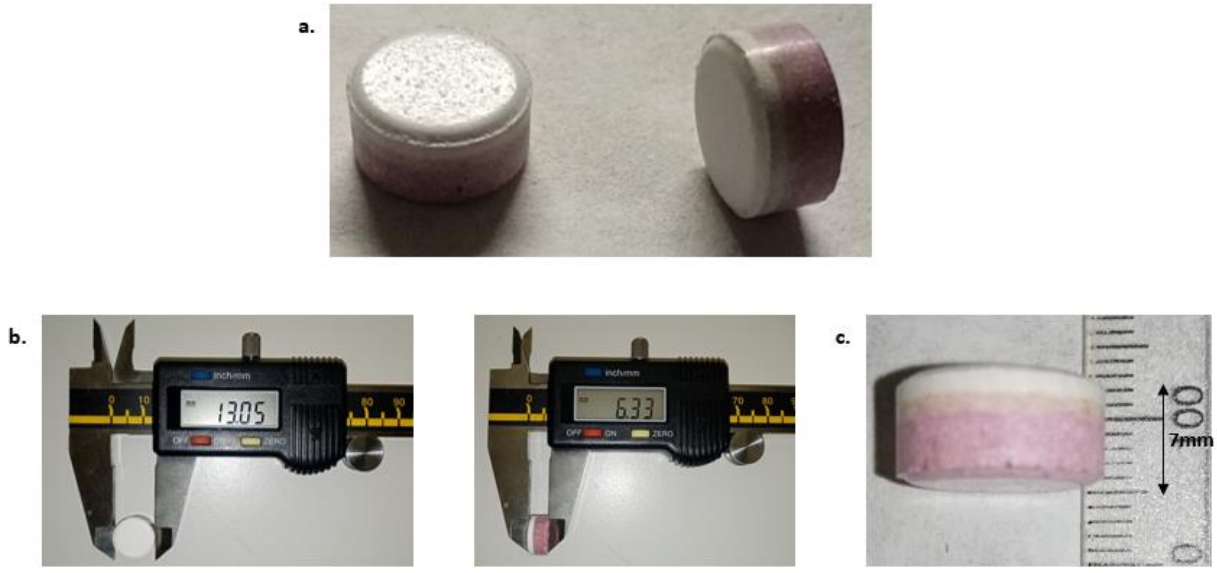

Figure 5.4: Digital images of **a**. the tablet **b.** Digital Calliper measurements of tablet dimensions**, c**. F1, showing the difference in thickness.

Table 5.4: Summary of results from in-process validation tests on tablets ± SD.

	Thickness (mm) (n=10)	Weight (mg) (n=10)	Hardness (kg)	Tensile Strength (MPa)	Friability % (n=10)	Layer integrity
F1	7.10±0.06	1223.91±30.81	15.57±0.29	1.053±0.02	0.41	√
F2	6.31±0.11	1157.33±18.51	14.17±0.13	1.079±0.009	0.43	√
F3	6.3 ±0.10	1171.44±14.38	14.4±0.22	1.097±0.02	0.30	√
Core pill uncoated (C2)	1.22±0.03	71.9±1.40	-	-	-	-
Coated core pill (C2)	3.62±0.06	232.18±1.60	11.27±0.21	2.155±0.04	0.23	√

5.3.2 Indentation Hardness Test

The densification of granules through compression conveys the mechanical strength of the tablet, which steadily declines as the system hydrates through the weakening of mechanical interlocks in the gastrointestinal milieu. An assessment of the force required to produce a dent on the tablet per mm^2 in its dry state is key in predicting the tablets' ability to withstand mechanical stress in the GIT to prevent unwanted erratic tablet erosion, maximizing the chance of more accurate *in vitro-in vivo* correlation. At the set parameters the cups showed significantly high resistance and higher force was generated on F3 (14.24 ± 0.19 N/mm^2) than 1 and 2 (12.39 ± 0.27 N/mm^2), the reason being the decreased amount of HPMC K15M and incorporation of HPMC E50LV. The concentration of matrix-forming polymers such as Eudragit L100-55 and HPMC K15M, particularly high viscosity grades of HPMC, is directly proportional to the mechanical strength of tablet formulations.

5.3.3 Gravimetric Analysis

Hydration behaviour in methocel cellulose ether tablet matrices is characterised by a glassy-to-rubbery state transition of the polymer (surface layer) forming a jelly-like structure around the matrix that keeps the core essentially dry. In the present system, the function of the methyl acrylic polymer (EL 100-55) was more pronounced than that of HPMC, evidenced by the complete lack of visible dissolution of the cup with minimal to no gel layer formation. Hence the incremental water uptake, though minute, and subsequent erosion from the surface in the first 2 hours of the analysis. At higher pH, the rate of water uptake became less than that of erosion, with a gradual decrease in the diameter of the cup, Figure 5.5. Notably, the surface of the core was observed to produce a well-defined jelly-like interface upon hydration. The reason for this behaviour can be ascribed to the fact that EL 100-55, although it cannot

dissolve at a pH below 5.5, possesses a greater affinity for water than EC. Consequently, the elevated concentration of EL 100-55 acted as a contributing factor to the high rate and magnitude of water imbibition supported by (Ranjan, Nayak and Reddy, 2014).

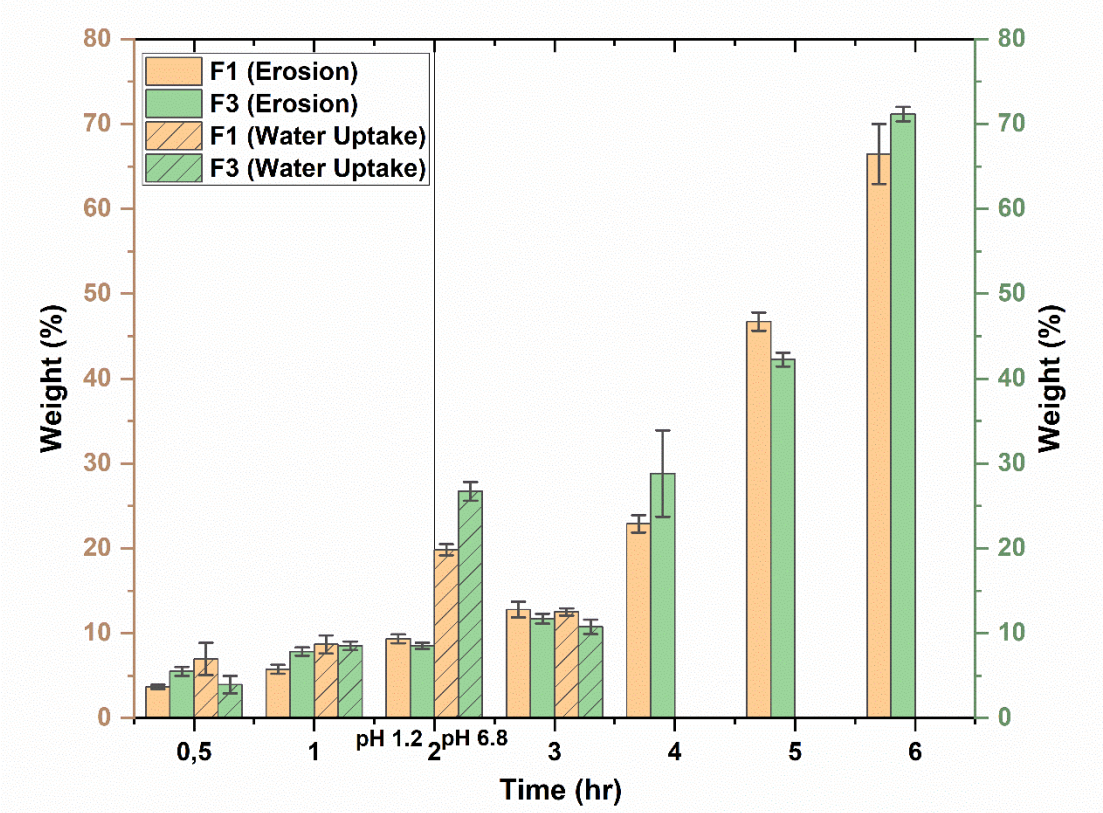

Figure 5.5: Mass gain and loss profiles of the tablets as a function of time.

5.3.4 Polymeric Structural Variations Analysis

The spectrum of the IR layer appears to be an overlap of that of PAR with all the characteristic bands of PAR still distinct in the fingerprint region (1500 cm^{-1} – 500 cm^{-1}) and the single bond O-H, N-H, C-H stretches (3500 cm^{-1} – 3000 cm^{-1}) as shown in Figure 5.6. Whilst DS peaks may have been masked by those of PAR, as the lesser API, the disappearance of certain characteristic peaks of the phenyl group (C=C) stretch at 1577 cm^{-1}, the substituted phenyl group stretch at 748 cm^{-1}, and the shift in characteristic peaks of the carbonyl group (C-O) stretches around 1735 cm^{-1} may be attributed to exhaustive favourable hydrogen bonding between DS and EL 100-55. That includes bonding between C-O of DS and O-H of EL 100-55, C-O of EL 100-55, and N-H of DS. These interactions reflect proper blending at a molecular level and therefore good compatibility (Shen *et al.,* 2011). FTIR spectrum of pure ESM is characterized by the absorption band of benzimidazole ring stretch at 1155 cm^{-1}, amino groups (C-N) in sulfonyl group (S=O) at 1076 cm^{-1}, secondary amine (C=N) in benzimidazole ring and pyridine ring stretched at 1589 cm^{-1} ,and a weak band at 2850–2800 cm^{-1} showing the

presence of a methoxy group at 1614 cm^{-1} (Van Nguyen, Baek and Lee, 2017). However, the ESM formulation spectrum demonstrated a considerable decrease in the intensity and transmittance at the above-mentioned wavelengths, for instance, transmittance values changed from 82.07% to 49.44%, 92.22% to 86.02% at wavelengths 1076 cm^{-1},1589 cm^{-1} respectively, and the 3500 cm^{-1} to 3000 cm^{-1} regions. Overall, no extra peaks were generated in the formulation spectra indicating no interaction of the drugs and excipients employed for each layer, this is consistent with literature findings on similar drug and polymer combinations (Udja, Han and Es, 2001; Malik and Singh, 2012; Swain, Nagamani and Panda, 2015; Van Nguyen, Baek and Lee, 2017; Jendrzejewska *et al.,* 2020).

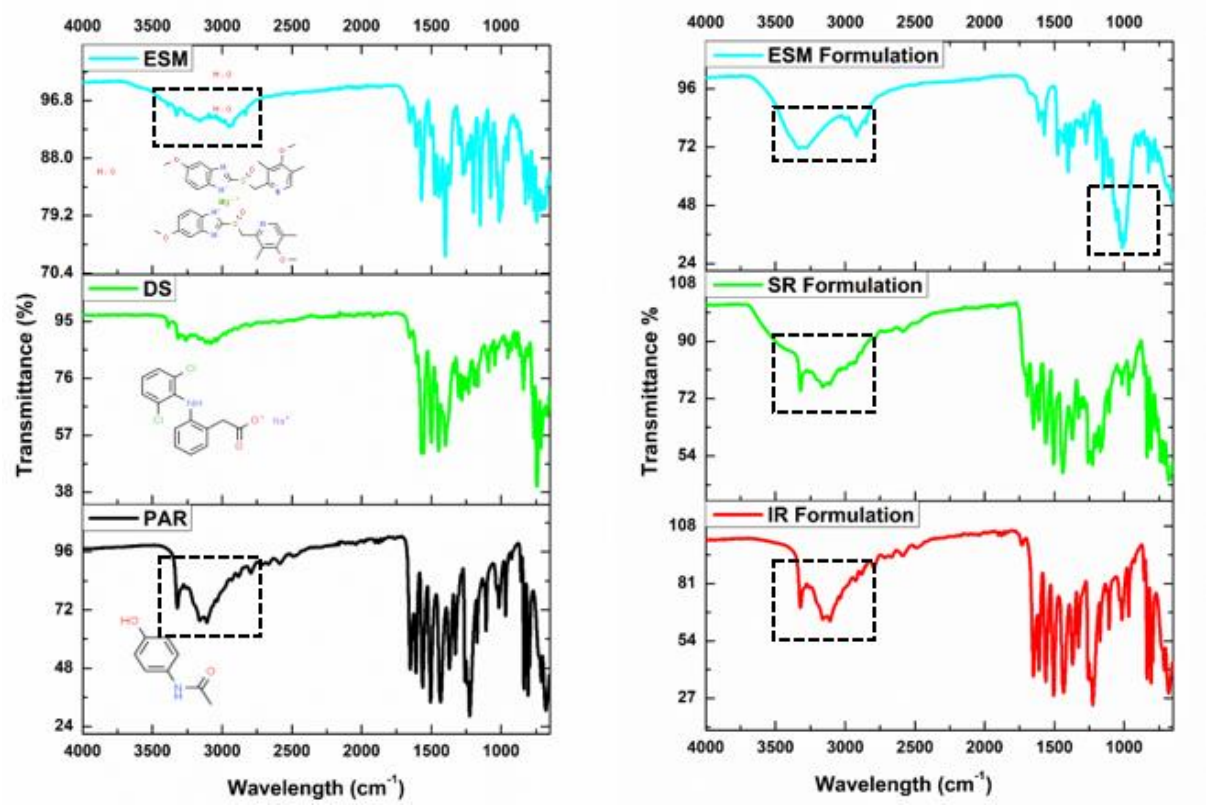

Figure 5.6: FTIR spectra of individual APIS and respective tablet formulation layers.

5.3.5 Determination of the Thermal Behaviour

Table 5.5 shows a comparative summary of DSC integration parameters, for each formulation layer and pure APIs, and corresponding thermograms in Figure 5.8. A <2˚C drop from the initial fusion, melting endothermic peak, characteristic of PAR from 173.06˚C in the IR layer was an indication of good compatibility of the formulation constituents and PAR within the layer. TGA results also affirmed the lack of drug-polymer interactions within the layer, an onset of degradation was observed at around 300°C for both pure drug and formulation, with a lower drop in sample weight to about 20% from 67% in the formulation, Figure 5.7 (Jendrzejewska

et al., 2020). Like the pure drug (ESM), the core formulation TGA curve showed an initial evaporation stage immediately after the heating started, this water loss resulted in a small mass change. In addition, the DSC core thermogram showed an endothermic peak at 153.72˚C, about 9˚C lower than the initially recorded fusion endotherm at 166.44˚C, indicating no relevant chemical or physical interaction between ESM and the entirety of the core constituents up to the studied temperature, consistent with the literature finding (Ferreira *et al.,* 2022; Panti, 2021). PAR being the dominant constituent in the DR cup layer, distinct peaks of DS were masked by those characteristic of PAR.

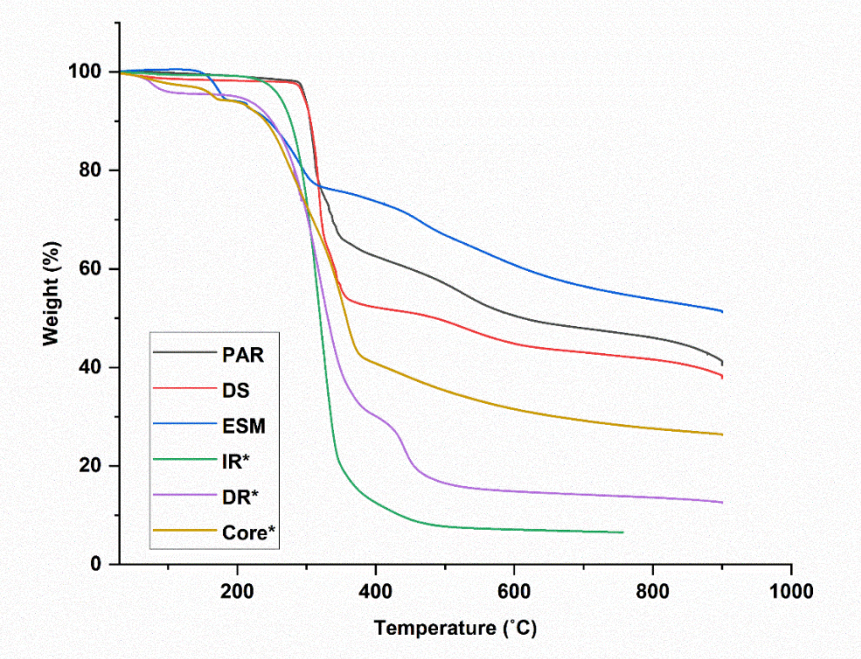

Figure 5.7: TGA thermograms for APIs and respective tablet formulation layers.

Table 5.5: Mean DSC integration data (n=3 samples).

	Mean Integral	Mean Onset Temperature	Mean Peak Temperature	Mean Endset Temperature
	(mJ±SD)	(°C±SD)		
PAR	-1189.76±110.56	169.39±0.31	173.06±0.22	178.36±16
DS	-528.94±75.5	282.69±0.56	289.84±0.53	293.58± 0.72
ESM	-331.17±34.1	164.35±0.11	166.44±0.33	168.71±0.44
IR Layer	-567.48±17.38	165.14±.023	171.55±0.12	176.92±0.93
DR Cup	-623.93±63.40	164.39±0.17	171.66±1.05	177.38±0.84
ESM Core	-264.34±23.39	153.62±1.02	153.72±0.05	157.16±1.41

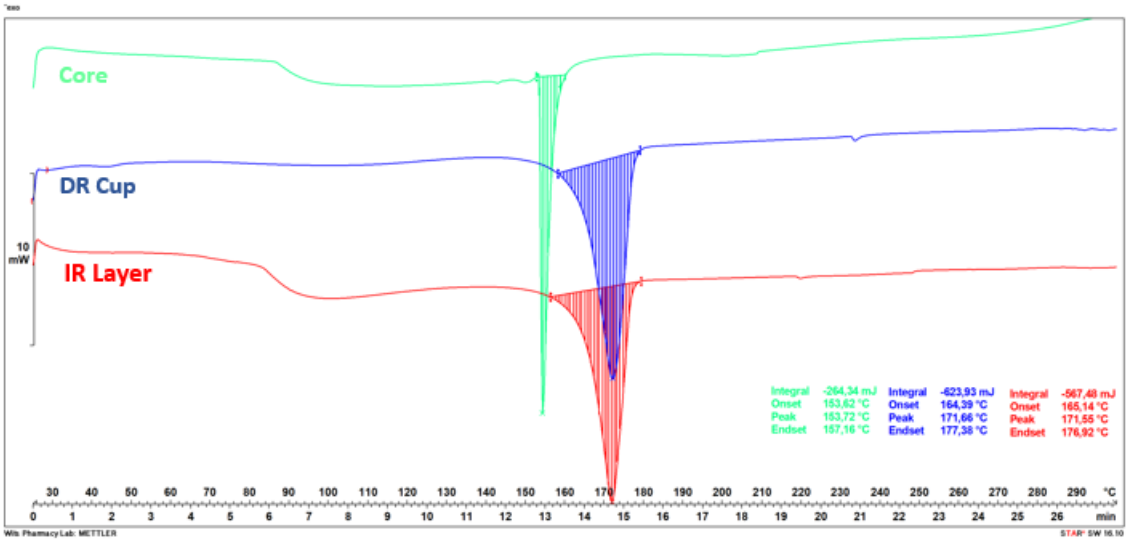

Figure 5.8: DSC thermograms for separate tablet formulation layers.

5.3.6 Determination of Surface Morphology Using Scanning Electron Microscopy

Figure 5.9.a shows the surface morphology for the core coat before dissolution was intact without perforations or troughs whilst b. shows the morphology of the ESM pill two hours into dissolution, at pH 1.2 a cross-sectional view of the core distinctly shows the gel layer and dry core of a fibrous network structure characteristic of MCC (Nasution *et al.,* 2017; Rasheed *et al.,* 2021). At 4 hours (pH 6.8), a fusion of the core contents and the coat was observed, explaining diffusion release mechanisms. A porous, surface view of the IR layer in Figure 5.9.1 comprising cross-linked carmellose sodium (CCS) explains the rapid swelling observed in the adjacent image upon hydration. Progressive deepening of the surface crazing in the cup was observed 2 hours and 4 hours into dissolution as the solvent front entered the matrix slowly towards the centre, indicative of a combination of bulk and surface gradual erosion mechanisms in a chemically controlled release system (Figure 5.1).

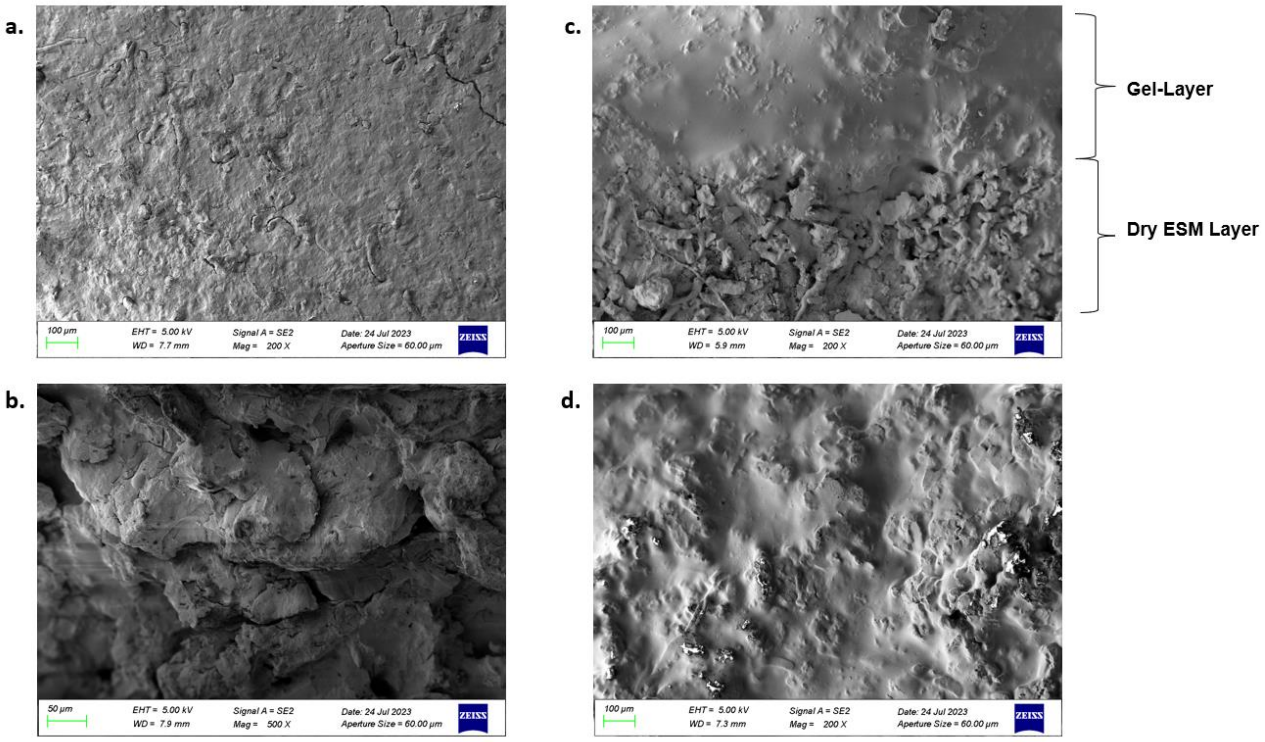

Figure 5.9: SEM Images of the core contents a. Surface view of the press coat, b. cross-sectional view of the ESM pill, c. Cross-sectional view 2 hours into dissolution in SGF, and d. 4 hours into dissolution in SSIF. In all cases, magnification was 200 *X*, except for b (500 *X*) at 5 kV.

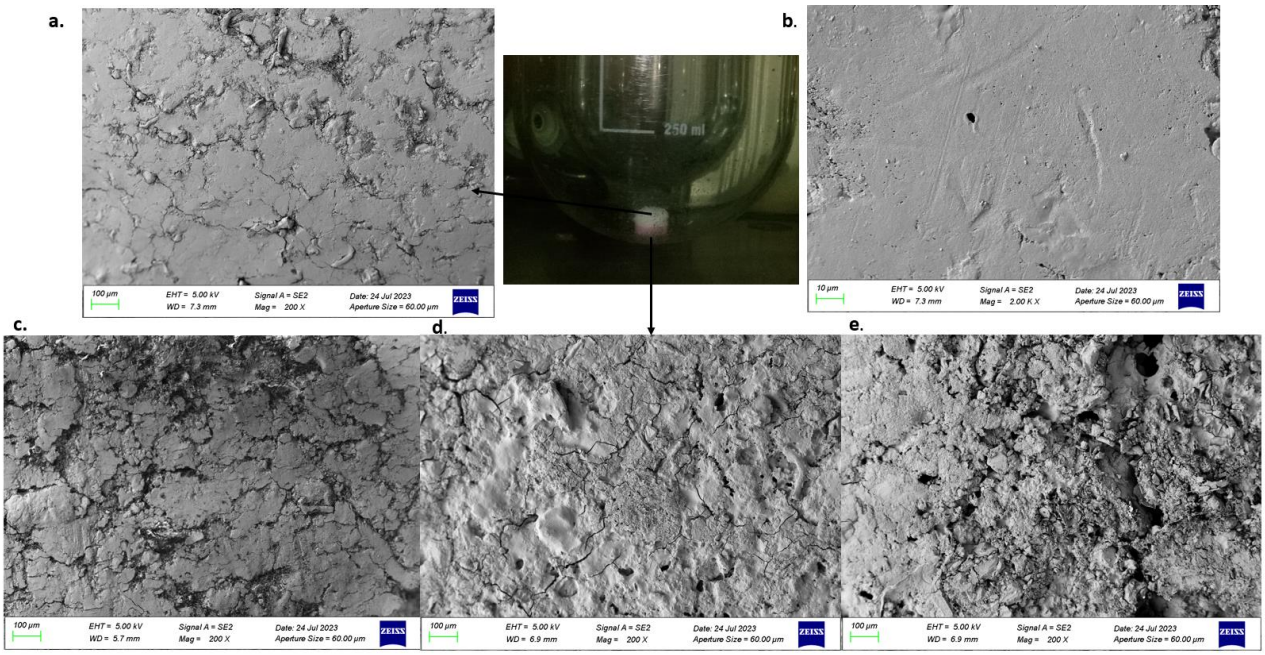

Figure 5.9.1: a. b. SEM images of the IR layer at 200X and 2kX, respectively before dissolution, c. DR cup surface morphology before dissolution, d. 2 hours, and e. 4 hours into dissolution in SGF and SSIF, respectively, at 200*X* magnification at 5kV.

5.3.7 *In Vitro* Drug Release Analysis

The results obtained showed little deviation from those obtained from the preliminary investigations in the previous Chapter**,** Figure 5.9.2. The release profiles were analysed by the regression coefficient method and regression coefficient value (r^2), see Table 5.6 below. ESM release from F1 was most linear in the first-order plots, whilst F2 and F3 zero-order plots showed the highest linearity. The difference may only be attributed to the difference in the barrier layers, where an earlier onset of surface hydration for the core was observed in F2 and F3 than in F1. The release of DS was consistently concentration-dependent (First Order) in all 3 formulations, despite the reduction in HPMC K15M concentration in F3. PAR, on the other hand, exhibited a hampered Fickian diffusion release mechanism deduced from the Kosmeyer Peppas release exponent (*n<0.45*) (Fosca, Rau and Uskoković, 2022).

Although EL 100-55 is insoluble in acidic environment and should prevent dissolution, hydration of the cup's surface may result in the dissolution and release of small amounts of PAR and DS, especially PAR due to its inherently higher solubility (20.3 mg/ml) than DS (0.0012 mg/ml) which resists dissolution at low pH (Kincl *et al.,* 2004; Lance *et al.,* 2005). Thus, the well-defined lag phase in the release of DS and lack thereof in that of PAR after the 50% (250 mg IR) mark, may not be interpreted as zero release of DS within the first 2 hours, evidenced by a mean cumulative release of DS 95.46 % ± 0.70.

Running the experiment for 24 hours allowed the simultaneous assessment of the extent of stability of the drugs in dissolution media. Both PAR and DS showed stability for more than 24 hours, considering each sample withdrawn was not immediately analysed at its withdrawal time. ESM on the contrary, after peaking at about the 8-hour mark started to degrade from about 12 hours, consistent with the pre-formulation stability investigations from Chapter 3.

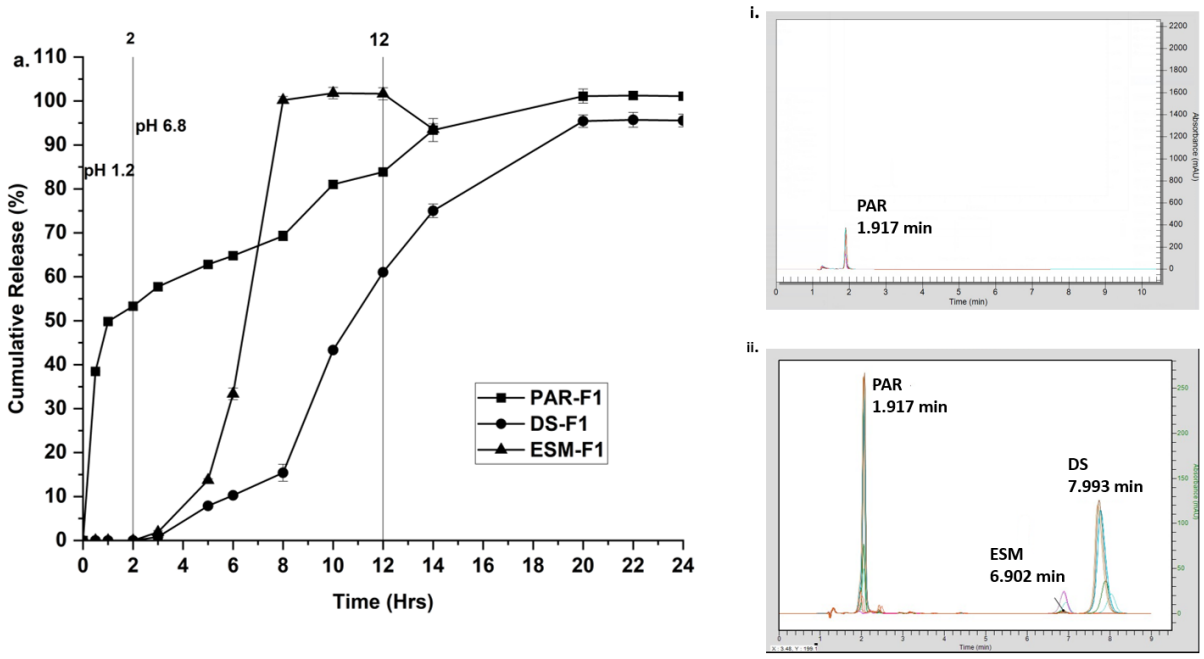
a.
2
12
pH 6.8
pH 1.2
Cumulative Release (%)
Time (Hrs)
PAR-F1
DS-F1
ESM-F1
i.
PAR
1.917 min
ii.
PAR
1.917 min
DS
7.993 min
ESM
6.902 min

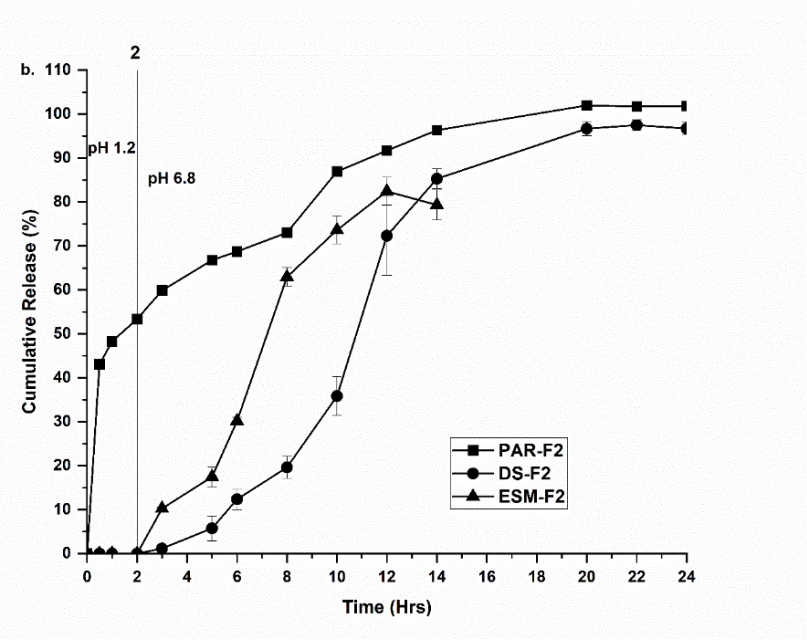
b.
2
pH 1.2
pH 6.8
Cumulative Release (%)
Time (Hrs)
PAR-F2
DS-F2
ESM-F2

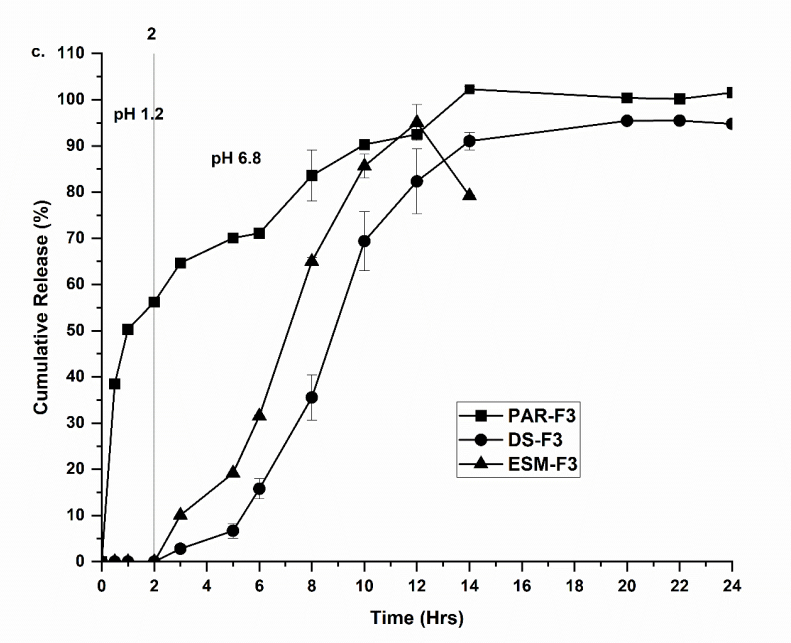

Figure 5.9.2: Cumulative drug release profiles in both SGF and SSIF (n=3) of a. F1 with respective overlain chromatograms showing the retention and detection of i. PAR only from samples withdrawn within the first 2 hours of dissolution and ii. ESM and DS from 2 hours onwards, b. F2 c. F3. Total Cumulative Amount Released, F1 PAR 101.09 % ± 0.80; DS 95,55 % ± 1.46; ESM 93.60 % ± 1.21. F2 101.81 % ±0.28; DS 9.71% ±1.39, ESM 82.43 % ± 3.16, and F3 PAR 101.53% ± 0.51; DS 95.46 % ± 0.70; ESM 95.07% ±3.89.

Table 5.6: Best of fit values for the different kinetic models.

		Zero Order	**First Order**	**Higuchi**	**Korsmeyer-Peppas**
F1	**PAR**	r^2=0.9649 k=5.593	r^2=0.9209 k_1=0.240	r^2=0.9890 k_H=24.048	r^2=0.9832 k=43.475. n=0.269
	DS	r^2=0.9656 k=4.302	r^2=0.9788 k_1=0.068	r^2=0.9752 k_H=16.619	r^2=0.9586 k=2.626. n=1.170
	ESM	r^2=0.9199 k=8.767	r^2=0.9353 k_1=0.136	r^2=0.9300 k_H=24.389	r^2=0.9003 k=3.031. n=1.477
F2	**PAR**	r^2=0.9467 k=5.750	r^2=0.9246 k_1=0.284	r^2=0.9852 k_H=24.840	r^2=0.9852 k=46.181. n=0.258
	DS	r^2=0.9451 k=4.466	r^2=0.9668* k_1=0.073	r^2=0.9668 k_H=17.314	r^2=0.9391 k=3.141. n=1.121
	ESM	r^2=0.9736* k=6.687	r^2=0.9720 k_1=0.095	r^2=0.9714 k_H=18.795	r^2=0.9671 k=2.699. n=1.407
F3	**PAR**	r^2=0.9006 k=5.843	r^2=0.9398 k_1=0.345	r^2=0.9652 k_H=25.420	r^2=0.9825 k=48.862. n=0.245
	DS	r^2=0.8953 k=4.750	r^2=0.9605 k_1=0.088	r^2=0.9340 k_H=18.896	r^2=0.9064 k=6.837. n=0.874
	ESM	r^2=0.9826* k=7.493	r^2=0.9724 k_1=0.109	r^2=0.9760 k_H=20.941	r^2=0.9774 k=2.333. n=1.522

5.4 Conclusion

A drug delivery system was successfully assembled for the simultaneous controlled release of PAR, DS, and ESM. Through in-process quality control tests, the validity of the manufacturing process was confirmed, with all results falling within pharmacopeial specifications. In addition to the deduced release models, the release behaviour from the cup of PAR (excluding the initial 250 mg) and DS from the 2-hour mark, distinctly follows the Hixson-Crowell model where the geometrical characteristic of the cup was maintained with surface erosion as dissolution occurred in planes parallel to the surface (Marcos, 2015). Visuals from SEM analysis, prior and during dissolution confirmed hydration gravimetric analysis results as well as erosion mechanisms. Considerable tensile strength and resistance complemented the overall slow and delayed release from the tablets. The disappearance, appearance, shift of peaks or a significant shift in the melting of the components is indicative of incompatibility. Through characterisation by FTIR and thermal analysis of the tablet formulation components, deleterious drug-polymer or excipient interactions were ruled out.

CHAPTER 6

EX VIVO PERMEABILITY ANALYSIS OF THE DRUG DELIVERY SYSTEM ACROSS PORCINE DUODENAL TISSUE

6.1 Introduction

The ability of a drug compound to pass biological membranes frames its pharmacokinetic profile in the body, i.e., absorption, distribution, excretion, and thus the duration of clinical efficacy. Oral formulations must have acceptable aqueous solubility alongside sufficient intestinal permeability to achieve therapeutic concentrations in the blood. As outlined in the Biopharmaceutics Classification System (BCS), aqueous solubility and membrane permeability are the two key factors that influence the bioavailability of a drug. Class II compounds, e.g., DS and ESM, have high permeability, but their solubility is below the class boundary at one or more pH values, e.g., at low pH for acids; thus, dissolution becomes the rate-limiting step in absorption.

Class III drugs, e.g., PAR, have low permeability and high solubility. The limiting factor in absorption becomes permeation (Kalantzi *et al.,* 2006; Chuasuwan *et al.,* 2008; Parr *et al.,* 2016; Latha, 2018). The inclusion of functional excipients such as cyclodextrin, disintegrants, surfactants, SMEDDS, and SNEDDS into solid dosage forms has been shown to increase bioavailability on many occasions (Kang *et al.,* 2004; Kou *et al.,* 2011; Suryadevara *et al.,* 2017; Conceição *et al.,* 2018; Dun *et al.,* 2018; Chaudhary *et al.,* 2019; van der Merwe *et al.,* 2020).

SLS is a common anionic surfactant whose inclusion in tableting both Class II and III drugs may favour overall bioavailability due to its function as a solubilising agent and permeability enhancer (Alshora *et al.,* 2022). SLS increases the solubility of poorly water-soluble active ingredients by incorporating the drug molecules into the lipophilic cores of the SLS-formed micelles in git fluid (van der Merwe *et al.,* 2020). Another mechanism by which SLS functions as a permeation enhancer is by altering the fluidity/integrity of the apical membrane of the enterocytes, which facilitates passive transcellular diffusion, or increasing the space of the tight junctions, which increases paracellular diffusion (Roos *et al.,* 2019). This explains the logic behind its inclusion in dissolution media instead of the actual formulation; in addition, SLS is a common bile salt surrogate in biorelevant media (Chokshi *et al.,* 2013; Koushik Ahamed, Banik and Salim Hossain, 2013; Silva *et al.,* 2022).

As innovations spike in the development and re-development of oral drug delivery systems, great impetus lies in implementing appropriate screening models with high capacity, low cost, and high predictability of *in vivo* permeability and absorption (Azman *et al.,* 2022). Because approximately 90% of the absorption of orally administered drugs occurs in the small intestinal region, several models and methodologies for intestinal permeability have been set out and tried for forecasting drug absorption in humans (Nunes, Silva and Chaves, 2015). These include *in silico, in* vitro permeation across a monolayer of cultured epithelial cells*, ex vivo* permeation studies using excised human or animal tissue*, and in vivo or in situ* intestinal perfusion studies in human or animal models. Nonetheless, regulatory authorities (e.g., EMA, FDA) continue to enforce the replacement of *in vivo* methods with *in vitro* and/or *ex vivo* models for ethical reasons. Besides, using *ex vivo* and *in vitro* models, particularly at early preclinical developmental stages, minimises the number of animals required, refines methods, and is less time-consuming and laborious (Liza, Nemes and Pet, 2023).

Ex vivo methods for the oral route may be classified into three main models: Diffusion chambers with separated tissue, Everted intestinal sacs, and InTESTine ™ (Masloh *et al.,* 2023). Depending on the direction of the solution flux, diffusion chamber setups can be horizontal (side-by-side), i.e., the Ussing Chamber, or vertical, i.e., the Franz Cell, Figure 6.1 (PermeGear Inc., 2014; Nunes, Silva and Chaves, 2015). Apart from the orientation, the difference in the two systems lies in the source and type of tissue employed; the Ussing Chamber is more suitable for mouse, rat, rabbit, dog, rat, and monkey tissues (Miyake *et al.,* 2017), whilst the Franz Cell is more suitable for thicker and larger surface area tissue, specifically porcine skin and canine buccal mucosa (Castro *et al.,* 2015; Ruela *et al.,* 2016). As the name suggests, everted intestinal sacs involve the use of excised intestinal tissue, 2 – 4 cm everted and tied at one end, filled with a buffer with a blunt needle, closed at the other end, and immersed in a container with an oxygenated solution at 37˚C (Nunes, Silva and Chaves, 2015; Masloh *et al.,* 2023).

The newest to the models is the InTESTine ™, developed to address the low throughput challenges of Diffusion Chambers (TNO, 2015). Equally significant is the overarching limitation of these *ex vivo* systems, that is, their inability to maintain tissue integrity for longer than 2-3 hours, an hour for the everted system; in addition, the Franz Cell does not offer temperature regulation for the donor compartment (Masloh *et al.,* 2023). Despite the drawback, the Franz Cell has been used successfully in assessing the permeability of solid oral formulations (Benetti *et al.,* 2016; Govender *et al.,* 2016)

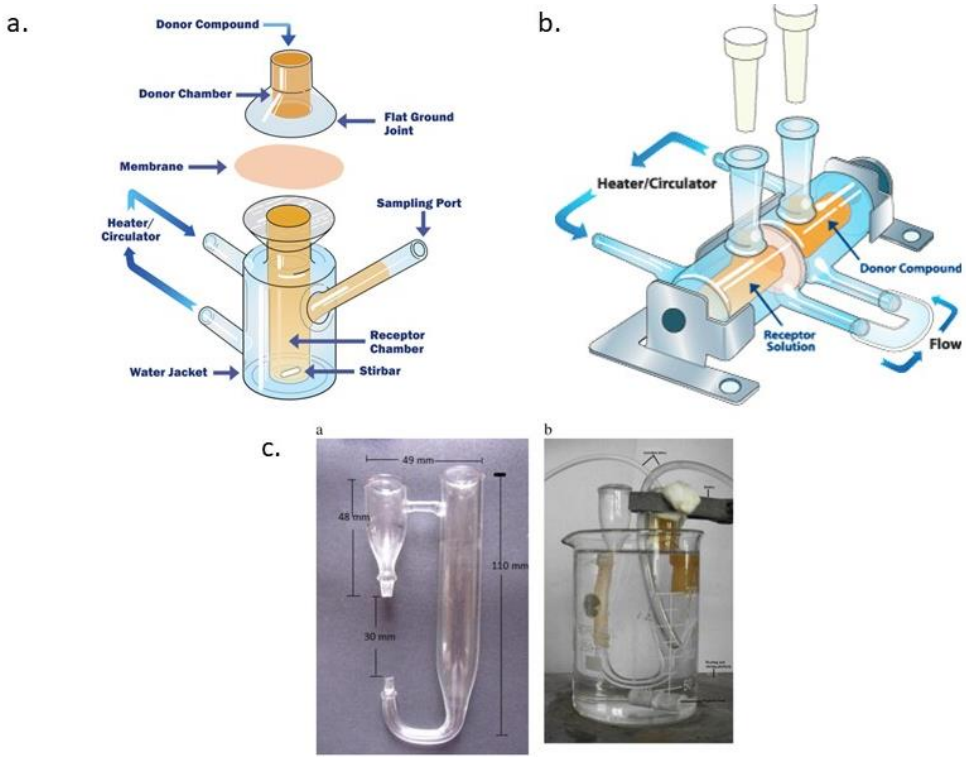

Figure 6.1: a. Oblique view of Franz Cell, b. Oblique view of Side-by-Side Cell, and c. Everted gut sac apparatus with dimensions a. and complete setup b. Reprinted with permission from (Dixit, Jain and Dumbwani, 2012).

Researchers have also demonstrated the use of the in-line flow-through perfusion system as a viable means of determining the git permeability of agents intended for oral administration, e.g., tablets (van Der Bijl and van Eyk, 2003; van Der Bijl, Seifart and van Eyk, 2003). The system is comparable to the vertical diffusion chamber; however, amongst other differences, it offers a permeation area about 5 times smaller than a standard Franz Cell, as shown in Figure 6.2.

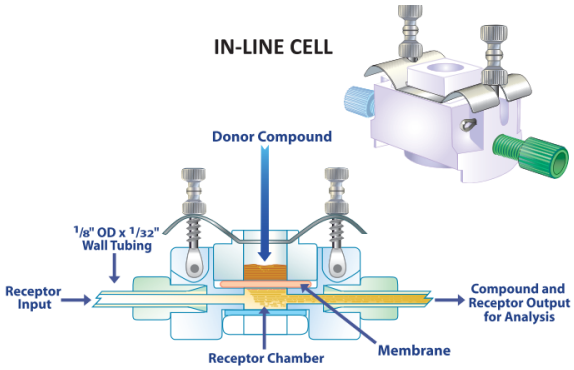

Figure 6.2: Cross-sectional view of an in-line cell with HPLC fittings. Reprinted with permission from (Inc., 2014).

A common observation made from all their findings was that the intestinal mucosa used in this model is not very permeable to molecules with weights (Mw) > 300 Da, with an upper limit of 500 Da, which may present a challenge for analysis of combinatorial solid multi-drug systems with high Mw weight compounds. The drugs in the present study are of Mw 151.2 g/mol (PAR), 318.1 g/mol (DS), and 767.2 g/mol (ESM) in combination; preliminary investigations on the flow-through in-line cell showed results consistent with the findings mentioned above with no penetration of DS and ESM.

Based on the aforementioned elucidations, such as larger surface area and zero detection of DS and ESM from the in-line cell set-up, as well as availability, the model of preference was determined to be the Franz Cell. This section will expound on the methodology applied in evaluating the *ex vivo* permeability characteristics of the drug compounds, in combination, through porcine duodenum.

6. 2 Material and Methods

6.2.1 Materials

The reference standards of paracetamol, diclofenac sodium, and esomeprazole magnesium trihydrate, all polymers and excipients employed, were purchased from Sigma-Aldrich (St. Louis, Missouri, USA). Analytical reagents used included pharmaceutical-grade purified water, Acetonitrile (HPLC grade) (Honeywell Burdick and Jackson, Muskegon, MI, USA), Orthophosphoric acid 85%(w/w) (HPLC grade) (Fluka, St. Louis, Missouri, USA). Excised porcine intestinal mucosa was sourced from Central Animal Services (University of the Witwatersrand, Johannesburg, South Africa).

6.2.2 Tissue Isolation and Preparation

Duodenum specimens were harvested from clinically healthy euthanised pigs. A waiver from the Wits Animal Research Ethics Committee (Waiver 02-06-2023), was obtained prior to tissue collection (Appendix 2). The specimens were transported in phosphate buffered saline (PBS); pH 7.4 within 1 hour, snap-frozen in liquid nitrogen, and stored at – 70°C. Before the start of each experiment, the frozen specimens were equilibrated in phosphate-buffered saline (PBS; pH 7.4) for 30 min at room temperature to thaw completely, after which the serosa and excess connective tissue were trimmed away, using forceps and a scalpel, as shown in Figure 6.3 (Pretorius and Bouic, 2009). The specimens were then carefully cut into 3 equal segments (≈ 4 x 4 cm) fit for the Franz Cell orifice, with a slight overlap.

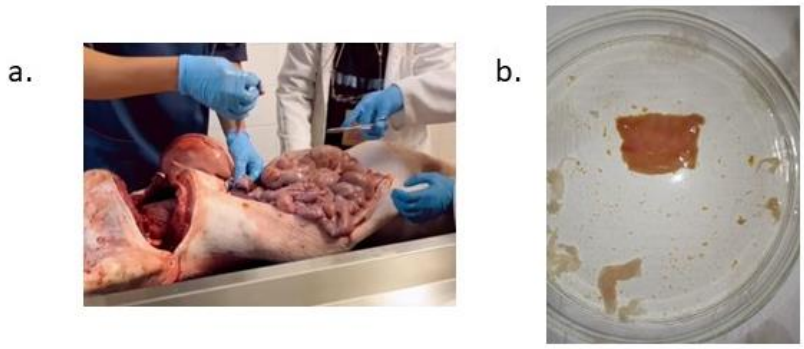

Figure 6.3: Digital Images of a. Specimen collection from euthanised white female pig and b. tissue preparation.

6.2.3 Sample Preparation and Experiment Set-Up

A three-cell Franz Diffusion Cell (FDC) (PermeGear Inc.Bethlehem, PA, USA) apparatus with a diffusion surface area of 1.7 cm², connected to a thermoregulated water bath, was used, Figure 6.4. The 12 ml receptor compartments were filled with PBS pH 7.4 and allowed to heat up to 37˚C. The cut segments were correctly mounted between the donor and receptor compartments, and each donor compartment was equilibrated with pH 6.8 SSIF, containing 1% (w/v) surfactant (SLS) for about 10 minutes. Weighed quantities of pure PAR/DS/ESM in the ratio 25:5:1, respectively, were dispersed in 10 ml of the same media and vortexed for about 15 minutes to provide solvent for the disintegration and dissolution of tablet components. The SSIF in the donor compartments was replaced with 1 ml aliquots of the drug mixture, and parafilm and aluminum foil were used as covers to avoid evaporation and photodegradation, respectively. Similarly, a pulverised tablet (F3) sample was analysed in triplicate (van der Bijl, Seifart and van Eyk, 2003; Govender *et al.,* 2014). The experiments were run for 8 hours, and 400 µl samples were collected at 15-minute intervals for the first 2 hours, followed by 2-hour intervals, and replaced with fresh 37˚C PBS pH 7.4 to maintain sink conditions.

Figure 6.4: Digital image of the Franz-Diffusion apparatus setup utilised for penetration analysis.

6.2.4 Analysis of Permeants

6.2.4.1 HPLC Quantification

Using the method established in Chapter 3, new standard curves were constructed to enable quantification of the low permeant concentrations and the same method was applied in analysing each sample withdrawn (Appendix 3). 0.45 µm nylon syringe filters were used to filter each collected sample before HPLC analysis. Cumulative amount (µg/cm^2) versus time graphs were plotted from the data obtained, Appendix 3 expands on the formula applied in calculating the cumulative amount.

6.2.4.2 Permeability Calculations

The average Steady State Flux (J) (µg/cm^2/min^1), the amount of each drug crossing the membrane per area per time from the cumulative amount per area versus time curves, was calculated from the gradient of the linear portion of the curves, applying the following Equation 6.1:

$$J = \frac{Q}{At} \qquad \textbf{Equation 6.1}$$

Where:

Q is the quantity of each drug that diffused through the intestinal mucosa into the receptor compartment (µg),

A is the area of exposed membrane in 1.767cm^2 , and

t is the drug exposure time to the intestinal mucosa (min) (Choonara and Kondiah, 2017).

The average permeability coefficient (P) (cm/min), representing the velocity of drug passage through the membrane, was calculated using Equation 6.2:

$$P = \frac{C_2 * V}{A * t * C_1} \qquad \textbf{Equation 6.2}$$

Where:

V (mL) is the volume of the acceptor compartment (12mL),

A (cm^2) is the effective permeation area (1.767cm^2),

t (min) is the time interval,

C_1 (µg/ml) is the concentration in the donor compartment, and

C_2 (µg/ml) is the concentration in the receptor compartment (Choonara and Kondiah, 2017).

The average apparent permeability coefficient (P_{app}) (cm/min), which represents the absorption constant, was calculated using Equation 6.3:

$$P_{app} = \frac{dQ/dt}{A*C_0} \qquad \textbf{Equation 6.3}$$

Where:

$\boldsymbol{dQ/dt}$ is the transport rate of each drug that diffused through the intestinal mucosa into the receptor compartment (µg/min),

A is the area of exposed membrane in 1.767cm^2, and

$\boldsymbol{C_0}$ is the initial concentration of each drug investigated in the donor compartment (µg/ml) (Kobus, 2006; Dezani *et al.,* 2013).

Statistical comparison of each set of results per drug, in and out of formulation, was done using ANOVA (Analysis of Variance). Results were considered significantly different when $p < 0.05$.

6.2.5 Integrity Analysis of the Intestinal Mucosa

Spectral images of excised intestinal mucosa samples utilised for the DDS permeation study were obtained before the experiment and at 24 hours. The tissue samples were placed on a diamond crystal of an Attenuated Total Reflectance-Fourier Transform Infrared (ATR-FTIR) spectrophotometer equipped with a single reflection diamond MIRTGS detector (PerkinElmer® Spectrum 100 Series FTIR Spectrometer PerkinElmerLtd., Beaconsfield, UK). Analysis was conducted over a wavenumber range of 6000–450 cm^{-1} at 20 scans.

6.3 Results and Discussion

6.3.1 Permeation Characteristics Analysis

Figure 6.5 a – d shows the cumulative drug permeated vs time profiles of PAR, DS, and ESM combined with and without excipients through porcine duodenal mucosa, as the cumulative amount of permeated drug per cm^2 over time. The profiles exhibited typical infinite dosing permeation behaviour (Selzer *et al.,* 2012), with a continual increase in the amount of drug permeated and no saturation point within the 8 hours. The tablet formulations generally showed similar permeation profiles, especially in the first 2 hours, (but overall lower) than those of the APIs without formulation components. This observation, in conjunction with the relatively high standard deviations, was attributed to the time-dependent formation of a suspension in the unstirred-donor cells, where the subsequently flocculated and floating drug was not available for permeation, resulting in decreased and variable permeability data, particularly in the tablet formulations constituting various formulation components some of

which insoluble. Despite the variations, the *p-values* for each pair of results for PAR, DS, and ESM, respectively were 0.45, 0.11, and 0.05 ≥ 0.05.

The obtained steady state flux rates for each drug both in and out of formulation were 5.63±0.43 (µg/cm^2/min), 8.66±1.03 (µg/cm^2/min) for PAR; 0.14±0.01 (µg/cm^2/min), 0.59±0.13 (µg/cm^2/min) for DS; 0.022±0.0013 (µg/cm^2/min), 0.053±0.006 (µg/cm^2/min) for ESM, respectively. As expected, the molecular weights of each drug correlated with the rate of permeation observed, i.e., PAR>DS>ESM (151.2 Da PAR, 318.1 Da DS, and 767.2 Da ESM). Unlike PAR, DS and ESM exhibited a delay in the onset of permeation with significant detection starting at approximately 1 hour into the experiment.

Although not much data is available for an equitable analogy, the P_{app} for pure PAR, as determined on a Sweetana-Grass diffusion model employing rat intestine, was found to be 3.061 x 10^{-6} cm/s (1,837x 10^{-4} cm/min), higher than the present 1.078x10^{-5} cm/min (Kobus, 2006). The lower permeation may be attributed to factors such as the tissue type, buffer type, donor compartment concentration, apparatus and area of tissue exposed. Considering the *in-vitro* results from the previous chapter, the release/dissolution of PAR is immediate and available for permeation in the gastric mucosa within the first 15 minutes; after that, the rest of the absorption will occur in the small intestinal region. Tables 6.1.a and b summarise the permeability parameters of each drug.

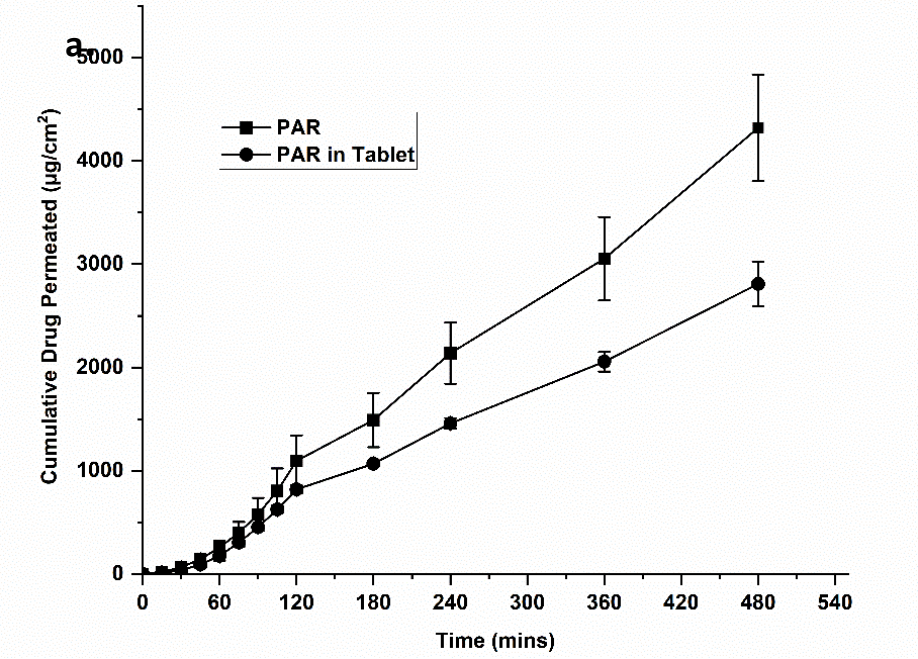

b.

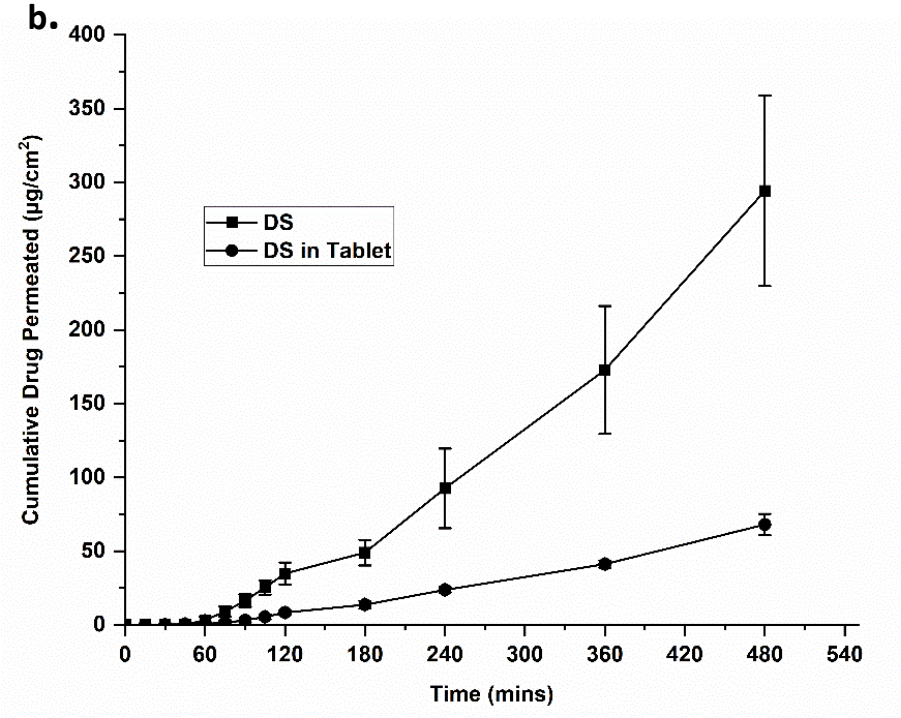
Cumulative Drug Permeated (µg/cm²)
Time (mins)
DS
DS in Tablet
0
50
100
150
200
250
300
350
400
0
60
120
180
240
300
360
420
480
540

c.

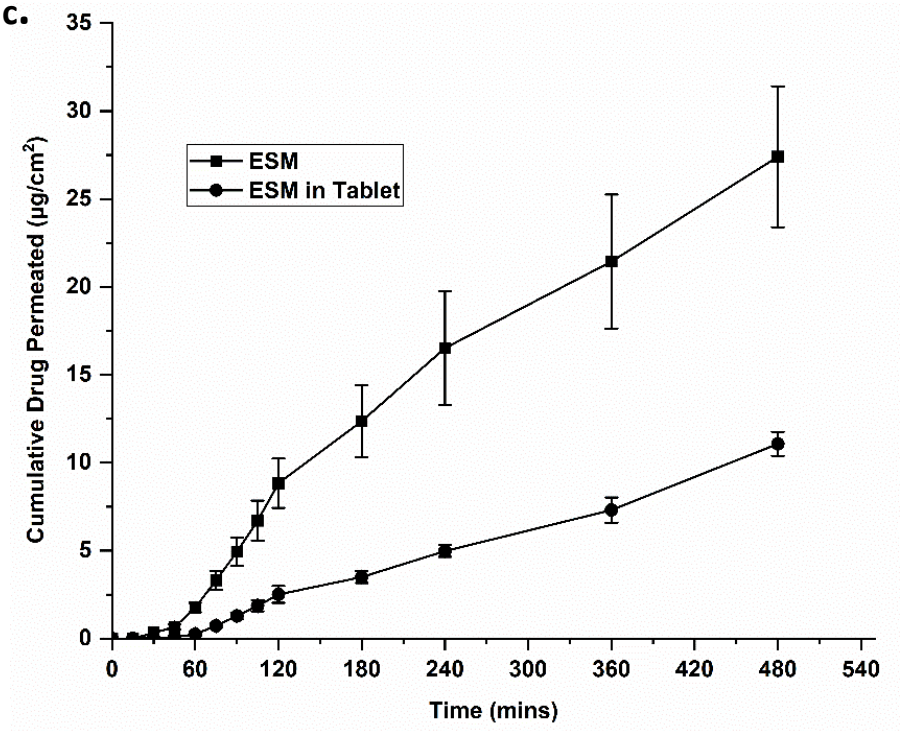
Cumulative Drug Permeated (µg/cm²)
Time (mins)
ESM
ESM in Tablet
0
5
10
15
20
25
30
35
0
60
120
180
240
300
360
420
480
540

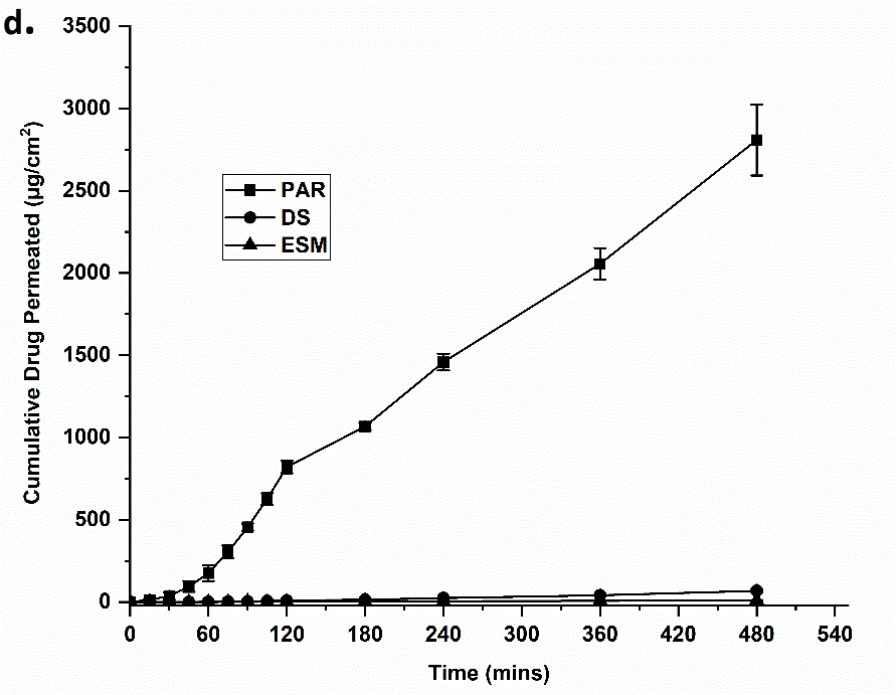

Figure 6.5: Cumulative permeation plots of a. PAR, b. DS, c. ESM in and out of formulation, d. Combined Tablet Plot (n=3).

Table 6.1a: Flux rates and permeability coefficients as determined through *ex vivo* permeation analysis.

	PAR			**DS**			**ESM**		
Cell	**J**	**P**	**P_{app}**	**J**	**P**	**P_{app}**	**J**	**P**	**P_{app}**
1	9.93	1.41×10^{-4}	2.04×10^{-4}	0.70	7.05×10^{-5}	6.84×10^{-5}	0.04	1.43×10^{-5}	3.55×10^{-5}
2	7.39	1.13×10^{-4}	1.78×10^{-4}	0.66	6.61×10^{-5}	6.49×10^{-5}	0.06	1.55×10^{-5}	2.97×10^{-5}
3	8.66	1.27×10^{-4}	1.53×10^{-4}	0.41	4.59×10^{-5}	3.87×10^{-5}	0.06	1.49×10^{-5}	2.39×10^{-5}
Mean	8.66	1.27×10^{-4}	1.78×10^{-4}	0.59	6.09×10^{-5}	5.74×10^{-5}	0.053	1.49×10^{-5}	2.97×10^{-5}
±Std.Dev	1.03	1.13×10^{-5}	2.10×10^{-5}	0.13	1.07×10^{-5}	1.32×10^{-5}	0.006	4.93×10^{-7}	4.77×10^{-6}

J *(µg/cm² /min),* ***P*** *(cm/min),* ***P_{app}*** *(cm/min).*

Table 6.1.b: Flux rates and permeability coefficients as determined through *ex vivo* permeation analysis (in formulation).

	PAR			DS			ESM		
Cell	**J**	**P**	**P_{app}**	**J**	**P**	**P_{app}**	**J**	**P**	**P_{app}**
1	5.77	8.12×10^{-5}	1.26×10^{-4}	0.15	1.56×10^{-5}	1.46×10^{-5}	0.022	9.61×10^{-6}	1.25×10^{-5}
2	6.08	8.68×10^{-5}	1.19×10^{-4}	0.14	1.47×10^{-5}	1.41×10^{-5}	0.023	9.65×10^{-6}	1.21×10^{-5}
3	5.04	5.85×10^{-5}	1.05×10^{-4}	0.12	1.01×10^{-5}	1.18×10^{-5}	0.02	9.07×10^{-6}	1.05×10^{-5}
Mean	5.63	7.55×10^{-5}	1.17×10^{-4}	0.14	1.35×10^{-5}	1.35×10^{-5}	0.022	9.44×10^{-6}	1.17×10^{-5}
±StdDev	0.43	1.22×10^{-5}	8.76×10^{-6}	0.01	2.43×10^{-6}	1.23×10^{-6}	0.0013	2.66×10^{-7}	8.17×10^{-7}

J *(µg/cm² /min),* ***P*** *(cm/min),* ***P_{app}*** *(cm/min).*

6.3.2 Integrity Analysis

The FTIR spectrum obtained after the experiment closely resembled that of the pre-exposed tissue; (Figure 6.6) below indicating maintenance of the intestinal mucosa's integrity throughout the experiment despite its fragile nature. As illustrated in the permeation plots, there was a continual increase in drug content permeating at a reasonably constant rate with no saturation in the intestinal membrane, nor were there leakages into the receptor chamber due to membrane rupture; transport was maintained throughout the run.

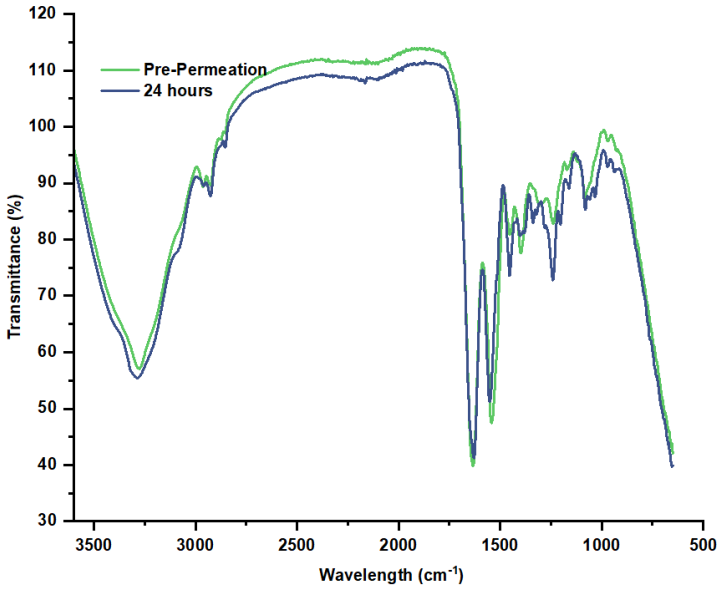

Figure 6.6: FTIR spectra of porcine duodenal tissue, pre- and post-exposure

6.4 Conclusion

The *ex vivo* analysis approach applied was able to successfully demonstrate the simultaneous penetration and permeation of the APIs from the DDS through porcine duodenal tissue as a human surrogate. Comparative analysis of the integrity of the tissue pre- and post-exposure provides further validation of the results obtained. (Kobus, 2006), in his study on the correlation of drug absorption in humans (Fa) to *in vitro* intestinal permeation, substantiated the fact that P_{app} values obtained using intestinal tissue in conventional diffusion models were significantly lower than those from cultured cell monolayers, i.e., Caco-2 models. Unfortunately, the data pool on the transport of various drug compounds that may be used comparatively is limited, consisting mainly of results obtained from Caco-2 cell culture models (Kamiya *et al.*, 2020). Nonetheless, these results may be used to forecast *in vivo* behavior from other *ex vivo/in vitro* models by using tools such as the one presented in Figure 6.7, where shallow and very high values are indicative of poor and good absorption, respectively. At the same time, the shaded intermediate section is a region of ambiguity in *in vivo* outcomes (Lüpfert and Reichel, 2005). Overall, the present results, in conjunction with the dissolution *in-vitro* release results, predict enhanced solubility and permeability of the BCS class II/III drugs in the DDS, which may in turn, have a positive impact on their bioavailability when further evaluated in a suitable *in vivo* model where the dissolution volume, media, motion and temperature are more representative of the human state.

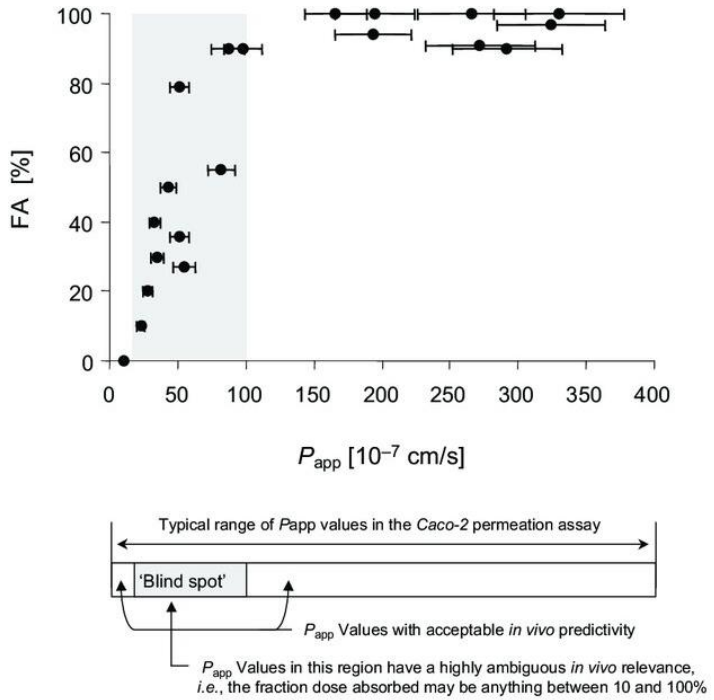

Figure 6.7: Graphical correlation plot of fraction absorbed versus apparent permeability coefficients of compounds observed in many higher throughput pharmacokinetic assays. Reprinted with permission (Lüpfert and Reichel, 2005).

CHAPTER 7

CONCLUSION AND RECOMMENDATIONS

7.1 Conclusion

The origins of the opioid epidemic can be traced back to the founders of Purdue Pharma L.P and their blockbuster prescription opioid OxyContin® from which over 450,000 people have died in the past two decades, with court proceedings still underway (Gale, 2022; Lawrence Hurley, 2023). The global crisis is evidently still a critical concern with documentary series such as Painkiller (2023, Netflix) bringing to the fore the realities of the dangers in prescribing opioid analgesics to opioid-naïve patients for chronic pain. Because the discontinuation of opioid analgesics is impractical, the impetuous lies on the pharmaceutical industry to discover, develop, and re-develop non-addictive medications for long-term pain management as a way of curbing the socio-economic consequences of the crisis, particularly in developing countries (Harker *et al*., 2020).

With the advent of advanced drug-delivery systems (DDSs), the pharmaceutical drug-delivery market is expected to rise from $1430 billion in 2020 to over $2015 billion by 2025, with oral DDSs making up more than 50% of this ever-rising market (Geraili, Xing and Mequanint, 2021b). As industries await the full implementation of the shift from traditional mass compression techniques to more economical on-demand, personalised 3D and 4D printing manufacturing technologies; revamped compression techniques continue to yield innovative controlled release systems.

The present study demonstrated the feasibility and practicality of the tablet design in delivering PAR, DS and ESM in one dosage form, the latter often prescribed separately. The pre-formulation stage in DDS development is not only important for characterisation or ruling out potential drug-excipient interactions but also as reference data for further proof of concept studies. For instance, in the context of this study where Hot Melt Extrusion-Fused Deposition Modelling 3D Printing techniques may be an alternative viable manufacturing technique, data on the thermal thresholds of the drugs in combination with commonly employed functional additives is key.

A publication detailing the proceedings of a workshop held on the future of permeability testing for tablets was recently put out, emphasizing on topics such as the potential effects of excipients on permeability and the use of label and literature data to designate permeability classes. The conclusion reached was the need for further improvements to currently

employed *in vitro* (and/or *ex vivo*) models for evaluating permeability, a more mechanistic approach to incorporating permeability data into physiologic-based pharmacokinetic (PBPK) models and refining tools to measure permeability *in vivo* (Mehta *et al*., 2023).

7.2 Recommendations

Whilst this study followed a proof-of-concept approach, with a clear motivation, many more unexplored non-addictive analgesic combinations are yet to be developed and this design may be efficiently applied. Porcine Intestinal permeability studies have demonstrated a promise of the APIs' systemic bioavailability, as a result, further testing may now be performed in an animal model and subsequently a human model.

REFERENCES

3D printing for healthcare market report 2021-2031. SWOT analysis.:https://www.visiongain.com/report/3d-printing-for-healthcare -market-2021/#download sampe_div111, (accessed 25 September 2021).

Abaci, A., Gedeon, C., Kuna, A., & Guvendiren, M. (2021). Additive Manufacturing of Oral Tablets : Technologies, Materials and Printed Tablets. *Adv Mech Eng;11(2),* 1–271.

Abdulhameed, O., Al-ahmari, A., Ameen, W., & Mian, S. H. (2019). Additive manufacturing : Challenges , trends , and applications. *11*(2), 1–27.

Abushouk, A. I., Sayed, A., Munir, M., Ghanem, E., Abdelfattah, O., Michos, E. D., Mentias, A., Kapadia, S., & Nissen, S. E. (2022). Fixed-Dose Combination (Polypill) for Cardiovascular Disease Prevention: A Meta-Analysis. *American Journal of Preventive Medicine*, *63(3),* 440 -449.

Algahtani, M. S. (2021). Assessment of Pharmacist's Knowledge and Perception toward 3D Printing Technology as a Dispensing Method for Personalized Medicine and the Readiness for Implementation. *Pharmacy, 9(68),*1–14.

Alhnan, M. A., Okwuosa, T. C., Sadia, M., Wan, K., & Ahmed, W. (2016). Emergence of 3D Printed Dosage Forms : Opportunities and Challenges. *Pharmaceutical Research*, 1817–1832.

Al-salloum, I., & Al-sabti, B. (2019). Stability Study of Esomeprazole Preparations in Different Packaging Material Using Stability. *World Journal of Pharmacy and Pharmaceutical Sciences*, *8*(9), 20–25.

Alshora, D. H., Ibrahim, M. A., Zayed, G., Al, M. A., Abou-taleb, H. A., & Ali, M. F. (2022). The role of sodium lauryl sulfate on formulation of directly compressed tablets containing simvastatin and aspirin : Effect on drugs dissolution and gastric mucosa. *Saudi Pharmaceutical Journal*, *30*(5), 635–645.

Alshora, D. H., Ibrahim, M. A., Zayed, G., Al, M. A., Abou-taleb, H. A., & Ali, M. F. (2022). The role of sodium lauryl sulfate on formulation of directly compressed tablets containing simvastatin and aspirin : Effect on drugs dissolution and gastric mucosa. *Saudi Pharmaceutical Journal*, *30*(5), 635–645.

Ammar, H. O., Ghorab, M. M., Felton, L. A., Gad, S., & Fouly, A. A. (2016). Effect of Antiadherents on the Physical and Drug Release Properties of Acrylic Polymeric Films. *AAPS PharmSciTech*, *17*(3), 682–692.

Andreadis, I. I., Gioumouxouzis, C. I., Eleftheriadis, G. K., & Fatouros, D. G. (2022). The Advent of a New Era in Digital Healthcare: A Role for 3D Printing Technologies in Drug Manufacturing? *Pharmaceutics, 14(3).*

Andrews, G. P., Jones, D. S., Senta-Loys, Z., Almajaan, A., Li, S., Chevallier, O., Elliot, C., Healy, A. M., Kelleher, J. F., Madi, A. M., Gilvary, G. C., & Tian, Y. (2019). The development of an inline Raman spectroscopic analysis method as a quality control tool for hot melt extruded ramipril fixed-dose combination products. *International Journal of Pharmaceutics*, *566*, 476–487.

Apeji, Y. E., & Olowosulu, A. K. (2020). Quantifying the effect of glidant on the compaction and tabletting properties of paracetamol granules. *Journal of Research in Pharmacy*, *24*(1), 44–55.

Arany, P., Papp, I., Zichar, M., Csontos, M., Elek, J., Regdon, G., Budai, I., Béres, M., Gesztelyi, R., Fehér, P., Ujhelyi, Z., Vasvári, G., Haimhoffer, Á., Fenyvesi, F., Váradi, J., Miklós, V., & Bácskay, I. (2020). In Vitro Tests of FDM 3D-Printed Diclofenac Sodium-Containing Implants. *Molecules, 25*(24).

Aulton, M. E., & Taylor, K. (2013). Aulton's pharmaceutics : The Design And Manufacture Of Medicines, (4th ed.). Churchill Livingstone/Elsevier.

Awad, A., Fina, F., Trenfield, S. J., Patel, P., Goyanes, A., Gaisford, S., & Basit, A. W. (2019). 3D Printed Pellets (Miniprintlets): A Novel, Multi-Drug, Controlled Release Platform Technology. *Pharmaceutics, 11(4),*148

Awad, A., Tren, S. J., Gaisford, S., & Basit, A. W. (2018). 3D printed medicines: A new branch of digital healthcare. *Pharmaceutics, 548*(4), 586–596.

Azad, M. A., Olawuni, D., Kimbell, G., Badruddoza, A. Z., Hossain, S., & Sultana, T. (2020). Polymers for Extrusion-Based 3D Printing of Pharmaceuticals : A Holistic Materials – Process Perspective. *Pharmaceutics,12(2),*124

Azman, M., Sabri, A. H., Anjani, Q. K., Mustaffa, M. F., & Hamid, K. A. (2022). Intestinal Absorption Study : Challenges and Absorption Enhancement Strategies in Improving Oral Drug Delivery. 1–24.

Banks, J. (2013). Adding Value in Additive Manufacturing : Researchers in the United Kingdom and Europe Look to 3D Printing for Customization. *IEEE Pulse 4(6),* 22–26.

Beamler. (2019). 3D Printing PEEK, PEI and ULTEM. Netherlands. https://www.beamler.com/high-performance- materials-for-3d-printing/, (accessed 9 September 2021).

Beitler, B. G., Abraham, P. F., Glennon, A. R., Tommasini, S. M., Lattanza, L. L., Morris, J. M., & Wiznia, D. H. (2022). Interpretation of regulatory factors for 3D printing at hospitals and medical centers, or at the point of care. *3D Print Med 8(7),* 1–7.

Benetti, C., Flammini, L., Vivo, V., Colombo, P., Colombo, G., Elviri, L., Scarpignato, C., Buttini, F., Bettini, R., Barocelli, E., & Rossi, A. (2016). Esomeprazole immediate-release tablets: Gastric mucosa ex vivo permeation, absorption and antisecretory activity in conscious rats. *Journal of Controlled Release*, *239*, 203–210.

Bhusnure, O. G., Gholve, S. V, Sugave, B. K., Dongre, R. C., Gore, S. A., & Giram, P. S. (2016). 3D Printing & Pharmaceutical Manufacturing: Opportunities and Challenges 3D Printing & Pharmaceutical Manufacturing : Opportunities and Challenges. *International Journal of Bioassays, 5(1),* 4723-4738.

Bijl, P. Van Der, & Eyk, A. D. Van. (2002). Permeability of human intestinal mucosa using a continuous flow-through perfusion system. *235*, 71–78.

Bijl, P. Van Der, & Eyk, A. D. Van. (2003). Comparative in vitro permeability of human vaginal , small intestinal and colonic mucosa. *261*, 147–152.

Bliesner, D. M. (2006). Appendix VI: Template for An Example Methods Validation Protocol. In *Validating Chromatographic Methods* (pp. 169–217). John Wiley & Sons, Inc.

Bloomquist, C. J., Mecham, M. B., Paradzinsky, M. D., Janusziewicz, R., Warner, S. B., Luft, J. C., Mecham, S. J., Wang, A. Z., & DeSimone, J. M. (2018). Controlling release from 3D printed medical devices using CLIP and drug-loaded liquid resins. *Journal of Controlled Release*, *278*, 9–23.

Boyer, C. J., Ballard, D. H., Weisman, J. A., Hurst, S., McGee, D. J., Mills, D. K., Woerner, J. E., Jammalamadaka, U., Tappa, K., & Alexander, J. S. (2018). Three-Dimensional Printing Antimicrobial and Radiopaque Constructs. *3D Printing and Additive Manufacturing*, *5*(1), 29–35.

Boyer, C. J., Woerner, J. E., Galea, C., Gatlin, C. A., Ghali, G. E., Mills, D. K., Weisman, J. A., McGee, D. J., & Alexander, J. S. (2018). Personalized Bioactive Nasal Supports for

Postoperative Cleft Rhinoplasty. *Journal of Oral and Maxillofacial Surgery : Official Journal of the American Association of Oral and Maxillofacial Surgeons*, *76*(7), 1562.e1-1562.e5.

Butler, R. J., Davis, T. K., Johnson, W. G., & Gardner, H. H. (2011). Effects of Nonadherence With Prescription Drugs Among Older Adults. *The American Journal Of Managed Care*,*17*(2), 153–160.

Cabiscol, R., Finke, J. H., Zetzener, H., & Kwade, A. (2018). Characterization of Mechanical Property Distributions on Tablet Surfaces. *Pharmaceutics, 10(4):* 184.

Castle, J. P., Jildeh, T. R., Abbas, M. J., Hennekes, M. E., Buckley, P. J., Shabet, C. L., Cotter, D. L., & Moutzouros, V. (2023). Patient factors influencing the choice of opioid versus non-opioid postoperative analgesia following common sports procedures: a prospective survey study. *Journal of Orthopaedics*, *40*, 1–6.

Castro, P., Madureira, R., Sarmento, B., & Pintado, M. (2015). Tissue-based *in vitro* and *ex vivo* models for buccal permeability studies. In *Concepts and Models for Drug Permeability Studies: Cell and Tissue based in Vitro Culture Models*. Elsevier Ltd, https://doi.org/10.1016/B978-0-08-100094-6.00012-2, (accessed 29 July 2023).

Chadha, R., & Bhandari, S. (2014). Drug-excipient compatibility screening-Role of thermoanalytical and spectroscopic techniques. In *Journal of Pharmaceutical and Biomedical Analysis (87),* 82–97.

Chakraborty, T. (2022). Tablets preparation, Excipients and Tests. *pHarmaVa (google.com),* https://www.researchgate.net/publication/360156539_Tablets_preparation_Excipients_and_Tests, (accessed 2 April 2022).

Challener, C. A. (2018). Selecting Excipients for Controlled Release. *Pharmaceutical Technology,42(7)*,24–26.

Chappidi, S. R., Bhargav, E., Marikunte, V., Chinthaginjala, H., Jyothi, M. V., Pisay, M., Jutur, M., Mahammad, M. S., Poura, M., Yadav, S., & Syed, M. (2019). A cost-effective (QbD) approach in the development and optimization of Rosiglitazone maleate mucoadhesive extended-release tablets – In vitro and ex vivo. *Advanced Pharmaceutical Bulletin*, *9(2),* 281–288.

Chaudhary, S., Aqil, M., Sultana, Y., & Kalam, M. A. (2019). Self-nanoemulsifying drug delivery system of nabumetone improved its oral bioavailability and anti-inflammatory effects in rat model. *Journal of Drug Delivery Science and Technology*, *51*, 736–745.

ChemSpider. (2021). *ChemSpider*. http://www.chemspider.com/Chemical-Structure.1906.html, (accessed 04 August 2023).

Chen, L., Yang, G., & Grosser, T. (2013). Prostanoids and inflammatory pain. *Prostaglandins and Other Lipid Mediators*, *104–105*, 58– 66

Chokshi, H., Miao, H., Tang, K., & Gray, V. (2013). Rationale for Selection of Dissolution Media: Three Case Studies. *Dissolution Technologies, 20(3),*6-13.

Choonara, Y. E., Toit, L. C., Kumar, P., & Kondiah, P. P. D. (2016). 3D-printing and the effect on medical costs : a new era ?. *Expert Rev. Pharmacoecon. Outcomes Res. 16(1),* 23–32.

Chou, P. Y., Chou, Y. C., Lai, Y. H., Lin, Y. T., Lu, C. J., & Liu, S. J. (2021). Fabrication of drug-eluting nano-hydroxylapatite filled polycaprolactone nanocomposites using solution-extrusion 3D printing technique. *Polymers*, *13*(3), 1–13.

Conceição, J., Adeoye, O., Cabral-Marques, H. M., & Lobo, J. M. S. (2018). Cyclodextrins as excipients in tablet formulations. *Drug Discovery Today*, *23*(6), 1274–1284.

Crouter, A., & Briens, L. (2014). The effect of moisture on the flowability of pharmaceutical excipients. *AAPS PharmSciTech*, *15(1),* 65–74.

Cruz, A. T., Garcia-Prats, A. J., Furin, J., & Seddon, J. A. (2018). Treatment of Multidrug-resistant Tuberculosis Infection in Children. *The Pediatric Infectious Disease Journal*, *37*(8), 831–834.

Danckwerts, M. P., & Watt, V. Der. (1998). Zero-Order Release of Theophylline from a Core-in-Cup Tablet. *Drug Development and Industrial Pharmacy* ,*24*(2), 163–167.

Dezani, A. B., Pereira, T. M., Caffaro, A. M., Reis, J. M., & Helena, C. (2013). Journal of Pharmacological and Toxicological Methods Determination of lamivudine and zidovudine permeability using a different ex vivo method in Franz cells. *Journal of Pharmacological and Toxicological Methods*, *67*(3), 194–202.

Di Carlo, M., Smerilli, G., & Salaffi, F. (2021). Mechanisms and Mediators of Pain in Chronic Inflammatory Arthritis. *Current Treatment Options in Rheumatology*, *7*(3), 194–207.

Dixit, P., Jain, D. K., & Dumbwani, J. (2012). Standardization of an ex vivo method for determination of intestinal permeability of drugs using everted rat intestine apparatus. *Journal of Pharmacological and Toxicological Methods*, *65*(1), 13–17.

Domsta, V., & Seidlitz, A. (2021). 3D-Printing of Drug-Eluting Implants : An Overview of the Current Developments Described in the Literature. *Molecules, 26*, 4066.

Dowel, D., Kathleen, R. R., & Christopher M. Jone. (2022). CDC Clinical Practice Guideline for Prescribing Opioids for Pain — United States, 2022 _ MMWR. *Morbidity and Mortality Weekly Report (MMWR)*, *71*(3).

Dressman, J.J., & Kramer, J. (Eds.). (2005). Pharmaceutical Dissolution Testing (1st ed.). CRC Press. https://doi.org/10.1201/9780849359170, (accessed 2 April 2022).

du Toit LC, Kumar P, Choonara YE, Pillay V .4D printing and beyond: where to from here? In: du Toit LC, Kumar P, Choonara YE, Pillay V, editors. Advanced 3d-Printed Systems and Nanosystems for Drug Delivery and Tissue Engineering. (2020). Duxford: Woodhead Publis.

Dun, J., Osei-yeboah, F., Boulas, P., Lin, Y., Sun, C., Dun, J., Osei-yeboah, F., Boulas, P., Lin, Y., Calvin, C., & Harvard, S. E. (2018). A systematic evaluation of dual functionality of sodium lauryl sulfate as a tablet lubricant and wetting enhancer Pharmaceutical Materials Science and Engineering Laboratory, Department of Pharmaceutics, University of Minnesota. *International Journal of Pharmaceutics*, *552(1-2),*139-147.

Dvoretskaya, A. (2020). The uses and prospects for 3D printing in pharmacology. https://www.europeanpharmaceuticalreview.com/article/119865/the-uses-and-prospects-for-3d-printing-in-pharmacology/ *(accessed 10 June 2022).*

Eduardo, D.-T., Ana, S.-E., & José B, F. (2021). A micro-extrusion 3D printing platform for fabrication of orodispersible printlets for pediatric use. *International Journal of Pharmaceutics*, *605*, 120854.

El-bassyouni, G. T. (2020). Advanced 3D-Printed Systems and Nanosystems for Drug Delivery and Tissue Engineering. Duxford: Woodhead Publis.

Eleftheriadis, G. K., & Fatouros, D. G. (2021). Haptic Evaluation of 3D-printed Braille-encoded Intraoral Films. *European Journal of Pharmaceutical Sciences*, *157*, 105605.

ElMeshad, A. N., Abdel-Haleem, K. M., Abdel Gawad, N. A., El-Nabarawi, M. A., & Sheta, N. M. (2020). Core in Cup Ethylmorphine Hydrochloride Tablet for Dual Fast and Sustained Pain Relief: Formulation, Characterization, and Pharmacokinetic Study. *AAPS PharmSciTech*, *21*(7).

Engel-Rebitzer, E., Dolan, A. R., Aronowitz, S. V., Shofer, F. S., Nguemeni Tiako, M. J., Schapira, M. M., Perrone, J., Hess, E. P., Rhodes, K. V., Bellamkonda, V. R.,

Cannuscio, C. C., Goldberg, E., Bell, J., Rodgers, M. A., Zyla, M., Becker, L. B., McCollum, S., & Meisel, Z. F. (2021). Patient Preference and Risk Assessment in Opioid Prescribing Disparities: A Secondary Analysis of a Randomized Clinical Trial. *JAMA Network Open*, *4*(7).

Evonik, N. (2018). An integrated portfolio of functional polymers, delivery technologies and services to release the true value of your oral solid dosage forms. *Oral Drug Delivery Solutions*, 1(07).

Evonik. (2022). *Evonic Eudragit® polymers – defining targeted drug release*. https://healthcare.evonik.com/en/pharmaceuticals/oral-drug-delivery/oral-excipients/eudragit-portfolio/sustained-release, (accessed 2 April 2022).

FabRx. *UK. https://www.fabrx.co.uk/technologies/ (*accessed 10 June 2022).

Farid, N. F., & Abdelaleem, E. A. (2016). Article HPTLC Method for the Determination of Paracetamol, Pseudoephedrine and Loratidine in Tablets and Human Plasma. *Journal of Chromatographic Science*, *54*(4), 647–652.

Fayed, M. H., Mahrous, G. M., Ibrahim, M. A., & Sakr, A. (2013). Influence of Carbopol 71G-NF on the release of dextromethorphan hydrobromide from extended-release matrix tablets. *Pharmaceutical Development and Technology*, *18(5),* 971–981.

FDA. (2022). FDA Takes Steps Aimed at Fostering Development of Non-Addictive Alternatives to Opioids for Acute Pain Management. https://www.fda.gov/news-events/press-announcements/fda-takes-steps-aimed-fostering-development-non-addictive-alternatives-opioids-acute-pain-management (accessed 24 June 2022).

Ferreira, M., Lopes, C. M., Gonçalves, H., Pinto, J. F., & Catita, J. (2022). Personalised Esomeprazole and Ondansetron 3D Printing Formulations in Hospital Paediatric Environment: I-Pre-Formulation Studies. *Applied Sciences*, *12*(20).

Fosca, M., Rau, J. V., & Uskoković, V. (2022). Factors influencing the drug release from calcium phosphate cements. *Bioactive Materials*,(7),341–363.

Freo, U. (2022). Paracetamol for multimodal analgesia. *Pain Management*, *12*(6), 737–750.

Gale, M. (2022). Sacklers Sacked But Purdue Still Caused Opioid Epidemic. https://www.ncbi.nlm.nih.gov/pmc/articles/PMC9339402/ (accessed 2 September 2023).

Gaziano, T. A., Opie, L. H., & Weinstein, M. C. (2006). Cardiovascular disease prevention with a multidrug regimen in the developing world: a cost-effectiveness analysis. *Lancet (London, England)*, *368*(9536), 679–686.

Gbureck, U., Vorndran, E., Müller, F. A., & Barralet, J. E. (2007). Low temperature direct 3D printed bioceramics and biocomposites as drug release matrices. *Journal of Controlled Release : Official Journal of the Controlled Release Society*, *122*(2), 173–180.

Genina, N., Boetker, J. P., Colombo, S., Harmankaya, N., & Rantanen, J. (2017). Anti-tuberculosis drug combination for controlled oral delivery using 3D printed compartmental dosage forms : From drug product design to in vivo testing. *Journal of Controlled Release*, *268* (10), 40–48.

Geraili, A., Xing, M., & Mequanint, K. (2021). Design and fabrication of drug-delivery systems toward adjustable release profiles for personalized treatment. *VIEW, 2(5).* John Wiley and Sons Inc.

Gioumouxouzis, C. I., Baklavaridis, A., Katsamenis, O. L., Markopoulou, C. K., Bouropoulos, N., Tzetzis, D., & Fatouros, D. G. (2018). A 3D printed bilayer oral solid dosage form combining metformin for prolonged and glimepiride for immediate drug delivery. *European Journal of Pharmaceutical Sciences*, *120*(4), 40–52.

GlobalData Healthcare. Medical Device Network, 3D printing of drugs can revolutionise personalised medicine and improve sustainability. (2021). New York. https://www.medicalde vice-network.com/comment/3d-printing-drugs-personalised-medicine-sustainability/99. Reddy VC, B V, Venkatesh, (accessed 21 September 2021).

González-Bueno, J., Sevilla-Sánchez, D., Puigoriol-Juvanteny, E., Molist-Brunet, N., Codina-Jané, C., & Espaulella-Panicot, J. (2021). Factors Associated with Medication Non-Adherence among Patients with Multimorbidity and Polypharmacy Admitted to an Intermediate Care Center. *International Journal of Environmental Research and Public, 18(18), 9606.*

Gorain, B., Choudhury, H., Pandey, M., Madheswaran, T., Kesharwani, P., & Tekade, R. K. (2018). Chapter 11. Drug–Excipient Interaction and Incompatibilities. *Dosage Form Design Parameters* (Issue January). Elsevier Inc. https://doi.org/10.1016/B978-0-12-814421-3.00011-7

Govender, M., Choonara, Y. E., Van Vuuren, S. F., & Du Toit, L. C. (2014). *Sequential Delivery Of Antibiotics And Probiotics Employing A Dual Release Mechanism*. Thesis Report. https://wiredspace.wits.ac.za/handle/10539/17357, (accessed 2 July 2023).

Govender, M., Choonara, Y. E., van Vuuren, S., Kumar, P., du Toit, L. C., Erlwanger, K., & Pillay, V. (2016). A Dual-Biotic System for the Concurrent Delivery of Antibiotics and Probiotics: In Vitro, Ex Vivo, In Vivo and In Silico Evaluation and Correlation. *Pharmaceutical Research*, *33*(12), 3057–3071.

Goyanes, A., Wang, J., Buanz, A., Telford, R., Gaisford, S., & Basit, A. W. (2015). 3D Printing of Medicines : Engineering Novel Oral Devices with Unique Design and Drug Release Characteristics. *Molecular Pharmaceutics,12,* 4077−4084

Gradman, A. H., Parisé, H., Lefebvre, P., Falvey, H., Lafeuille, M. H., & Duh, M. S. (2013). Initial combination therapy reduces the risk of cardiovascular events in hypertensive patients: A matched cohort study. *Hypertension*, *61*(2), 309–318.

Gross, B. C., Erkal, J. L., Lockwood, S. Y., Chen, C., & Spence, D. M. (2014). Evaluation of 3D printing and its potential impact on biotechnology and the chemical sciences. *Analytical Chemistry*, *86*(7), 3240–3253.

Gu, X., Sun, X., Sun, Y., Wang, J., Liu, Y., Yu, K., Wang, Y., & Zhou, Y. (2021). Bioinspired Modifications of PEEK Implants for Bone Tissue Engineering. *Frontiers in Bioengineering and Biotechnology*, *8*, 631616.

Guedes, J. da S., & Guedes, M. L. da S. (2006). Step-by-Step Analytical Methods Validation and Protocol in the Quality System Compliance Industry. *Revista de Saúde Pública*, *40*(6), 951–961.

Hagrasy, A. S., Cruise, P., Jones, I., & Litster, J. D. (2013). In-line Size Monitoring of a Twin Screw Granulation Process Using High-Speed Imaging. *Journal of Pharmaceutical Innovation*, *8*(2), 90–98.

Harker, N., Lucas, W. C., Laubscher, R., Dada, S., Myers, B., & Parry, C. D. (2020). Is South Africa being spared the global opioid crisis? A review of trends in drug treatment demand for heroin, nyaope and codeine-related medicines in South Africa (2012–2017). *International Journal of Drug Policy*, *83*.

Healy, A. V, Fuenmayor, E., Doran, P., Geever, L. M., Higginbotham, C. L., & Lyons, J. G. (2019). Additive Manufacturing of Personalized Pharmaceutical Dosage Forms via Stereolithography. *Pharmaceutics, 11(12),* 645.

Hilson, M., & Nhonoli, A. M. (1991). Public health associations. In *World Health Forum* (Vol. 12, Issue 4).

Hiremath, P., Nuguru, K., & Agrahari, V. (2018). Material attributes and their impact on wet granulation process performance. In *Handbook of Pharmaceutical Wet Granulation: Theory and Practice in a Quality by Design Paradigm*, (pp. 263–315).

Hobbs, K. M. (2009). Development Of A Novel Rate-Modulated Fixed Dose Analgesic Combination For The Treatment Of Mild To Moderate Pain. Thesis Report.

Horst, D. J. (2018). 3D Printing of Pharmaceutical Drug Delivery Systems. *Archives of Organic and Inorganic Chemical Sciences*, *1*(2), 3–8.

Hummler, H., Page, S., Stillhart, C., Meilicke, L., Grimm, M., Mannaa, M., Gollasch, M., & Weitschies, W. (2023). Influence of Solid Oral Dosage Form Characteristics on Swallowability, Visual Perception, and Handling in Older Adults. *Pharmaceutics*, *15*(4), 151-153.

Huynh, C. T., & Lee, D. S. (2015). Controlled Release. *Encyclopedia of Polymeric Nanomaterials* (pp. 439–449). Springer Berlin Heidelberg.

Hwang, Y.-C., Kang, M., Ahn, C. W., Park, J. S., Baik, S. H., Chung, D. J., Jang, H. C., Kim, K.-A., Lee, I.-K., Min, K. W., Nam, M., Park, T. S., Son, S. M., Sung, Y.-A., Woo, J.-T., Park, K. S., & Lee, M.-K. (2013). Efficacy and safety of glimepiride/metformin sustained release once daily vs. glimepiride/metformin twice daily in patients with type 2 diabetes. *International Journal of Clinical Practice*, *67*(3), 236–243.

ICH. (2009). International Conference On Harmonisation Of Technical Requirements For Registration Of Pharmaceuticals For Human Use Pharmaceutical Development Q8(R2).

ICHQ2R1. (2014). International Conference on Harmonisation. *Encyclopedia of Toxicology: Third Edition*, *2*(November 1994), 1070–1072.

Id, T. E., Abualsamen, M. M., Almomani, B. A., Al-, N. A., & Alali, F. Q. (2021). Acceptance and attitudes toward COVID-19 vaccines: A cross-sectional study from Jordan. *Plos One*, *816*, 1–15.

Inc., P. (2014). Diffusion Testing Fundamentals. *www.Permegear.Com*, (accessed 7 July 2023).

Inzana, J. A., Trombetta, R. P., Schwarz, E. M., Kates, S. L., & Awad, H. A. (2015). 3D printed bioceramics for dual antibiotic delivery to treat implant-associated bone infection. *European Cells & Materials*, *30*, 232–247.

Jain, A., Bansal, K. K., Tiwari, A., Rosling, A., & Rosenholm, J. M. (2018). Role of Polymers in 3D Printing Technology for Drug Delivery - An Overview Role of Polymers in 3D Printing Technology for Drug Delivery - An Overview. *Pharmaceutical Methods, 2(3),*167-172.

Jain, D. K., Jain, N., Charde, R., & Jain, N. (2011). The RP-HPLC method for simultaneous estimation of esomeprazole and naproxen in binary combination. *Pharmaceutical Methods*, *2*(3), 167–172.

Jamróz, W., Szafraniec, J., Kurek, M., & Jachowicz, R. (2018). 3D Printing in Pharmaceutical and Medical Applications – Recent Achievements and Challenges. *Pharm Res, 35*(176).

Jendrzejewska, I., Goryczka, T., Pietrasik, E., Klimontko, J., & Jampilek, J. (2020). X-ray and Thermal Analysis of Selected Drugs Containing Acetaminophen. *Molecules, 25*(24).

Jindal, S., & Dua, K. (2016). Development of Bilayer Tablets with Modified Release of Selected Incompatible Drugs. *Polim Med,46(1),*5-15.

Juban, A., Briançon, S., Puel, F., Hoc, T., & Nouguier-Lehon, C. (2017). Experimental study of tensile strength of pharmaceutical tablets: effect of the diluent nature and compression pressure. *EPJ Web of Conferences, 140,* 13002.

Kadry, H., Wadnap, S., Xu, C., & Ahsan, F. (2019). Digital light processing (DLP) 3D-printing technology and photoreactive polymers in fabrication of modified-release tablets. *European Journal of Pharmaceutical Sciences*, *135*, 60–67.

Kalantzi, L., Reppas, C., Dressman, J. B., Amidon, G. L., Junginger, H. E., Midha, K. K., Shah, V. P., Stavchansky, S. A., & Barends, D. M. (2006). Biowaiver monographs for immediate release solid oral dosage forms: Acetaminophen (Paracetamol). *Journal of Pharmaceutical Sciences*, *95*(1), 4–14.

Kamerman, P. R., Bradshaw, D., Laubscher, R., Pillay-Van Wyk, V., Gray, G. E., Mitchell, D., & Chetty, S. (2020). Almost 1 in 5 South African adults have chronic pain: A prevalence study conducted in a large nationally representative sample. *Pain*, *161*(7), 1629–1635.

Kamiya, Y., Takaku, H., Yamada, R., Akase, C., Abe, Y., Sekiguchi, Y., Murayama, N., Shimizu, M., Kitajima, M., Shono, F., Funatsu, K., & Yamazaki, H. (2020). Determination and prediction of permeability across intestinal epithelial cell monolayer of a diverse range of industrial chemicals/drugs for estimation of oral absorption as a putative marker of hepatotoxicity. *Toxicology Reports*, *7*(10), 149–154.

Kang, B. K., Lee, J. S., Chon, S. K., Jeong, S. Y., Yuk, S. H., Khang, G., Lee, H. B., & Cho, S. H. (2004). Development of self-micro emulsifying drug delivery systems (SMEDDS) for oral bioavailability enhancement of simvastatin in beagle dogs. *International Journal of Pharmaceutics*, *274*(1–2), 65–73.

Kang, J., Zhang, J., Zheng, J., Wang, L., Li, D., & Liu, S. (2021). 3D-printed PEEK implant for mandibular defects repair - a new method. *Journal of the Mechanical Behavior of Biomedical Materials*, *116*, 104335.

Karavasili, C., Gkaragkounis, A., Moschakis, T., Ritzoulis, C., & Fatouros, D. G. (2020). Pediatric-friendly chocolate-based dosage forms for the oral administration of both hydrophilic and lipophilic drugs fabricated with extrusion-based 3D printing. *European Journal of Pharmaceutical Sciences: Official Journal of the European Federation for Pharmaceutical Sciences*, *147*, 105291.

Kassem, T., Sarkar, T., & Nguyen, T. (2022). 3D Printing in Solid Dosage Forms and Organ-on-Chip Applications. *Biosensors,12*(186),1 -17.

Kempin, W., Domsta, V., Grathoff, G., Brecht, I., Semmling, B., Tillmann, S., Weitschies, W., & Seidlitz, A. (2018). Immediate Release 3D-Printed Tablets Produced Via Fused Deposition Modeling of a Thermo-Sensitive Drug. *Pharmaceutical Research*, *35*(6).

Khaled, S. A., Burley, J. C., Alexander, M. R., Yang, J., & Roberts, C. J. (2015a). 3D printing of five-in-one dose combination polypill with defined immediate and sustained release profiles. *International Journal of Pharmaceutics, 217,* 308–314.

Khaled, S. A., Burley, J. C., Alexander, M. R., Yang, J., & Roberts, C. J. (2015b). 3D printing of tablets containing multiple drugs with defined release profiles. *International Journal of Pharmaceutics, 494*, 643–650.

Khan, F., Ahmad, I., Akhtar, M., Rauf, H. A., Altaf, H., & Hayat, M. M. (2016). *RP-HPLC* Method Development And Validation For Simultaneous Determination Of Esomeprazole And Diclofenac Sodium In Pharmaceutical Dosage Forms. *Pharmaceutical Chemistry Journal,49*(11), 788–794.

Khan, Z. (2012). Configuration Of a Multi-Layered Multi-Disk Tablet For Specialized Drug Delivery. Thesis Report.

Kincl, M., Meleh, M., Veber, M., & Vrečer, F. (2004). Study of physicochemical parameters affecting the release of diclofenac sodium from lipophilic matrix tablets. *Acta Chim. Slov* 51.

Kingwell, K. (2022). New non-opioid pain drug pushes through to pivotal trials. *Nat Rev Drug Discov, 21(11),* 783-785.

Kobus., S. (2006). 'A study to correlate drug absorption in humans (Fa) to in vitro intestinal permeation using the sweetana-grass diffusion model', Ph.D. Thesis, North-West University, Potchefstroom.

Korte, C., & Quodbach, J. (2018). Formulation development and process analysis of drug-loaded filaments manufactured via hot-melt extrusion for 3D printing of medicines. *Pharmaceutical Development and Technology*, *23*(10), 1117–1127.

Kou, W., Cai, C., Xu, S., Wang, H., Liu, J., Yang, D., & Zhang, T. (2011). In vitro and in vivo evaluation of novel immediate-release carbamazepine tablets: Complexation with hydroxypropyl-β-cyclodextrin in the presence of HPMC. *International Journal of Pharmaceutics*, *409*(1–2), 75–80.

Koushik Ahamed, S., Banik, S., & Salim Hossain, M. (2013). in-Vitro Release Characterization of Ketorolac Tromethamine Loaded Matrix Tablets. *Ijpsr*, *4*(3).

Kwon, T. K., Kang, J. H., Na, S. B., Kim, J. H., Kim, Y. Il, Kim, D. W., & Park, C. W. (2022). Novel Esomeprazole Magnesium-Loaded Dual-Release Mini-Tablet Polycap: Formulation, Optimization, Characterization, and In Vivo Evaluation in Beagle Dogs. *Pharmaceutics*, *14*(7).

Kwon, T. K., Kang, J. H., Na, S. B., Kim, J. H., Kim, Y. Il, Kim, D. W., & Park, C. W. (2022). Novel Esomeprazole Magnesium-Loaded Dual-Release Mini-Tablet Polycap: Formulation, Optimization, Characterization, and In Vivo Evaluation in Beagle Dogs. *Pharmaceutics*, *14*(7), 1407-1411.

Lance R Shaw, William J Irwin, Tim J Grattan, & Barbara R Conway. (2005). The Effect of Selected Water-Soluble Excipients on the Dissolution of Paracetamol and Ibuprofen. *Drug Dev Ind Pharm,31(6),* 515–525.

Langer, R., Basu, A., & Domb, A. J. (2016). Special issue: Polylactide (PLA) Based Biopolymers. In *Advanced drug delivery reviews* (Vol. 107, pp. 1–2). https://doi.org/10.1016/j.addr.2016.11.002 (accessed 3 August 2021).

Latha, K. (2018). Formulation And Evaluation Of Press Coated Tablets Of Esomeprazole. *World Journal Of Pharmaceutical Research,7,(9),* 1711-1741.

Lawrence Hurley, N. N. (2023). *Supreme Court puts Purdue Pharma bankruptcy deal on hold over Sackler provision.* https://www.nbcnews.com/politics/supreme-court/supreme-court-puts-purdue-pharma-bankruptcy-deal-hold-rcna98148, (accessed 2 July 2023).

Lazzaroni, M., & Porro, G. B. (2009). Management of NSAID-Induced Gastrointestinal Toxicity Focus on Proton Pump Inhibitors. *Drugs, 69 (1),* 51-69.

Li, K., Zhu, M., Xu, P., Xi, Y., Cheng, Z., Zhu, Y., & Ye, X. (2015). Three-dimensionally plotted MBG/PHBHHx composite scaffold for antitubercular drug delivery and tissue regeneration. *Journal of Materials Science. Materials in Medicine*, *26*(2), 102.

Ligon, S. C., Liska, R., Stampfl, J., Gurr, M., & Mülhaupt, R. (2017). Polymers for 3D Printing and Customized Additive Manufacturing. *Chemical Reviews*, *117*(15), 10212–10290.

Liltorp, K., Larsen, T. G., Willumsen, B., & Holm, R. (2011). Solid state compatibility studies with tablet excipients using non-thermal methods. *Journal of Pharmaceutical and Biomedical Analysis*, *55*(3), 424–428.

Lim, S. H., Ng, J. Y., & Kang, L. (2017). Three-dimensional printing of a microneedle array on personalized curved surfaces for dual-pronged treatment of trigger finger. *Biofabrication*, *9*(1), 15010.

Lisa, N. (2021). *Melting Point Theory*. The LibreTexts Libraries, https://chem.libretexts.org/Bookshelves/Organic_Chemistry/Organic_Chemistry_Lab_Techniques_(Nichols)/06%3A_Miscellaneous_Techniques/6.01%3A_Melting_Point/6.1C%3A__Melting_Point_Theory (accessed 04 August 2023).

Liu, J. Y., Zhang, X. X., Huang, H. Y., Lee, B. J., Cui, J. H., & Cao, Q. R. (2018). Esomeprazole magnesium enteric-coated pellet-based tablets with high acid tolerance and good compressibility. *Journal of Pharmaceutical Investigation*, *48*(3), 341–350.

Liza, J., Nemes, D., & Pet, Á. (2023). Recent Options and Techniques to Assess Improved Bioavailability : *In Vitro* and *Ex Vivo* Methods. *Pharmaceutics, 2023; 15(4),*1146.

Lobo, M. S., & Costa, P. (2001). Modelling and comparison of dissolution profiles. *Eur J Pharm Sci,13(2)*, 123–133.

Long, J., Gholizadeh, H., Lu, J., Bunt, C., & Seyfoddin, A. (2017). Application of Fused Deposition Modelling (FDM) Method of 3D Printing in Drug Delivery. *Current Pharmaceutical Design*, *23*(3), 433–439.

López-Jaramillo, P., González-Gómez, S., Zarate-Bernal, D., Serrano, A., Atuesta, L., Clausen, C., Castro-Valencia, C., Camacho-Lopez, P., & Otero, J. (2018). Polypill: an affordable strategy for cardiovascular disease prevention in low-medium-income countries. *Therapeutic Advances in Cardiovascular Disease*, *12*(6), 169–174.

Lubrizol Corporation. Hot melt extrusion, life science. (2019). Cleveland, *1620,* 1–5.

Lukin, I., Musquiz, S., Erezuma, I., Al-tel, T. H., Dolatshahi-pirouz, A., & Orive, G. (2019). Expert Opinion on Drug Discovery Can 4D Bioprinting Revolutionize Drug Development ? *Expert Opinion on Drug Discovery*, *14*(10), 953–956.

Lüpfert, C., & Reichel, A. (2005). Development and application of physiologically based pharmacokinetic-modeling tools to support drug discovery. *Chemistry and Biodiversity*, *2*(11), 1462–1486.

Maclean, N., Khadra, I., Mann, J., Abbott, A., Mead, H., & Markl, D. (2023). Formulation-dependent stability mechanisms affecting dissolution performance of directly compressed griseofulvin tablets. *International Journal of Pharmaceutics*, *631*.

Maity, S., & Sa, B. (2016). Compression-Coated Tablet for Colon Targeting: Impact of Coating and Core Materials on Drug Release. *AAPS PharmSciTech*, *17*(2), 504–515.

Malik, D., & Singh, I. (2012). Formulation and evaluation of press-coated tablets of esomeprazole for colonic delivery. *Asian Journal of Pharmaceutics 6(4),*252

Marcos, L. B. (2015). Mathematical models of drug release. *Strategies to Modify the Drug Release from Pharmaceutical Systems*, 63–86.

Masloh, S., Culot, M., Gosselet, F., Chevrel, A., Scapozza, L., & Labouebe, M. Z. (2023). Challenges and Opportunities in the Oral Delivery of Recombinant Biologics. *Pharmaceutics,15(5),*1415.

Mehta, M., Polli, J. E., Seo, P., Bhoopathy, S., Berginc, K., Kristan, K., Cook, J., Dressman, J. B., Mandula, H., Munshi, U., Shanker, R., Volpe, D. A., Gordon, J., Veerasingham, S., Welink, J., Almeida, S., Gonzalez, P., Painter, D., Tsang, Y. C., … Velagapudi, R. (2023). Drug Permeability - Best Practices for Biopharmaceutics Classification System (BCS)-Based Biowaivers: A workshop Summary Report. In *Journal of Pharmaceutical Sciences*, *112(7),* 1749–1762.

Melchels, F. P. W., Feijen, J., & Grijpma, D. W. (2010). Biomaterials A review on stereolithography and its applications in biomedical engineering. *Biomaterials*, *31*(24), 6121–6130.

Miyake, M., Koga, T., Kondo, S., Yoda, N., Emoto, C., Mukai, T., & Toguchi, H. (2017). Prediction of drug intestinal absorption in human using the Ussing chamber system: A comparison of intestinal tissues from animals and humans. *European Journal of Pharmaceutical Sciences*, *96*, 373–380.

Mohurle, Mr. S. M., J. Asnani, Ms. Dr. A., R. Chaple, Dr. D., Kurian, Mr. J., & G. Bais, Mr. A. (2019). Quality by Design (QbD): An Emerging Trend in Improving Quality and Development of Pharmaceuticals. *Saudi Journal of Medical and Pharmaceutical Sciences*, *05*(12), 1132–1138.

Mužíková, J., Muchová, S., Komersová, A., & Lochař, V. (2015). Compressibility of tabletting materials and properties of tablets with glyceryl behenate. *Acta Pharmaceutica*, *65*(1), 91–98.

Nagaraju, R., Meera, D. S., Kaza, R., Arvind, V. V., & Venkates-, V. (2009). Core-in-Cup Tablet Design of Metoprolol Succinate and its Evaluation for Controlled Release. *Current Drug Discovery Technologies, 6(4),* 299-305.

Najmi, A., & Sultan, M. H. (2022). Mathematical Modeling of Drug Release Kinetics of Different Brands of Rosuvastatin Calcium IR Tablets Marketed in Saudi Arabia. *Dissolution Technologies*, *29(2)*.

Nakajima, R., Watanabe, F., & Kamei, M. (2021). Factors Associated with Medication Non-Adherence among Patients with Lifestyle-Related Non-Communicable Diseases. *Pharmacy, 9(*90),1–11.

Nalwade, S. U., Reddy, V. R., Rao, D. D., & Morisetti, N. Kumar. (2012). A validated stability indicating ultra-performance liquid chromatographic method for determination of impurities in Esomeprazole magnesium gastro-resistant tablets. *Journal of Pharmaceutical and Biomedical Analysis*, *57*(1), 109–114.

Nandi, K., Sen, D. J., Patra, F., & Nandy, B. (2020). *Angle Of Repose Walks On Its Two Legs : Carr Index And Hausner Ratio*. *World Journal of Pharmacy and Pharmaceutical Sciences* ,*9*(5), 1565–1579.

Nasution, H., Yurnaliza, Veronicha, Irmadani, & Sitompul, S. (2017). Preparation and characterization of cellulose microcrystalline (MCC) from fibre of empty fruit bunch palm oil. *IOP Conference Series: Materials Science and Engineering*, *180*(1).

National Library of Medicine. USA. (2021). https://clinicaltrials.gov/ct2/home, (accessed 1 October 2021).

National Library of Medicine. USA. (2021).https://pubmed.ncbi.nlm.nih.gov/?term=3d +printing118, (accessed 21 September 2021).

Ngo, T. T., Hoffman, L., Hoople, G. D., Trevena, W., Shakya, U., & Barr, G. (2020). Surface morphology and drug loading characterization of 3D-printed methacrylate-based polymer facilitated by supercritical carbon dioxide. *The Journal of Supercritical Fluids*, *160*, 104786.

Nunes, R., Silva, C., & Chaves, L. (2015). Tissue-based in vitro and ex vivo models for intestinal permeability studies. In *Concepts and Models for Drug Permeability Studies: Cell and Tissue based in Vitro Culture Models*. (1st ed). Chapter 203-236.

Okwuosa, T. C., Pereira, B. C., Arafat, B., Cieszynska, M., Isreb, A., & Alhnan, M. A. (2017). Fabricating a Shell-Core Delayed Release Tablet Using Dual FDM 3D Printing for Patient-Centred Therapy. *Pharmaceutical Research*, *34*(2), 427–437.

Panti, M. (2021). Influence of the Impregnation Technique on the Release of Esomeprazole from Various *Bioaerogels*, *13(11),* 1-17.

Parfati, N., & Rani, K. C. (2018). The effects of croscarmellose sodium concentration on the physicochemical characteristics of orodispersible tablets of atenolol. *Pharmaciana*, *8*(1), 87.

Parr, A., Hidalgo, I. J., Bode, C., Brown, W., Yazdanian, M., Gonzalez, M. A., Sagawa, K., Miller, K., Jiang, W., & Stippler, E. S. (2016). The Effect of Excipients on the Permeability of BCS Class III Compounds and Implications for Biowaivers. *Pharmaceutical Research*, *33*(1), 167–176.

Paul A Dieppe, Shah Ebrahim, & Peter Jüni. (2004). Lessons From The Withdrawal Of Rofecoxib. *BMJ,329*, 867–8.

Payne, R. A., & Avery, A. J. (2011). Polypharmacy: one of the greatest prescribing challenges in general practice. *The British Journal of General Practice: the journal of the Royal College of General Practitioners, 61(583),* 83–84.

Peppas, N. A., & Narasimhan, B. (2014). Mathematical models in drug delivery: How modelling has shaped the way we design new drug delivery systems. *Journal of Controlled Release*,*190*,75–81.

Pereira, B. C., Isreb, A., Forbes, R. T., Dores, F., & Habashy, R. (2019). European Journal of Pharmaceutics and Biopharmaceutics 'Temporary Plasticiser ': A novel solution to

fabricate 3D printed patient-centred cardiovascular ‘ Polypill ’ architectures. *European Journal of Pharmaceutics and Biopharmaceutics*, *135*(12), 94–103.

PermeGear Inc. (2014). Diffusion Testing Fundamentals. *Www.Permegear.Com*, (accessed 2 July 2023).

pharmaeducation.net. (2023). Difference between Lubricant and Glidant What is the definition of Lubricant vs Glidant? https://pharmaeducation.net/difference-between-lubricant-and-glidant/, (accessed 2 April 2022).

Piepoli, M. F., Hoes, A. W., Agewall, S., Albus, C., Brotons, C., Catapano, A. L., Cooney, M.-T., Corrà, U., Cosyns, B., Deaton, C., Graham, I., Hall, M. S., Hobbs, F. D. R., Løchen, M.-L., Löllgen, H., Marques-Vidal, P., Perk, J., Prescott, E., Redon, J., … Binno, S. (2016). European Guidelines on cardiovascular disease prevention in clinical practice: The Sixth Joint Task Force of the European Society of Cardiology and Other Societies on Cardiovascular Disease Prevention in Clinical Practice. *European Heart Journal*, *37*(29), 2315–2381.

Ponsar, H., Wiedey, R., & Quodbach, J. (2020). Hot-Melt Extrusion Process Fluctuations and their Impact on Critical Quality Attributes of Filaments and 3D-printed Dosage Forms. *Pharmaceutics*, *12*(6).

Poudel, I., Annaji, M., Arnold, R. D., Kaddoumi, A., Shamsaei, N., Lee, S., Pegues, J., Ahmadi, Z., Samani, M. M., Corriveau, K., & Babu, R. J. (2020). Dexamethasone eluting 3D printed metal devices for bone injuries. *Therapeutic Delivery*, *11*(6), 373–386.

Press release. Healthcare 3D printing Market Size 2021 report offers opportunities, challenges, risks and influences factors analysis, and industry trends. Friday. 2021 Jul 30;4:54.AM CDT. https://www.news channelnebraska.com/story/44418826/healthcare-3d-printing- market-size-2021-report-offers-opportunities-challenges-risks-and-influences-factors-analysis, (accessed 21 September 2021).

Pretorius, E., & Bouic, P. J. D. (2009). Permeation of four oral drugs through human intestinal mucosa. *AAPS PharmSciTech*, *10*(1), 270–275.

Przybyła, G. W., Szychowski, K. A., & Gmiński, J. (2021). Paracetamol – An old drug with new mechanisms of action. *Clinical and Experimental Pharmacology and Physiology, 48(1),* 3–19.

Psimadas, D., Georgoulias, P., Valotassiou, V., & Loudos, G. (2012). Molecular Nanomedicine Towards Cancer : *Journal of Pharmaceutical Sciences*, *101*(7), 2271–2280.

Pugliese, R., Beltrami, B., Regondi, S., & Lunetta, C. (2021). Annals of 3D Printed Medicine Polymeric biomaterials for 3D printing in medicine : An overview. *Annals of 3D Printed Medicine*, *2*, 100011.

Rahman, A.N. (2019). HPLC Method for Determination of Paracetamol in Pharmaceutical Formulations and Environmental Water Samples*. Chemical Science Transactions, 8(2),* 237-243.

Raj, B., Surendra, G., Dong, P., & Kim, W. (2021). Cellulose and its derivatives for application in 3D printing of pharmaceuticals. *Journal of Pharmaceutical Investigation*, *51*(1), 1–22.

Rajabi-siahboomi, A. R., & Tiwari, S.B. (2008). Modulation of drug release from hydrophilic matrices. *Pharmaceutical Technology Europe, 20(9).*

Rancis, F., Han, K. L. C., Ung, A. C. T. H., Uen, Y. S., Ustin, J., Ee, E. C. L., Eung, I. K. S. L., Ui, R. J. H., Eung, A. K. L., Ong, I. W. S. W., Ydney, S. C. S., Hung, C., Oseph, J., & Ung, J. Y. S. (2002). Celecoxib Versus Diclofenac and Omeprazole in Reducing the Risk Of Recurrent Ulcer Bleeding In Patients With Arthritis. *N Engl J Med,* 347(26), 1-7.

Ranjan, O. P., Nayak, U. Y., & Reddy, M. S. (2014). Optimization of Chronomodulated Delivery System Coated with a Blend of Ethyl Cellulose and Eudragit L100 by Central Composite Design : In Vitro and In Vivo Evaluation. *Journal of Pharmaceutical Innovation 9(2),*95-105

Rasheed, M., Jawaid, M., Parveez, B., Bhat, A. H., & Alamery, S. (2021). Morphology, structural, thermal, and tensile properties of bamboo microcrystalline cellulose/poly(Lactic acid)/poly(butylene succinate) composites. *Polymers*, *13*(3), 1–15.

Rathbone, M. J. (2012). *Advances in Delivery Science and Technology*. http://www.springer.com/series/8875, (accessed 17 July, 2022).

Reddy, V. C., V., B., Venkatesh, M. P., & Pramod Kumar, T. M. (2020). First FDA Approved 3D Printed Drug Paved New Path for Increased Precision in Patient Care. In *Applied Clinical Research, Clinical Trials and Regulatory Affairs (Discontinued), 7(2),*93–103.

Repka, M. A., Bandari, S., Kallakunta, V. R., Vo, A. Q., Mcfall, H., Pimparade, M. B., & Bhagurkar, A. M. (2018). Melt extrusion with poorly soluble drugs – An integrated review. *International Journal of Pharmaceutics*, *535*(1–2), 68–85.

Robles-martinez, P., Xu, X., Trenfield, S. J., Awad, A., Goyanes, A., Telford, R., Basit, A. W., & Gaisford, S. (n.d.). 3D Printing of a Multi-Layered Polypill Containing Six Drugs Using a Novel Stereolithographic Method. *Pharmaceutics, 11*(274), 1-16.

Roos, C., Dahlgren, D., Sjögren, E., Sjöblom, M., Hedeland, M., & Lennernäs, H. (2019). Effects of absorption-modifying excipients on jejunal drug absorption in simulated fasted and fed luminal conditions. *European Journal of Pharmaceutics and Biopharmaceutics*, 142(5), 387–395.

Ruela, A. L. M., Perissinato, A. G., Lino, M. E. de S., Mudrik, P. S., & Pereira, G. R. (2016). Evaluation of skin absorption of drugs from topical and transdermal formulations. *Brazilian Journal of Pharmaceutical Sciences*, *52(3),* 527–544.

Rycerz, K., Stepien, K. A., Czapiewska, M., Arafat, B. T., Habashy, R., Isreb, A., Peak, M., & Alhnan, M. A. (2019). Embedded 3D Printing of Novel Bespoke Soft Dosage Form Concept for Pediatrics. *Pharmaceutics*, *11*(12).

Safi, S., Thiessen, T., & Schmailzl, K. J. (2018). Acceptance and Resistance of New Digital Technologies in Medicine: Qualitative Study. *JMIR Research Protocols*, *7*(12), e11072.

Sahoo, C. K., Sahoo, N., Rao, S. R. M., Sudhakar, M., & Satyanarayana, K. (2015). A review on controlled porosity osmotic pump tablets and its evaluation. *Bulletin of Faculty of Pharmacy, Cairo University*, *53*, 195–205.

Sahoo, C. K., Sahoo, N. K., Ram, S., Rao, M., & Sudhakar, M. (2015). Madridge Journal of Novel Drug Research Formulation and Optimization of Controlled Porosity Osmotic Pump Tablets of Lamivudine using Sodium Chloride as Osmogen for the Treatment of AIDS. *Madridge J Nov Drug Res,2(1),* 94–101.

Salt, A. (2021). A data set to verify volume and sample removal correction calculations for dissolution testing. *Dissolution Technologies*, *28*(2), 16–20.

Samlayawala, Z. A., & Koradia, S. K. (2014). Development and validation of RP-HPLC method for simultaneous estimation of paracetamol, diclofenac potassium and famotidine in its combined pharmaceutical dosage form. *International Journal of Pharmaceutical Research*, *6*(4), 95–99.

Sateesh. (2017). Compression Coating-an Approach to Colon-Specific Drug Delivery: Review. *Modern Applications of Bioequivalence & Bioavailability*, *1*(3).

Segall, A. I. (2019). Preformulation: The use of FTIR in compatibility studies. *Journal of Innovations in Applied Pharmaceutical Science*, *4*(3), 01–06.

Seidel, M. F., Hügle, T., Morlion, B., Koltzenburg, M., Chapman, V., MaassenVanDenBrink, A., Lane, N. E., Perrot, S., & Zieglgänsberger, W. (2022). Neurogenic inflammation as a novel treatment target for chronic pain syndromes. *Experimental Neurology* (Vol. 356). Academic Press Inc.

Selzer, D., Abdel-mottaleb, M. M. A., Hahn, T., Schaefer, U. F., & Neumann, D. (2012). Finite and infinite dosing : Difficulties in measurements, evaluations and predictions. *Adv Drug Deliv Rev, 65(2),*278-94.

Shah, K. U., & Khan, G. M. (2012). Regulating drug release behavior and kinetics from matrix tablets based on fine particle-sized ethyl cellulose ether derivatives: An in vitro and in vivo evaluation. *The Scientific World Journal*, 842348.

Shahi, S. R., Zadbuke, N. S., Gulecha, B., Shivanikar, S. S., & Shinde, S. B. (2012). Design and development of controlled porosity osmotic tablet of diltiazem hydrochloride. *Journal of Advanced Pharmaceutical Technology & Research*, *3*(4), 229–236.

Shahrubudin, N., Koshy, P., Alipal, J., Kadir, M. H. A., & Lee, T. C. (2020). Challenges of 3D printing technology for manufacturing biomedical products : A case study of Malaysian manufacturing firms. *Heliyon*, *6*(3), e03734.

Shaqour, B., Samaro, A., Verleije, B., Beyers, K., Vervaet, C., & Cos, P. (2020). Production of Drug Delivery Systems Using Fused Filament Fabrication: A Systematic Review. *Pharmaceutics, 12(*6).

Sharma, H., & Medical, S. (2018). Validated RP-HPLC Method For Simultaneous Estimation Of Paracetamol , Pamabrom And Dicyclomine , Hydrochloride In Bulk Dicyclomine Hydrochloride is chemically 2- Dicyclomine Hydrochloride in combination with other drugs. *International Journal of Pharmaceutical Sciences And Research, 7(1),* 316-24.

Sharma, M. C., Sharma, S., Vishwavidyalaya, D. A., & Indore, M. P. (2011). Determination and Validation of UV- Spectrophotometric method for Estimation of Paracetamol and Diclofenac Sodium in Tablet Dosage Forms Using Hydrotropic Solubilizing Agents. *International Journal of PharmTech Research*, *3(1),* 244–247.

Sharma, P. K., Choudhury, D., Yadav, V., Murty, U. S. N., & Banerjee, S. (2022). 3D printing of nanocomposite pills through desktop vat photopolymerization (stereolithography) for drug delivery reasons. *3D Printing in Medicine*, *8(3)*,1–10.

Shen, X., Yu, D., Zhu, L., Branford-White, C., White, K., & Chatterton, N. P. (2011). Electrospun diclofenac sodium loaded Eudragit® L 100-55 nanofibers for colon-targeted drug delivery. *International Journal of Pharmaceutics*, *408*(1–2), 200–207.

Silva, D. A., Davies, N. M., Bou-chacra, N., & Ferraz, H. G. (2022). Update on Gastrointestinal Biorelevant Media and Physiologically Relevant Dissolution Conditions. *Dissolution Technologies, 29(2),*62-75.

Simão, J., Chaudhary, S. A., & Ribeiro, A. J. (2023). Implementation of Quality by Design (QbD) for development of bilayer tablets. *European Journal of Pharmaceutical Sciences*, (*184).*

Sithole, M. N., Oosthuysen, E., Jaarsveld, J. Van, Preez, J. L. D., Plessis, J. Du, & Gerber, M. (2021). Development and validation of an HPLC method to be used for simultaneous detection and quantification of different statins after ex vivo skin diffusion studies. *Die Pharmazie*, *76*(12), 583–587.

Siyawamwaya M., Choonara, Y. E., & Kondiah, P. P. D. (2017). Three-Dimensional Printed Controlled Release Tritherapeutic Tablet (3D CRTT) For The Delivery Of Anti-Hiv Drugs. Thesis Report.

Siyawamwaya, M., Choonara, Y. E., Kondiah, P. P. D., & Toit, L. Du. (2017). A humic acid-polyquaternium-10 stoichiometric self-assembled fibrilla polyelectrolyte complex: Effect of pH on synthesis, characterization, and drug release. *International Journal of Polymeric Materials, 65(11),* 550–560.

Siyawamwaya, M., Toit, L. C., Kumar, P., Choonara, Y. E., Kondiah, P. P. P. D., & Pillay, V. (2019). European Journal of Pharmaceutics and Biopharmaceutics 3D printed, controlled release, tritherapeutic tablet matrix for advanced anti-HIV-1 drug delivery. *European Journal of Pharmaceutics and Biopharmaceutics*, *138*(4), 99–110.

Sokar, M. S., Hanafy, A. S., El-Kamel, A. H., & El-Gamal, S. S. (2013). Pulsatile core-in-cup valsartan tablet formulations: In vitro evaluation. *Asian Journal of Pharmaceutical Sciences*, *8*(4), 234–243.

Srinija, K., & Lakshmi, P. K. (2016). Novel core in cup (In-lay) tablets of lamotrigine for mucoadhesive drug delivery system. *International Current Pharmaceutical Journal 5(2),*9–13.

STANDARD TREATMENT GUIDELINES AND ESSENTIAL MEDICINES LIST FOR SOUTH AFRICA HOSPITAL LEVEL 2015 EDITION. (2015).

Stansbury, J. W., & Idacavage, M. J. (2016). 3D printing with polymers: Challenges among expanding options and opportunities. *Dental Materials : Official Publication of the Academy of Dental Materials*, *32*(1), 54–64.

Stewart, S. A., Domínguez-Robles, J., McIlorum, V. J., Gonzalez, Z., Utomo, E., Mancuso, E., Lamprou, D. A., Donnelly, R. F., & Larrañeta, E. (2020). Poly(caprolactone)-Based Coatings on 3D-Printed Biodegradable Implants: A Novel Strategy to Prolong Delivery of Hydrophilic Drugs. *Molecular Pharmaceutics*, *17*(9), 3487–3500.

Stewart, S. A., Domínguez-Robles, J., McIlorum, V. J., Mancuso, E., Lamprou, D. A., Donnelly, R. F., & Larrañeta, E. (2020). Development of a Biodegradable Subcutaneous Implant for Prolonged Drug Delivery Using 3D Printing. *Pharmaceutics*, *12*(2).

Suryadevara, V., Lankapalli, S. R., Danda, L. H., Pendyala, V., & Katta, V. (2017). Studies on jackfruit seed starch as a novel natural superdisintegrant for the design and evaluation of irbesartan fast-dissolving tablets. *Integrative Medicine Research*, *6*(3), 280–291.

Swain, R. P., Nagamani, R., & Panda, S. (2015). Formulation, in vitro Characterization and Stability Studies of Fast Dispersing Formulation, in vitro Characterization and Stability Studies of Fast Dispersing Tablets of Diclofenac Sodium. *Journal of Applied Pharmaceutical Science, 5(07),* 094-102.

Takka, S., Sakr, A. M., Takka, S., Singh Bharaj, S., & Sakr, A. (2003). Influence of methacrylic acid and hydroxypropylmethylcellulose on the tablet properties and in vitro release of dextromethorphan hydrobromide. *Pharmazie, 58(12),*886-90.

Tanuwijaya, J. (2013). The Effects of Crospovidone and Croscarmellose Sodium as Superdisintegrants On the Characteristics Of Piroxicam Nanoparticles ODT (L-). *International Journal of PharmTech Research,*5(4).

Thakral, S., Thakral, N. K., & Majumdar, D. K. (2013). Eudragit: a technology evaluation. *Expert Opinion on Drug Delivery*, *10*(1), 131–149.

Thanawuth, K., Sutthapitaksakul, L., Konthong, S., & Suttiruengwong, S. (2021). Impact of Drug Loading Method on Drug Release from 3D-Printed Tablets Made from Filaments Fabricated by Hot-Melt Extrusion and Impregnation Processes. *Pharmaceutics,13(1607), 1-13.*

TNO. (2015). InTESTine ™ Study processes that determine intestinal absorption. https://www.tno.nl/media/4327/intestine_food.pdf, (accessed 15 July 2023).

Trenfield, S. J., Awad, A., Goyanes, A., Gaisford, S., & Basit, A. W. (2018). 3D Printing Pharmaceuticals: Drug Development to Frontline Care. *Trends in Pharmacological Sciences*, *39*(5), 440–451.

Trombetta, R. P., Ninomiya, M. J., El-Atawneh, I. M., Knapp, E. K., de Mesy Bentley, K. L., Dunman, P. M., Schwarz, E. M., Kates, S. L., & Awad, H. A. (2019). Calcium Phosphate Spacers for the Local Delivery of Sitafloxacin and Rifampin to Treat Orthopedic Infections: Efficacy and Proof of Concept in a Mouse Model of Single-Stage Revision of Device-Associated Osteomyelitis. *Pharmaceutics*, *11*(2).

Udja, P. T., Han, M. Z. I. K., & Es, E. M. (2001). Thermal Behaviour of Diclofenac Sodium : Decomposition and Melting. *Chem Pharm Bull,49(10),* 1245–1250.

van Der Bijl, P., Seifart, H. I., & van Eyk, A. D. (2003). Permeability of intestinal mucosa to crystalline and tabletted isoniazid (INH) [11]. *South African Medical Journal*, *93*(2), 127–128.

van der Merwe, J., Steenekamp, J., Steyn, D., & Hamman, J. (2020). The role of functional excipients in solid oral dosage forms to overcome poor drug dissolution and bioavailability. *Pharmaceutics*, *12*(5).

van Gils, P. F., Over, E. A. B., Hamberg-van Reenen, H. H., de Wit, G. A., van den Berg, M., Schuit, A. J., & Engelfriet, P. M. (2011). The polypill in the primary prevention of cardiovascular disease: cost-effectiveness in the Dutch population. *BMJ Open*, *1*(2), e000363.

Van Nguyen, H., Baek, N., & Lee, B. J. (2017). Enhanced gastric stability of esomeprazole by molecular interaction and modulation of microenvironmental pH with alkalizers in solid dispersion. *International Journal of Pharmaceutics*, *523*(1), 189–202.

Van Soest, E. M., Sturkenboom, M. C. J. M., Dieleman, J. P., Verhamme, K. M. C., Siersema, P. D., & Kuipers, E. J. (2007). Adherence to gastroprotection and the risk of

NSAID-related upper gastrointestinal ulcers and haemorrhage. *Alimentary Pharmacology and Therapeutics*, *26*(2), 265–275.

Varghese, R., Salvi, S., Sood, P., Karsiya, J., & Kumar, D. (2022). 3D printed medicine for the management of chronic diseases: The road less travelled. *Annals of 3D Printed Medicine*, *5*, 100043.

Ventola, C. L. (2014). *Medical Applications for 3D Printing: Current and Projected Uses*. *39*(10), 704–711.

Vidushi, Y., & Meenakshi B. (2017). A Review On HPLC Method Development And Validation. *RJLBPCS, 2(6),* 166-180.

Vodáčková, P., Vraníková, B., Svačinová, P., Franc, A., Elbl, J., Muselík, J., Kubalák, R., & Solný, T. (2018). Evaluation and Comparison of Three Types of Spray Dried Coprocessed Excipient Avicel® for Direct Compression. *BioMed Research International*, 2739428.

Vorndran, E., Klammert, U., Ewald, A., Barralet, J., & Gbureck, U. (2010). Simultaneous Immobilization of Bioactives During 3D Powder Printing of Bioceramic Drug-Release Matrices. *Advanced Functional Materials*, *20*, 1585–1591.

Wall, M. J., Hill, E., Huckstepp, R., Barkan, K., Deganutti, G., Leuenberger, M., Preti, B., Winfield, I., Carvalho, S., Suchankova, A., Wei, H., Safitri, D., Huang, X., Imlach, W., La Mache, C., Dean, E., Hume, C., Hayward, S., Oliver, J., & Frenguelli, B. G. (2022). Selective activation of Gαob by an adenosine A1 receptor agonist elicits analgesia without cardiorespiratory depression. *Nature Communications*, *13*(1), 6–7.

Wallace, J. L. (2008). *Prostaglandins, NSAIDs, and Gastric Mucosal Protection: Why Doesn't the Stomach Digest Itself?* https://doi.org/10.1152/physrev.00004.2008.-Except

Wang, Y., Yang, M., Shen, R., Shao, S., Chen, L., Gong, W., Shan, L., & Gao, C. (2018). Development of metoprolol tartrate-loaded sustained-release pellets: effect of talc on the mechanism of drug release. *Pharmaceutical Development and Technology*, *23*(7), 664–673.

Webster, R., Castellano, J. M., & Onuma, O. K. (2017). Polypills 2 Putting polypills into practice: challenges and lessons learned. *The Lancet*, *389*(10073), 1066–1074.

Weisman, J. A., Ballard, D. H., Jammalamadaka, U., Tappa, K., Sumerel, J., D'Agostino, H. B., Mills, D. K., & Woodard, P. K. (2019). 3D Printed Antibiotic and Chemotherapeutic

Eluting Catheters for Potential Use in Interventional Radiology: In Vitro Proof of Concept Study. *Academic Radiology*, *26*(2), 270–274.

Wesholowski, J., Hoppe, K., Nickel, K., Muehlenfeld, C., & Thommes, M. (2019). European J1. Melchels FPW, Feijen J, Grijpma DW. Biomaterials A review on stereolithography and its applications in biomedical engineering. *European Journal of Pharmaceutics and Biopharmaceutics*, *142*(1), 396–404.

Weverling, G. J., Lange, J. M., Jurriaans, S., Prins, J. M., Lukashov, V. V, Notermans, D. W., Roos, M., Schuitemaker, H., Hoetelmans, R. M., Danner, S. A., Goudsmit, J., & de Wolf, F. (1998). Alternative multidrug regimen provides improved suppression of HIV-1 replication over triple therapy. *AIDS (London, England)*, *12*(11), 117-22.

Williams, B. S., & Buvanendran, A. (2011). Nonopioid Analgesics: NSAIDs, COX-2 Inhibitors, and Acetaminophen. *Essentials of Pain Medicine*, 130-139.

Windolf, H., Chamberlain, R., Breitkreutz, J., & Quodbach, J. (2022). 3D Printed Mini-Floating-Polypill for Parkinson Disease: Combination of Levodopa, Benserazide, and Pramipexole in Various Dosing for Personalized Therapy. In *Pharmaceutics, 14* (5).

World Health Organization. (2020). Hearts: technical package for cardiovascular disease management in primary health care. https://www.who.int/publications/i/item/9789240001367 (accessed 21 April 2021).

Wright, H. (2005). Global data. In *Offshore, 65(7).*

Wu, W., Ye, C., Zheng, Q., & Wu, G. (2016). *A therapeutic delivery system for chronic osteomyelitis via a multi-drug implant based on three-dimensional printing technology*. *31*(2), 250–260.

Wu, W., Zheng, Q., Guo, X., & Huang, W. (2009). The controlled-releasing drug implant based on the three-dimensional printing technology. *Journal of the Wuhan University of Technology-Mater. Sci. Ed.*, *24*, 977–981.

Wu, W., Zheng, Q., Guo, X., & Sun, J. (2009). *A programmed release multi-drug implant fabricated by three-dimensional printing technology for bone tuberculosis*.

Xu, X., Robles-martinez, P., Madla, C. M., Joubert, F., Goyanes, A., Basit, A. W., & Gaisford, S. (2020). Stereolithography (SLA) 3D printing of an antihypertensive polyprintlet : Case study of an unexpected photopolymer-drug reaction. *Additive Manufacturing*, *33*(12).

Yadav, G., Bansal, M., Thakur, N., & Khare, P. (2013). *Multilayer Tablets and Their Drug Release Kinetic Models for Oral Controlled Drug Delivery System*. *16*(6), 782–795.

Yang, Z., Jin, L., Yan, Y., & Mei, Y. (2018). Filament Breakage Monitoring in Fused Deposition Modeling Using Acoustic Emission Technique. In *Sensors 18* (3).

Youssef, S. H., Mohamed, D., Hegazy, M. A. M., & Badawey, A. (2019). Analytical methods for the determination of paracetamol, pseudoephedrine and brompheniramine in Comtrex tablets. *BMC Chemistry*, *13*(3).

Yusuf, S., Pais, P., Afzal, R., Xavier, D., Teo, K., Eikelboom, J., Sigamani, A., Mohan, V., Gupta, R., & Thomas, N. (2009). Effects of a polypill (Polycap) on risk factors in middle-aged individuals without cardiovascular disease (TIPS): a phase II, double-blind, randomised trial. *Lancet (London, England)*, *373*(9672), 1341–1351.

Zhang, J., Feng, X., Patil, H., Tiwari, R. V, & Repka, M. A. (2017). Coupling 3D printing with hot-melt extrusion to produce controlled-release tablets. *International Journal of Pharmaceutics*, *519*(1–2), 186–197.

Zheng, Y., Deng, F., Wang, B., Wu, Y., Luo, Q., Zuo, X., Liu, X., Cao, L., Li, M., Lu, H., Cheng, S., & Li, X. (2021). Melt extrusion deposition (MED^{TM}) 3D printing technology – A paradigm shift in design and development of modified release drug products. *International Journal of Pharmaceutics*, *602*, 120639.

Zhu, M., Li, K., Zhu, Y., Zhang, J., & Ye, X. (2015). 3D-printed hierarchical scaffold for localized isoniazid/rifampin drug delivery and osteoarticular tuberculosis therapy. *Acta Biomaterialia*, *16*, 145–155.

Zhu, X., Li, H., Huang, L., Zhang, M., & Fan, W. (2020). Biomedicine & Pharmacotherapy 3D printing promotes the development of drugs. *Biomedicine & Pharmacotherapy*, *131*(8), 110644.

APPENDICES

Appendix 1: Abstract of Review Paper

EXPERT OPINION ON DRUG DELIVERY
https://doi.org/10.1080/17425247.2022.2121816

REVIEW

Customized 3D printed multi-drug systems: an effective and efficient approach to polypharmacy

Kundai R. Mazarura, Pradeep Kumar and Yahya E. Choonara

Wits Advanced Drug Delivery Platform Research Unit, Department of Pharmacy and Pharmacology, School of Therapeutic Science, Faculty of Health Sciences, University of the Witwatersrand, Johannesburg, South Africa

ABSTRACT

Introduction: Combination therapies continue to improve therapeutic outcomes as currently achieved by polypharmacy. Since the introduction of the polypill, there has been a significant improvement in adherence and patient outcomes. However, the mass production of polypills presents a number of technical, formulation, and clinical challenges. The current one-size-fits-all approach ignores the unique clinical demands of patients, necessitating the adoption of a more versatile tool. That will be the novel, but not so novel, 3D printing.

Areas covered: The present review investigates this promising paradigm shift from one medication for all, to customized medicines, providing an overview of the current state of 3D-printed multi-active pharmaceutical forms, techniques applied and printing materials. Details on cost implications, as well as potential limitations and challenges are also elaborated.

Expert opinion: 3D printing of multi-active systems, is not only beneficial but also essential. With growing interest in this field, a shift in manufacturing, prescribing, and administration patterns is, at this point, unavoidable. Addressing limitations and challenges, as well as data presentation on clinical trial results, will aid in the acceleration of this technology's implementation. However, it is clear that 3D printing is not the end of it, as evidenced by the emerging 4D printing technology.

ARTICLE HISTORY
Received 17 April 2022
Accepted 02 September 2022

KEYWORDS
3D-printing; customized; multi-drug systems; polypharmacy; polypill

Appendix 2: Ethics Waiver Certificate

ANIMAL RESEARCH ETHICS COMMITTEE
Registration number: AREC-101210-002

Date: 02/02/2023

Certificate reference: Waiver 02-06-2023-O
Category: O
Applicant: Kundai Mazarura
Department: Department of Pharmacy and Pharmacology (WITS)
Tel: 011 717 2552; **Email**: 1589308@students.wits.ac.za

Re: Waiver from the Animal Ethics Research Committee of the University of the Witwatersrand

This letter is to confirm that Kundai Mazarura (#1589308), MSc in Pharmacy Student under the supervision of Prof Yahya Choonara, Prof Pradeep Kumar, Dr Armorel van Eyk and Dr Mohamed Irhuma (Department of Pharmacy and Pharmacology), does not require full Animal Ethics Research Committee clearance to undertake the work titled ***"3D printed fixed dose combination with low abuse potential for the treatment of chronic pain"***.

Reason for waiver
The project is using intestinal tissue from domestic pig *(sus scrofa domesticus)* already euthanized at WRAF. The applicant should liaise with WRAF.

Details of the study
The *ex-vivo* study will be conducted to determine the permeability of chronic pain treatment drugs. *Ex vivo* permeation will be carried out in pigs duodenum (n = 6 to 12). Six (6)× 6 cm pieces will be cut, and mounted on the metal ring of the Franz cells. The *ex vivo* permeation study will be performed in Franz diffusion cells where duodenum portions will be placed between the receptor and donor compartments with the basal side in contact with the receiving medium and the apical side in contact with the donor chamber to avoid the bubble formation. Drug concentrations will be analysed.

The individuals covered by the waiver are Kundai Mazarura, Prof Yahya Choonara, Prof Pradeep Kumar, Dr Armorel van Eyk and Dr Mohamed Irhuma (Department of Pharmacy and Pharmacology, WITS).

Please contact me should you require further information.

Yours sincerely

A/Prof Frederic Michel
Chair: Animal Research Ethics Committee
University of the Witwatersrand

Appendix 3: Permeability Regression Lines and Cumulative Amount Formula

A3.1 Standard Curves

a. Paracetamol

Linearity range: 0.1 – 5 µg/ml
$y = 7628.3x + 87.002$, $r^2 = 0.9999$

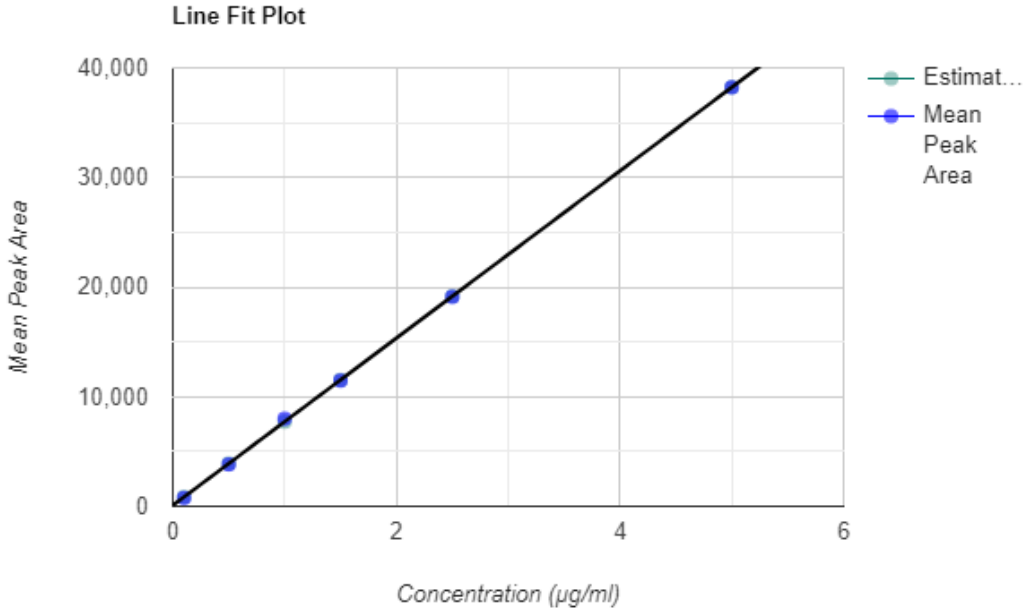

b. Diclofenac Sodium

Linearity range: 0.5 – 5 µg/ml
$y = 10577x - 127.46$, $r^2 = 0.9995$.

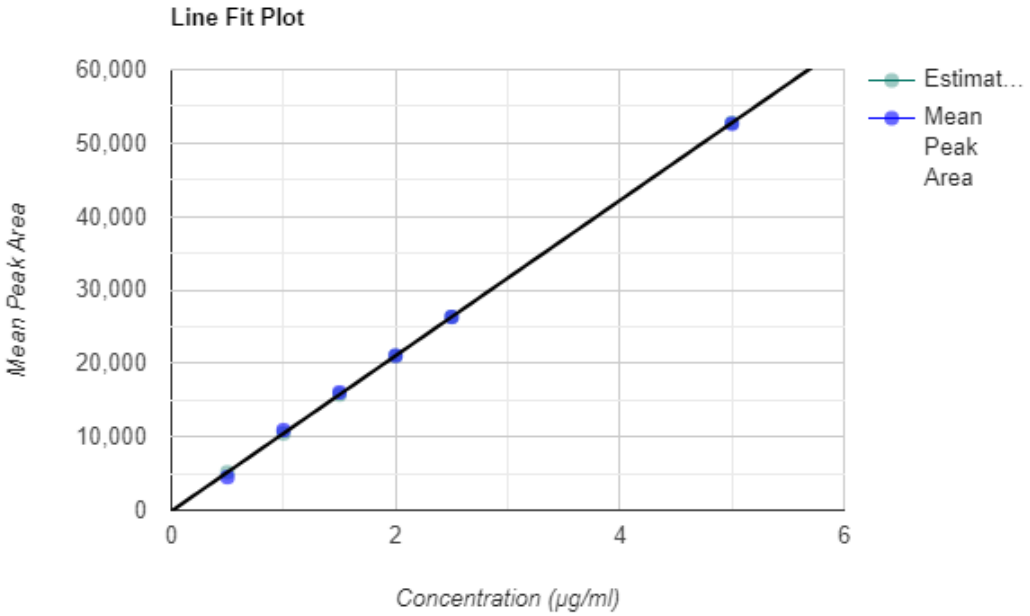

c. Esomeprazole Magnesium Trihydrate

Linearity range: 0.1 – 2.5 µg/ml

$y = 23684x + 138.34$, $r^2 = 0.9976$

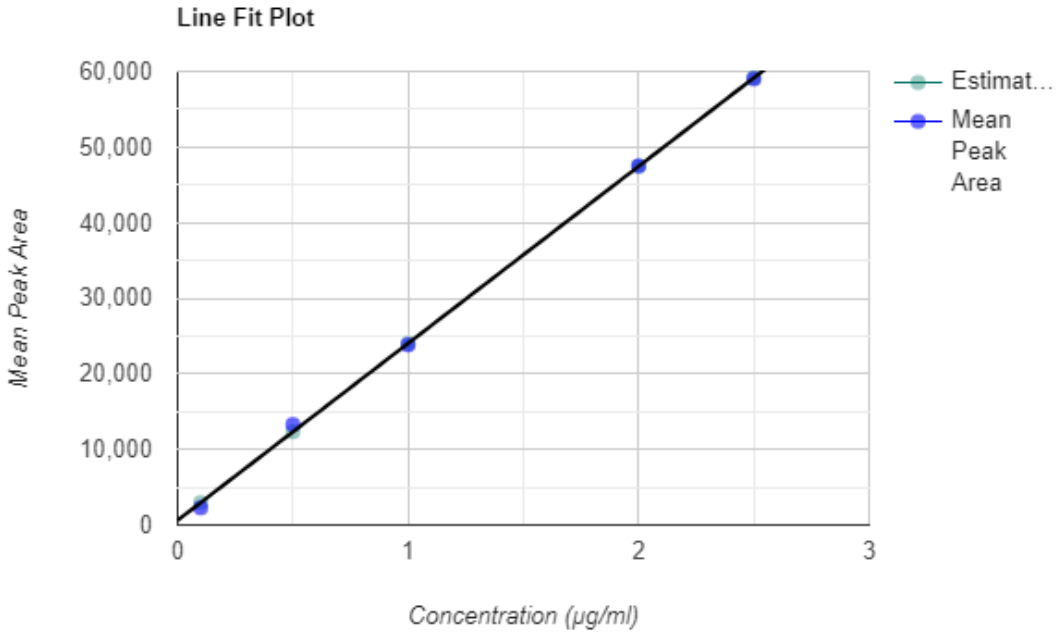

A3.2 Cumulative Amount Formula

e.g. PAR

Time (min)	**µg/ml**	**/12ml** **Receptor Volume**	**Cumulative Mass of drug per sample drawn (0.4 ml)**	**µg/cm²**
0	0.000	0.000	0.000	0.000
15	(Peak area - 87.002)/7628.3 = A	A * 12 = A1	A1 * 0.4 = A2	A2/1.767
30	(Peak area - 87.002)/7628.3 = B	B * 12 = B1	B1 * 0.4 + (A2) = B2	B2/1.767